HIGHLY CO_2-PHILIC LIQUID OLIGOMERS AND PHASE CHANGE-SOLVENTS FOR THE ABSORPTION OF CO_2

by

Matthew B. Miller

B.S. in Chemical Engineering, SUNY at Buffalo, 2006

Submitted to the Graduate Faculty of

Swanson School of Engineering in partial fulfillment

of the requirements for the degree of

Doctor of Philosophy

University of Pittsburgh

2011

UNIVERSITY OF PITTSBURGH

SWANSON SCHOOL OF ENGINEERING

This dissertation was presented

by

Matthew B. Miller

It was defended on

June 13th, 2011

and approved by

J. Karl Johnson, PhD, Chairman and Professor, Department of Chemical and Petroleum Engineering

Sachin S. Velankar, PhD, Associate Professor, Department of Chemical and Petroleum Engineering

David R. Luebke, PhD, Research Scientist, National Energy Technology Laboratory, NETL,

Dissertation Director: Robert M. Enick, PhD, Professor, Department of Chemical and Petroleum Engineering

HIGHLY CO_2-PHILIC LIQUID OLIGOMERS AND PHASE CHANGE-SOLVENTS FOR THE ABSORPTION OF CO_2

Matthew B. Miller, PhD

University of Pittsburgh, 2011

Integrated gasification combined cycle (IGCC) power plants are "the power plants of the future" due to their increased thermal efficiency compared to the current fleet of pulverized coal (PC) power plants employed throughout the US. An additional advantage they have is the range of possible fuels that can be used in their employ including, coal, biomass, recycled plastics, etc. Although there are no commercial scale IGCC plants currently in use in the US today, the increase in energy demand in the US compounded with the decommissioning of current PC plants each year will result in their construction soon.

As with all fossil fuel using processes the IGCC plant will give off CO_2 as a major waste stream that today is currently vented to the atmosphere. With the rising levels of atmospheric CO_2 and the concern of global climate change, and the contribution from CO_2, technology has been developed to capture CO_2 from this IGCC fuel stream. This capture process is done via physical absorbents because of the inherent high pressure driving force present in this fuel stream.

The overall objective of this work is to identify the most CO_2-philic compounds from three classes of compounds made up of C, N, O, and H intended to be used in the carbon capture process associated with the IGCC plant. The three classes of compounds in question are low volatility CO_2-philic oligomers, volatile organic solvents, and solid CO_2-philic compounds that are capable of melting in the presence of CO_2.

Phase behavior experiments have been carried out in order to construct phase diagrams for each solvent and CO_2. These diagrams quantify the miscibility of CO_2 in each solvent which helps determine the best possible solvent for absorbing CO_2 from a mixed gas high pressure stream in a typical counter-current absorption column. The higher the miscibility of CO_2 in the absorbent, the lower the pressure of phase separation will be throughout the phase behavior diagram.

Several solvents classified as low volatile CO_2-philic oligomers were tested with CO_2. A mixture of low volatility CO_2-philic oligomers known as poly(ethylene glycol) di-methyl ether, PEGDME, is the current solvent of choice in the IGCC capture process. Poly(dimethylsiloxane), PDMS, and poly(propylene glycol) di-methyl ether, PPGDME, are potentially better solvents, compared to PEGDME, in this process due to their limited miscibility or immiscibility with water, a constituent in the fuel stream, and their low viscosity, an important property for gas transport in and out of the liquid phase solvent.

Volatile organic solvents, while not prevalent in the IGCC capture process, are very widely used as solvents for a range of separation applications and are used extensively in CO_2 capture primarily in the sweetening process of natural gas. Commercial scale sorbents including methanol and propylene carbonate have been in use for years under the proprietary names of Rectisol^{TM} and the Fluor process. Several organic solvents were examined in this study in binary mixtures with CO_2. It was determined that acetone is the best solvent on a weight basis due to its small spherical size and shape and the CO_2-philic ketone functionality. It cannot be used commercially however due to its high vapor pressure that would cause significant evaporative losses in practice. The best solvents compared on a molar basis include 2-(2-butoxyethoxy)ethyl acetate, 2-methoxyethyl acetate, both discovered in this work, and methyl acetate. Overall the

best solvents on a weight or molar basis are those that are highly oxygenated compounds, rich in carbonyl and/or ether groups that favor Lewis acid:Lewis base interactions with CO_2.

CO_2-philic solids are from the last group of potential solvents examined with CO_2 and were found in the past by our group and two others. Originally investigated to be valuable as sand binders, these solids' unique ability to melt and then mix with CO_2 has great potential value in energy savings and initial capital equipment cost savings. This potential stems from these solvents' ability to release all CO_2 absorbed at a moderate pressure, approximately 5 MPa as opposed to a liquid solvent that releases CO_2 at 0.1 MPa. The solids were chosen from two classes known as sugar acetates and tert-butylated aromatics and were tested in a binary mixture with pure CO_2 and also a ternary mixture with an equimolar mixed gas CO_2/H_2. Four compounds, sucrose octaacetate, 1,3,5-tri-*tert*-butylbenzene, 2,4-di-*tert*-butylbenzene, and 1,3,5-trioxane, were determined to be viable candidates for the selective absorption of CO_2 from a CO_2/H_2 mixture that are capable of melting and selectively absorbing CO_2.

Lastly, higher molar mass PDMS solvents were examined and compared to PEGDME (molar mass = 310) at elevated temperatures. These PDMS solvents are all substantially larger than the PDMS hexamer tested in conjunction with the other hexamers and oligomers tested. The major benefit these higher molar mass solvents have is that they allow the capture step to be carried out at higher temperatures. Additionally these PDMS solvents are completely immiscible with water up to 68.95 MPa and 393 K. This change in the capture process allows for the elimination of heat exchangers needed to lower the temperature of the fuel gas stream, and also eliminates a condenser step that is typically needed to eliminate much of the water out of the fuel stream for the hydrophilic PEGDME solvent. Each PDMS solvent, PDMS10 (viscosity, μ, equals 10 cSt at 298.15 K, and average molar mass, $\overline{MW}$ equals 1,250 g/mol), PDMS 20 (μ = 20

cSt at 298.15 K and $\overline{MW}$ = 2,000 g/mol), and PDMS50 (μ = 50 cSt at 298.15 K and $\overline{MW}$ = 3,780 g/mol), was examined in a binary mixture with CO_2 at 353 K, 373 K, and 393 K, respectively, at PDMS weight fractions between 0.60 and 0.95. Each PDMS solvent displayed comparable CO_2 miscibility compared with PEGDME at each temperature. Additionally each PDMS solvent was mixed with H_2 at the same temperatures, and was able to mix and form a single homogeneous liquid phase however, only at substantially higher PDMS weight fractions, 0.995 to 0.999. While it is not clear which solvent has the highest miscibility with H_2, the comparison of H_2 miscibility to CO_2 miscibility in each solvent illustrates the difference in selectivity that these solvents have for CO_2 over H_2.

TABLE OF CONTENTS

LIST OF TABLES

LIST OF FIGURES

PREFACE

I wish to express my gratitude to my adviser Dr. Enick for his enlightenment, wisdom, and knowledge throughout my graduate studies. His use of his cheerful and always friendly enthusiasm is something that we should all try to emulate, especially on the really frustrating days, and will be remembered. I would also like to thank Dr. David R. Luebke, Dr. J. Karl Johnson, and Dr. Sachin S. Velankar for their guidance and support throughout my time at the University of Pittsburgh.

I would also like to thank Dr. Deepak Tapriyal, Dazun Xing, Bing Wei, Hussein Belied and Dr. Katie Barillas for the many constructive discussions and support throughout my time as a graduate student.

Lastly, I would like to thank my parents, my wife Lindsay, and Tyson, for their unconditional love and support that has shaped me into the individual I am today

1.0 INTRODUCTION

Recently there has been growing concerns about CO_2 emissions into the atmosphere from the burning of fossil fuels. These fossil fuels provide us with a large percentage of our primary energy such as heat and power. With the availability, ease of extraction and current infrastructure already in place, fossil fuels will undoubtedly continue to dominate the energetic landscape for several decades, and CO_2 will continue to be one of the byproducts of these processes.

The global production of primary energy in 2008 claims that 33.2 % of energy produced worldwide comes from oil, 27.0 % from coal, 21.1 % from gas, 12.2 % from renewables, (hydro, and combustible renewable wastes), and 5.8 % from nuclear sources. (1) Figure 1 shows the source of CO_2 emissions based on industry sector and fuel type as of 2006. Public heat and power, or electricity generation, comprises the largest part, contributing approximately 35 % of the CO_2 released into the atmosphere. Additionally, approximately 15 % is produced by the Industrial sector. These sources of CO_2 which make up 50 % of the anthropogenically released CO_2 present the greatest opportunities for CO_2 capture and sequestration, because most of the CO_2 produced from these sectors comes from large point sources that are capable of being retrofitted with carbon capture technology. Figure 2 shows some contributing industrial processes to CO_2 emissions based on the partial pressure of CO_2 present in the flue gas exit streams. The examples illustrated in Figure 2 are some of the largest processes in the world

including 133 million metric tons of ammonia produced in 2009, (2) 19 million metric tons of ethylene oxide produced in 2009, (3) approximately 50 million metric tons of H_2 consumed per year as of 2006, (4) and 110.5 trillion ft^3 of methane produced from natural gas processing in 2008. (5)

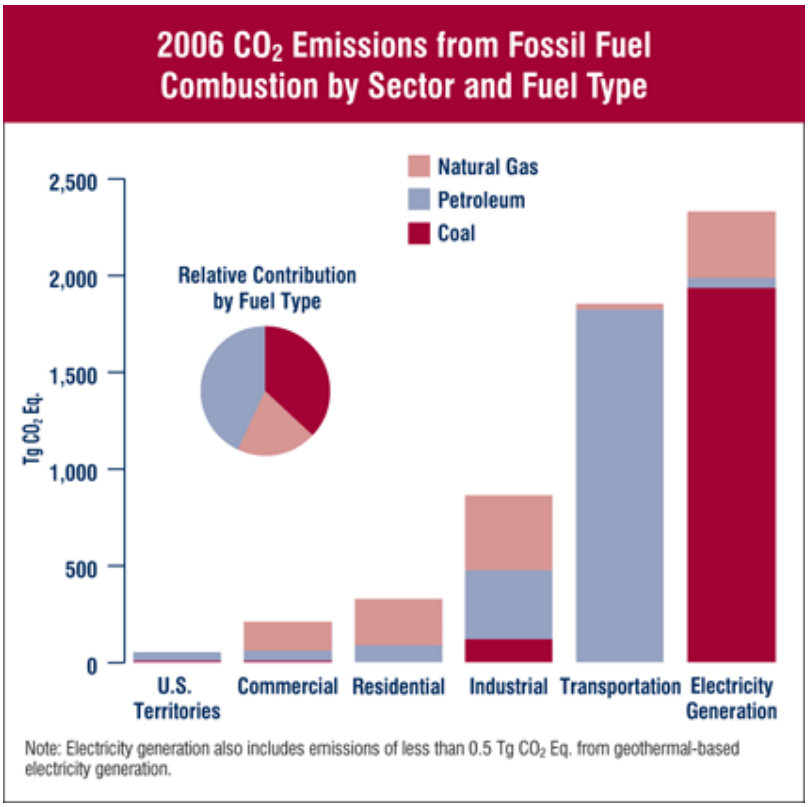

Figure 1. Global CO_2 emissions. (Figure obtained from (6))

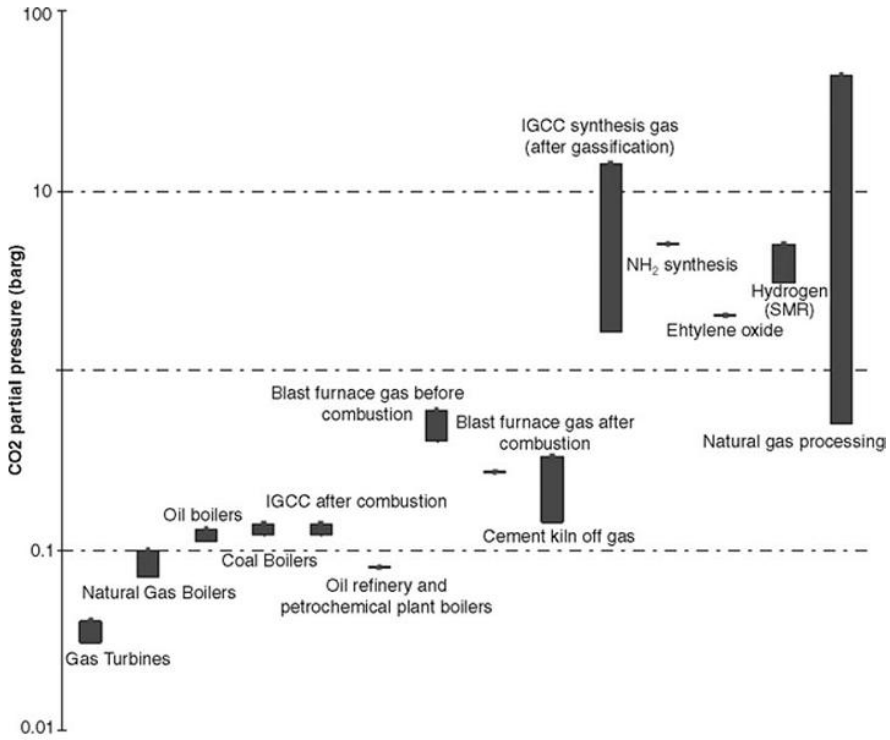

Figure 2. Partial pressure of CO_2 from the most important CO_2 producing stationary processes.(Figure obtained from (7))

There are many different strategies for the removal of CO_2, all of them with needed and ongoing research efforts from governments and the private sector across the globe. One way to look at them is putting them in three different categories illustrated by the cartoon in Figure 3. The strategies fall into three main categories, post-combustion capture, pre-combustion capture or oxycombustion. In post-combustion capture the fuel is burned and the energy used to produce electricity. The flue streams from the burning of the fuel contain CO_2 which would then be separated and recovered. Post-combustion capture is applied to more conventional combustion technologies such as pulverized coal-fired plants. In a pre-combustion process the CO_2 is captured prior to power generation, after the gasification of the fuel and a water gas shift step is used to convert partially combusted CO to CO_2. The H_2 is then oxidized to produce energy or

alternatively could be used to make a variety of synthetic chemicals. The pre-combustion process can be used in processes such as an Integrated Gasification Combined Cycle (IGCC) plant, which operates at higher thermal efficiencies than typical power plants, such as pulverized coal (PC). (8) Oxycombustion technology is a technique that produces ideally a pure CO_2 stream and a pure water stream (which can be readily condensed) during the power generation step.

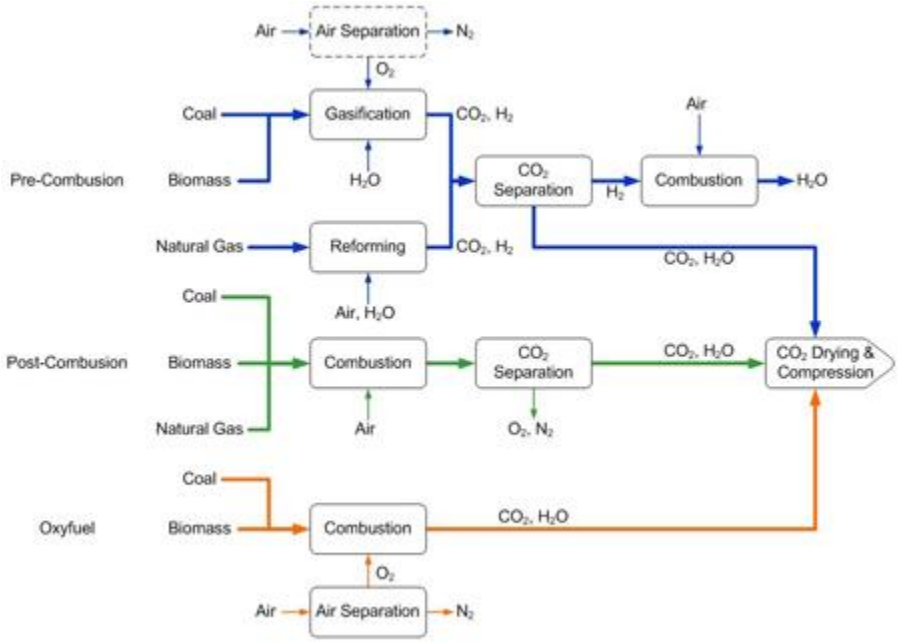

Figure 3. Main CO_2 capture routes.(Figure obtained from (9))

The solvent-based CO_2 capture strategies for pre-combustion and post-combustion can also be classified according to the pressure of the stream containing the CO_2. The post-combustion removal strategy is utilized when the stream is of low pressure, typically around 1-2 atmospheres and the flue gas temperature is between 323 K and 398 K. Because the CO_2 partial pressure and total pressure of the stream are very low the absorbent (solvent) should be one that relies on chemical absorption in order to be able to bond with the CO_2 and remove it from the stream. The pre-combustion removal strategy is utilized when the CO_2 containing stream is a high pressure

stream typically between 2.41 MPa and 8.27 MPa with similar temperatures as the post-combustion streams. In this case, the CO_2 partial pressure is high enough that the use of physical solvents is preferred; absorption is achieved through physical solvation in this case. Pre-combustion solvents utilizing physical absorption must have a particularly strong affinity for CO_2, and is the major topic that will be focused on in this dissertation. The two high pressure systems, seen in Figure 2, best suited for eventual implementation of new absorbents are IGCC synthesis gas production and natural gas processing.

1.1 CO_2-PHILIC FUNCTIONAL GROUPS AND CO_2-PHILICITY

In general there are no hard and fast rules that make a compound CO_2-philic, or make it able to readily mix with CO_2 at various concentrations and conditions. There are however, several guidelines about the structure of a compound that have been established over the years that lend that compound towards being CO_2-philic. Carbon dioxide has no dipole moment due to its symmetry, however it is polar and has a large quadrupole moment,(10)(11) shown in Figure 4; additionally each oxygen carries two sets of lone pairs of electrons. These characteristics allow CO_2 to interact via Lewis acid:Lewis base interactions,(12)(13) and allows it to effectively mix with other weakly polar and non-polar compounds.(14) Pearson's hard and soft acid-base principles classifies CO_2 as a hard acid and gives a set of guidelines for functional groups that should be able to interact with CO_2, classified as hard bases.(15)(16) Functional groups that readily interact with CO_2 in this fashion, some of which were explicitly listed by Pearson as hard bases, are perfluorinated compounds, and oxygen rich moieties such as carbonyl, ether, and acetate groups; the hydroxyl group is a CO_2-phobic moiety despite the fact it is classified as a

hard base. Interactions between CO_2 and these groups have also been shown via *ab initio* calculations (17) and Fourier transform IR spectroscopy. (18) High molecular weight polymers that have shown CO_2-philic nature via the incorporation of these CO_2-philic moieties include poly(vinyl acetate), (19) (20) (21) (22) poly(dimethylsiloxane) (PDMS), (23) (24) (25) (26) (27) PDMS that incorporated acetate groups throughout the backbone, (28) (29) poly(propylene glycol), PPG, and poly(ethylene glycol), PEG, capped with trifluoroacetate groups, (30) and PEG and PPG monomethylethers. (31) Some other examples include compounds specifically utilizing the carbonyl group (32) as well as varying degrees of fluorination. (33) (34) (35) (36) Increased CO_2-philicity via addition of acetate groups has also been seen in solid CO_2-philes such as sugar acetates including maltose octaacetate, (37) peracetylated α and β glucose, (38) (39) (40) peracetylated α and β galactose, (38) (39) (41) (42) (43) sucrose octaacetate, (44) (45) and peracetylated variations of cyclodextrins. (41) (46) (47)

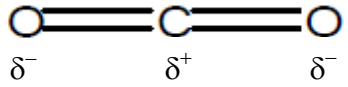

Figure 4. Charge distribution across CO_2.

The interactions between solute and solvent noted above increase CO_2 solvency in each of those examples, but just as important are the solvent-solvent interactions not involving CO_2. If a solvent is capable of strong interactions with itself such as hydrogen bonding, it will likely be a poor CO_2 solvent because these like-like interactions become dominant. This is illustrated with water, that experiences large amounts of hydrogen bonding, and benzene which interacts with itself via pi-pi stacking. Similarly the alcohol functional group is a CO_2-phobic moieties

because it promotes these strong solvent-solvent interactions. Functional groups, such as heavily branched alkane chains like tert butyl groups, that can decrease these interactions via steric hindrance can increase CO_2 solubility in solvents that share these characteristics. (48) (49) It is thought that the inclusion of these alkane groups lowers the cohesive energy density of the compound which directly correlates to solvent-solvent interactions. (50) Examples of this can be seen in a few benzene derivative compounds studied including tri-*tert*-butylbenzene, (50) tri-*tert*-butylphenol, (51) and several other benzene derivatives that have various alkane and iso-alkane groups bonded to the benzene. (52)

In light of all these correlations, a good CO_2 solvent should be one that has, slightly polar characteristics, multiple sites for Lewis acid:Lewis base interactions, and sites for hydrogen bonding so long as they do not allow the solvent-solvent interaction to become dominant. A solvent accountable for these considerations via a structure containing CO_2-philic functional groups will be an effective CO_2 solvent.

2.0 BACKGROUND

2.1 CHEMISORPTION

2.1.1 Introduction

Carbon dioxide is commonly removed from gas mixtures via a variety of absorption processes. The gas mixtures at low pressures employing chemical absorption typically use aqueous amine solutions (i.e. amine scrubbing) because the reaction between primary, secondary and tertiary amines (needs water present) and CO_2 occurs at low CO_2 partial pressures. A mixture of 30 wt% monoethanolamine, MEA, in water is the current leading technology for commercial scale CO_2 capture from PC power plants. Mixtures of MEA and MDEA, (N-methyldiethanolamine, $CH_3N(CH_2CH,OH)_2$), as well as mixtures including tertiary amines have also been studied and are growing in popularity. Solvent regeneration is achieved by temperature swing desorption (TSD), as heating to a moderate temperature causes the solutes to dissociate from the solvent.

2.1.2 Alkonolamines

Solvents such as MEA and MDEA are also referred to as alkanolamines and are frequently used in industry for the removal of acid gases, such as CO_2, SO_2, and COS, from

various waste streams. They are utilized in systems where said flue stream has a low pressure around or just above one atmosphere, whereas physical solvents are commonly used at higher pressures. Alkanolamines provide a good solution for exit streams at low pressures due to their low cost, ease of use, ease of reclamation, as well as low absorption of hydrocarbons. (53) Here the only driving force is a favorable chemical driving force, at the conditions of the waste stream, that allows the absorbent to bond to the CO_2 with favorable kinetics at low temperatures (less than 50 ^oC) and pressures around 1 atm. The reaction takes place via the formation of ammonium carbamates ($RNH_3^+ {}^-O_2CNHR$) between either primary or secondary amines with the CO_2. Typically aqueous MEA (2-aminoethanol, $H_2NCH_2CH_2O$) is used with 30 wt% being MEA. This 30 wt% MEA aqueous solution is used in order to decrease the viscosity of MEA, which is 20 times that of water at ambient pressure and 30^{o}C. (54) Also upon reaction with CO_2 the formed carbamate greatly increases the viscosity of the solvent and more concentrated solutions of MEA would experience mobility problems in the process. Water is also used in this fashion with mixtures of MEA, DEA (diethanolamine, $HOCH_2CH_2NHCH_2CH_2OH$), and MDEA (*N*-methyldiethanolamine, $CH_3N(C_2H_4OH)_2$) because it is a safe, inexpensive solvent capable of dissolving these amines as well as the amine-CO_2 carbamate complexes formed upon reaction. Figure 5 illustrates a comparison of the loading of CO_2 into Selexol$^{\mathbf{TM}}$, the physical absorbent of choice in IGCC plants, and MEA. The Selexol$^{\mathbf{TM}}$ solvent is able to continually absorb and mix with CO_2 as the composition of CO_2 increases with increasing pressure. The MEA-CO_2 solution reaches an asymptote however (2:1 molar ratio of amine:CO_2, illustrated for each MEA concentration as vertical lines), as a result of the stoichiometric limit of two MEA molecules being required for each CO_2 molecule present when forming the carbamate. Slight increases in

loading continue to occur via other routes such as physical absorption of the CO_2, or zwitterion formation.

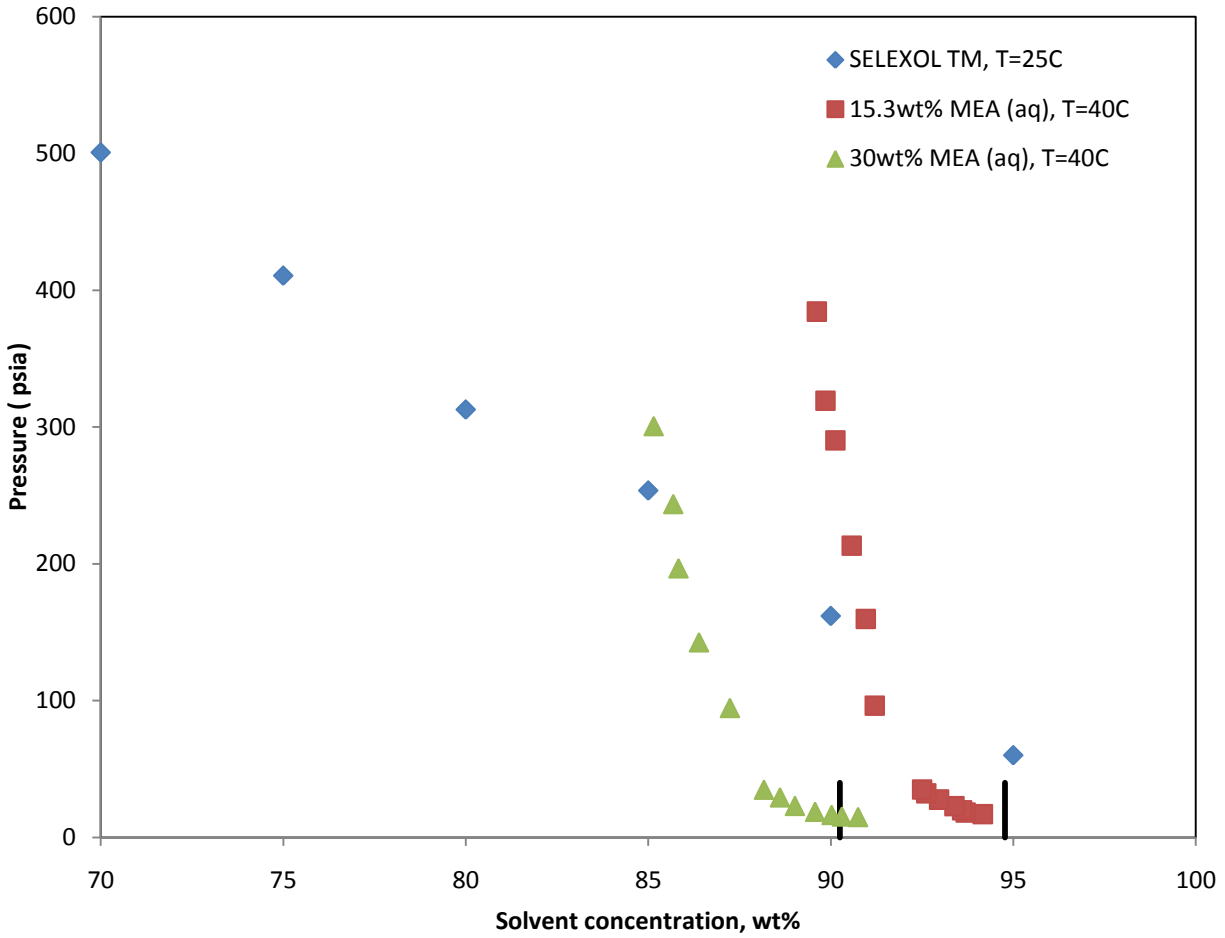

Figure 5. Illustration of absorptive capacity of Selexol™ and two compositions of MEA in water, lines represent 2:1 theoretical molar ratio of amine:CO_2. (55)

The MDEA is advantageous in this mixture because reaction with CO_2 requires a 1:1:1 molar ratio of CO_2:H_2O:MDEA. This improved "loading" however, comes at the cost of increased molecular weight of the amine (molecular weight of MEA is 61.08 g/mol and the molecular weight of MDEA is 119.2 g/mol) and a decreased rate of reaction. The tertiary amine binding energy to the CO_2 is smaller than that of primary or secondary amines, thus needing less energy to break this bond later on during solvent regeneration. (55) The MDEA also performs very well in absorbing H_2S, another acid gas present in smaller quantities in many flue gas streams from power plants and natural gas wells. While the MDEA does not greatly affect the loading of CO_2 on a weight basis, these mixtures bring about higher loading capacities, which is an important improvement because the stoichiometry of carbamate formation requires two primary or secondary amines for every one CO_2. Overall, these mixtures are able to improve CO_2 and H_2S loading, as well as reduce the energy required to release the absorbed gases upon temperature swing regeneration. (55) (56)

2.1.3 Chilled Ammonia

The chilled ammonia process is another process that chemically binds to CO_2 in order to remove it from flue gas streams. It is a relatively new process, but has recently received much publicity because of involvement from industrial and research partners such as Alstom and Electric Power Research Institute (EPRI). This process occurs between 0-10^oC and involves many elementary reaction steps that, from an overall perspective, takes one CO_2, one NH_3 and one H_2O molecule to form ammonium bicarbonate, NH_4HCO_3. The ammonia and water are liquid at the low temperatures and pressures of around one atmosphere. The CO_2 in its gas state is reacted with the ammonia as it is sprayed in a counter current flow path, at approximately 7-

10% concentration in water, with the CO_2. The product of the reaction, ammonium bicarbonate, exists as a solid. The largest advantage of this process is the high capture capacity of CO_2, approximately 1.2 kg CO_2 per kg NH_3. (57) Another major advantage is that with the CO_2 existing in a solid state it can be regenerated at a high pressure, immediately ready for sequestration. The solvent used is very cheap and available, and also has a lower binding energy than other chemical absorbers such as MEA or MDEA. The low concentration of ammonia throughout the process ensures safety to equipment and from potential explosive hazards. One major disadvantage of this process is the added energy and equipment necessary to cool and keep cooled all components operating at the low temperatures experienced in this process. Another disadvantage is the solids that are formed present a mobility problem and newer technologies such as fluidized beds or entrained beds must be used in order to transfer the ammonium bicarbonate from the absorber to regenerators.

2.2 PHYSICAL SOLVENT PROCESSES

2.2.1 Introduction

When the gas mixture to be separated is at high pressure the physical absorption technique becomes favorable to remove CO_2 because the high partial pressure of CO_2, like that seen in IGCC synthesis gas and natural gas processing, is sufficient to attain high loadings of CO_2 in the solvent. The rich solvent from the high pressure absorber is then regenerated at low pressures via pressure swing desorption (PSD) and occasionally TSD as well because CO_2 solubility in the solvent is inversely proportional to temperature.

Recently, the use of alkanes, such as dodecane, has been suggested for CO_2 removal from high pressure mixed gas streams.(58) Methanol has also been used commercially used as a solvent for CO_2 under the process name of Rectisol^{TM}, but the solvent must be chilled to prevent excessive evaporative losses of the alcohol. Another solvent process, primarily used in the sweetening of natural gas, is the Morphysorb® process. This process uses a mixture of morpholines such as N-formylmorpholine as well as N-acetylmorpholine, and is a good choice when the natural gas has larger concentration of CO_2 compared to typical concentrations found in natural gas wells. (59)

Figure 6 presents a comparison of literature values for the wt% solubility of CO_2 in propylene carbonate, isooctane, and methanol as a function of pressure and a temperature representative of the absorption column, 25 ^{o}C. Figure 6 also contains data for the solubility of CO_2 in Selexol determined during the course of this study. Figure 6 illustrates the high miscibility of CO_2 and Selexol and why it is a popular solvent; it exhibits high loadings of CO_2 at any given pressure (or the lowest pressure to attain a given loading) and it is much less volatile than methanol.

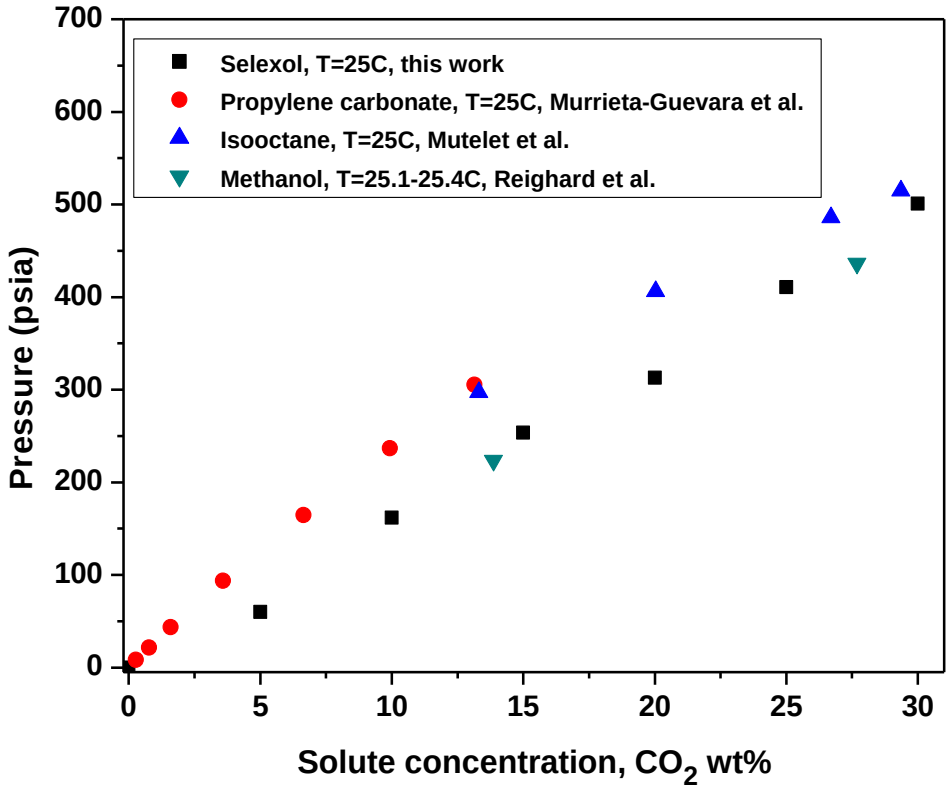

Figure 6. Comparison of common physical absorbents in commercial use at 25°C. (60) (61) (62)

2.2.2 Selexol™

The Selexol™ process is one of the leading physical absorption processes applied when the removal of acid gases is critical. It is well suited to be used in IGCC coal fired power plants (63) and is currently licensed by UOP LLC. The Selexol™ process was originally utilized to remove CO_2 from ammonia plants then used to remove acid gases from synthesis gas derived from petroleum stock and was then used in the sweetening of natural gas. (64)

Currently in the U.S. there are 617 facilities that produce electricity from coal, (65) and out of those, 476 facilities are owned by power plants that sell the electricity generated to the general public, the rest being plants that produce electricity strictly for onsite industrial use. As of September 2004, out of those 476 facilities only 2 of those are IGCC power plants, neither of them being commercial scale. (66) Figure 7 is an illustration of how an IGCC plant might be laid out. First the coal comes in and forms a slurry with water which is then gasified using air, or O_2 from an air separation unit when capturing the CO_2, to produce syngas, a combination of CO_2, CO, H_2, and H_2O. The fuel gas stream is then sent to a water-gas-shift, WGS, reactor in order to convert all remaining CO to CO_2 and produce more H_2, the wanted fuel. After that, the fuel gas goes through several cleanup stages to remove constituents such as mercury, organic sulfur compounds, and CO_2 which would employ the Selexol™ process. After the fuel stream is cleaned it contains primarily H_2, and is sent to combustion turbines in order to produce electricity. IGCC plants are versatile and can be tailored to produce synthesis gas, syngas, instead of power. If that is the goal then there would be no WGS step, and instead the syngas stream would be taken off to make a wide range of organic chemicals utilizing the Fischer-Tropsch process capable of combing CO and H_2 to form a wide range of different alkanes, alkenes, and alkynes ranging from methane up to long chain paraffin waxes.

The Selexol™ process employs a physical absorption solvent to absorb CO_2 as well as other acidic gases present in the stream such as H_2S. The Selexol™ solvent is also capable of absorbing many other components out of the gas stream such as small hydrocarbons, carbonyl sulfide, and water. The highest affinities for absorption are owned by water, H_2S, and CO_2, while the other components are not absorbed in significant quantities due to their low relative solubilities. The solvent itself has desirable vapor pressure and viscosity values low enough to inhibit evaporative losses and facilitate pumping, respectively, during the regeneration of the solvent.(67) This fundamental advantage, low vapor pressure, is what separates the Selexol™ solvent, and all oligomeric solvents, from other volatile organic solvents such as, chilled methanol.

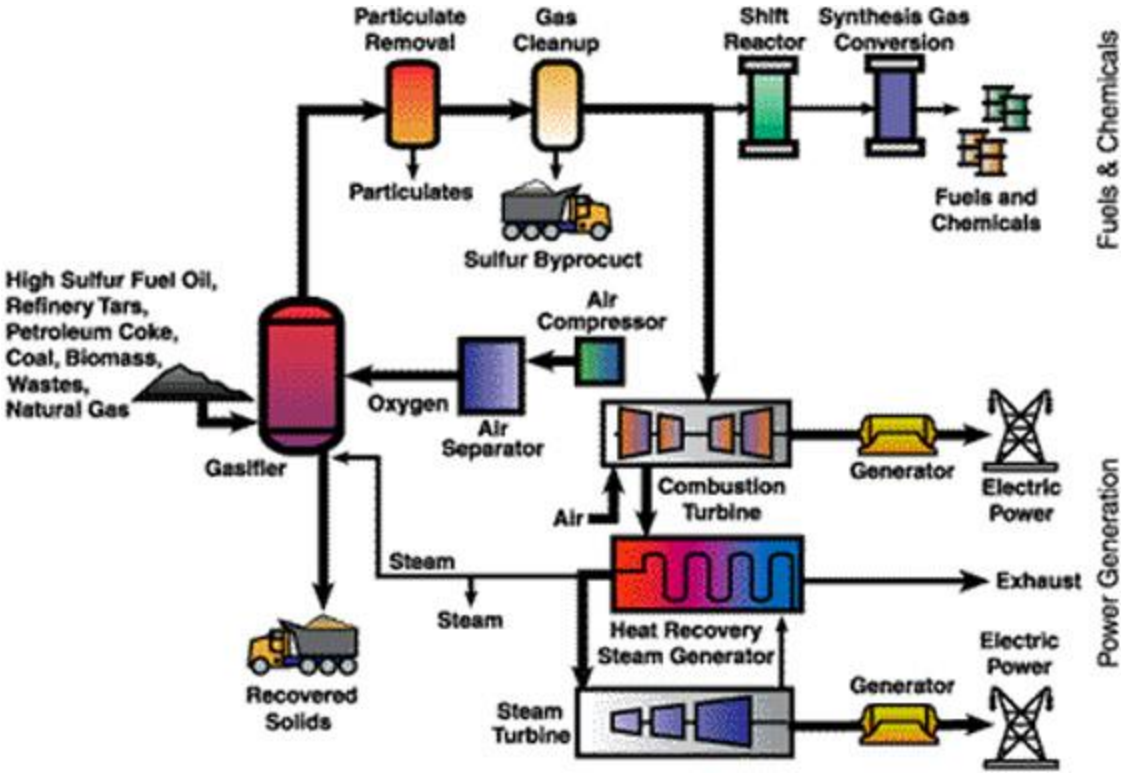

Figure 7. Cartoon of IGCC plant. (68)

2.2.3 Rectisol™

The Rectisol™ process was originally developed and patented by Linde and Lurgi; (64) now the patents and trademark are used in common. The Rectisol™ process is extensively used in the natural gas industry in order to strip out unwanted CO_2, and works very much like any physical absorber in that an exit stream that contains acid gases needs to be cleaned prior to being vented to the atmosphere or used somewhere else. As of 1996 there were more than 100 units in operation and under construction.(69) The solvent used in this process is chilled methanol, which lends many advantages to this process, the first being that the use of methanol absorbs all water and possible ice buildup. This is very important because a standard Rectisol™ plant operates between -75^o to -100^{o}F.(64) The Rectisol™ solvent uses pressure as its driving force to absorb all that it can at given conditions. The rich solvent stream is regenerated using pressure swing desorption and temperature swing desorption if necessary to change solubility conditions and release the unwanted components contained therein. This ultra cold temperature combined with pressure as the driving force for absorption allows the Rectisol™ process to absorb some troublesome components that might not be possible in other processes, such as, hydrogen cyanide, aromatics, organic sulfur compounds, and gum-forming hydrocarbons.(64) Another major benefit of the Rectisol™ process conditions is that it has the capability to release the CO_2 and H_2S fraction in separate streams and the capability to collect H_2S and CO_2 separately. With this CO_2 present in a stream by itself it can readily be pressurized and transported for sequestration or some other pertinent use. Rectisol™ is however, very costly because the solvent in use needs to be chilled to the subzero temperatures stated above in order to increase the solubility of acid gases in the solvent. This leads to increasingly complex flow diagrams as well as an increase in the number of heat exchangers necessary and energy needed to

cool the solvent to sub-zero temperatures resulting in high capital and operating costs of the process.

2.2.4 Fluor®

The Fluor® process is another physical absorbent process available that is licensed by Fluor Daniel, Inc., and was introduced in 1960 by Kohl and Buckingham.(70) This process uses propylene carbonate as its solvent of choice and is most attractive when exit streams contain high concentrations of CO_2, such as 30-70%, relative, for example, to the typical 10-14% CO_2 in a PC plant exit stream from the boiler. The attractiveness of propylene carbonate is not so much due to its affinity for CO_2, but rather for its low affinity for H_2S compared to other physical absorbents. Propylene carbonate can absorb 10.6 mL H_2S per mL of solvent whereas it can only absorb 3.22 mL of CO_2 per mL of solvent, a selectivity of approximately 3.3:1, H_2S:CO_2.(71) This selectivity may still seem rather high, but when compared to other physical processes such as Rectisol^{TM}, which has a selectivity of 6.1:1, H_2S:CO_2 at only -22^{o}F,(72) it becomes apparent that the Fluor® process is very apt to be used with high concentrations of CO_2 and low to insignificant concentrations of H_2S. The Fluor® process is primarily used in natural gas sweetening but has also been used in processing ammonia synthesis gas and hydrogen synthesis gas with a total of 13 commercial units throughout the world.(64) While the solvent used has a very high capacity for CO_2 it is also expensive.

2.2.5 Morphysorb®

The Morphysorb® process is a relatively new process researched at the Gas Technology Institute and licensed through Uhde, a company of ThyssenKrupp Technologies. The Morphysorb® solvent is made up of a mixture of N-formyl-morpholine (NFM) and N-acetyl-morpholine (NAM). This solvent's major advantage is a high capacity for acid gases like CO_2 and H_2S, along with a very low capacity for small hydrocarbons, C_1-C_3.(59) It also has the ability to remove mercaptans from the feed gas and is capable of removing other impurities such as benzene, toluene, ethylbenzene and other benzene derivatives potentially present in natural gas streams. This low capacity for light hydrocarbons and ability to remove benzene and its derivatives lends Morphysorb® to being an excellent candidate for the sweetening of natural gas. The solvent itself is relatively cheap, inert, and has very low vapor pressure, all adding up to reduced capital investment and operational costs.

2.3 OXYCOMBUSTION

In the oxycombustion process the fuel is oxidized with pure O_2 that allows for the products to be made up of primarily CO_2 and H_2O. Along with these major products any impurities contained in the fuel would ideally be oxidized typically forming NO_x, and SO_x. The water in the exit stream can readily be condensed out yielding just a pure H_2O stream and nearly pure CO_2 stream. In order to accomplish this, an air separation unit (ASU) needs to be added which supplies the reactor with pure O_2. Current ASU technology relies on cryogenic separation

which is a costly process both in terms of initial capital and the energy required to carry out this cryogenic cooling during operation.

Efforts have been made however, in utilizing chemical looping to bring O_2 into the reactor via oxygen carriers typically made up of metallic compounds, M. This technique involves taking a metallic compound, oxidizing it in an air reactor, transporting it to the fuel combustion reactor, where the metallic compound would then be reduced by the fuel, and then transporting the oxygen carrier back to the oxidation reactor to be re-oxidized, as illustrated in Figure 8.

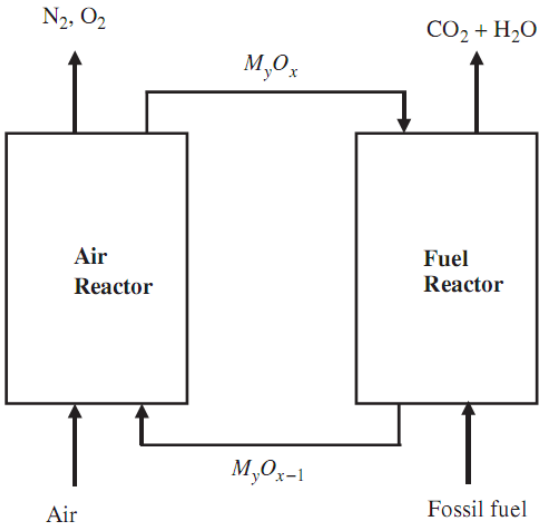

Figure 8. Schematic of chemical looping combustion technology. (73)

The main advantage of oxycombustion via chemical looping resides in the product streams, separated, pure CO_2 and H_2O. Many challenges still remain however, regarding the scale up of this technology including, optimization of metal and combinations of metal alloys and supports to be used, solid/metal transportation, reduction and oxidation kinetics, lifetime of

oxygen carriers, effects of impurities such as sulfur compounds in fuels, and potential coke build up.(73)

3.0 RESEARCH OBJECTIVES

The primary objective of this project is to identify the most CO_2-philic compounds from three classes of compounds made up of C, N, O, and H intended to be used in carbon capture and sequestration systems on large industrial point sources of CO_2. The three classes of compounds in question are low volatility CO_2-philic oligomers, volatile organic solvents, and solid CO_2-philic compounds that are capable of melting in the presence of CO_2.

3.1 CO_2-PHILIC OLIGOMERS

The objective of this study is to assess the viability of several oligomeric (repeat units of 2-7), CO_2-philic CO_2 capture solvents, and to compare their CO_2 absorption, hydrophobicity, and viscosity with the commercial oligomeric CO_2 solvent used in the Selexol^{TM} process. The identification of a CO_2 solvent with superior properties to the Selexol^{TM} solvent (high CO_2 absorption, hydrophobic, low viscosity) has the potential to lead to greater IGCC power plant efficiency. This study does not include comparisons of other properties that are very relevant to a large-scale absorption process, including the determination of solvent vapor pressure, corrosion rates with common materials of construction, or rates of solvent thermal degradation. The choice of solvents has been limited to oligomeric versions of polymers that have already been

established as "CO_2-philic" by their ability to completely dissolve in CO_2 in dilute concentrations at elevated pressures. (53) (56) (58) (60) (61)

The solvents examined include poly(propyleneglycol) dimethyl ether (PPGDME), poly(ethyleneglycol) dimethyl ether (PEGDME), poly(dimethylsiloxane) (PDMS), perfluoropolyether (PFPE) which is a perfluorinated oligomer with a PPG backbone, poly(propyleneglycol) diacetate (PPGDAc), poly(butyleneglycol) diacetate with a linear (-C_4H_8O-) monomer unit, also known as poly(tetramethyleneetherglycol) diacetate, (PTMEGDAc), poly(butylenegylcol) (PBG) with a branched monomer (-$CH(C_2H_5)CH_2O$-), was transformed into poly(butyleneglycol) diacetate (PBGDAc), glyceryl triacetate (GTA), and the Selexol^{TM} solvent. Ideally the solvent should have a high affinity for CO_2, low viscosity, in order to reduce pumping requirements and also reduce mass transfer limitations, low affinity for water, low vapor pressure to reduce evaporative losses, low cost, and minimal environmental toxicity issues.

3.2 VOLATILE ORGANIC SOLVENTS FOR CO_2 CAPTURE

The use of volatile organic solvents for the absorption of CO_2 based solely on their ability to absorb CO_2 has been proposed as a potential commercial CO_2 solvent and examined. Other solvent qualities such as volatility, cost, health and safety, and environmental toxicity issues have not been included in the assessment and would need to be done elsewhere on a per process basis. The choice of candidates was based on compounds with low molecular weight that possess functional groups that demonstrate CO_2-philic behavior. The ideal functional groups are those

that are oxygen rich, such as carbonyl, ether, and acetate, in order to provide ample sites for the CO_2 to interact favorably with.

Some of the chosen compounds have been studied in the past at various temperatures or at the CO_2 rich end of the phase diagram. The list of candidates includes 1,4-dioxane, (74) (75) (76) acetone, (77) (78) (79) (80) (81) methyl acetate, (82) (83) (84) acetylacetone, (85) 2-butoxyethyl acetate, 2-(2-butoxyethoxy)ethyl acetate, 1-nitropropane, 2-nitropropane, *N*,*N*-dimethylacetamide, 2-methoxyethyl acetate, and *N*-*tert*-butylformamide. Other low molecular weight oxygenated hydrocarbons with at least one carbonyl or ether oxygen atom were considered. Formaldehyde is unfortunately only available in aqueous solution. Acetaldehyde and dimethyl ether are inappropriate for use as liquid organic solvents due to their near or sub-ambient boiling points, 294 K and 248 K, respectively. Finally diethyl ether may be a promising candidate because it is made up of four carbons and an ether oxygen however, safety concerns associated with its flammability and stability barred its use in this examination.

3.3 NOVEL SOLID CO_2-PHILES

The last objective of this work is to assess the ability of novel CO_2-philic solvents to serve as CO_2 absorption solvents that can be regenerated with small pressure drops (to values just below the vapor-liquid-solid, VLS, three-phase pressure) that induce solidification (freezing) of the compound to release the CO_2 at a relatively high pressure (~3 MPa to 6 MPa) during regeneration. This regeneration at higher pressures also makes the CO_2 immediately transport ready, which is necessary for sequestration and avoids the costly compression of the CO_2 often

incurred after solvent regeneration. Two classes of compounds have been identified as candidates for this technology, sugar acetates and tert-butylated aromatics. The list of sugar acetates examined includes β-D-ribofuranose 1,2,3,5-tetraacetate (BRF-Ac), D-(+)-sucrose octaacetate (SOA), β-D-maltose octaacetate (MOA), α-D(+)-glucose pentaacetate (AGLU-Ac), and β-D-galactose pentaacetate (BGAL-Ac). The list of butylated aromatics includes 2,6-di-*tert*-butyl-4-methylphenol, 1,2,4-triacetoxybenzene, 2,4-di-*tert*-butylphenol, 2,4,6-tri-*tert*-butylphenol (TTBP), 1,3,5-tri-*tert*-butylbenzene (TTBB), and 3,5-di-*tert*-butylphenol. The last solid CO_2-phile, 1,3,5-trioxane, was chosen due to excellent solubility shown from 1,4-dioxane in our work with organic volatile solvents.

The binary phase behavior of these new compounds with CO_2 has been examined. Any of the compounds that were capable of melting in pure CO_2 and experienced a melting point depression were then further tested with an equimolar mixture of CO_2/H_2 and the tertiary phase behavior was examined.

3.4 HIGH MOLECULAR WEIGHT PDMS

Physical absorption of CO_2 is the capture strategy that will be employed in the IGCC power plant because it presents excellent capture opportunities due to the single high pressure fuel gas stream it produces that contains large amounts of CO_2 (41 %) and H_2 (56 %). (63) This fuel stream comes out of the gasifier then quenched, and cooled before being sent to a COS hydrolysis process that converts all organic sulfur compounds to CO_2 and H_2S. The exit stream of the COS hydrolysis process is between 479 K and 497 K. This stream is then sent through a water gas shift (WGS) reactor in order to convert CO and H_2O to CO_2 and H_2. Then it has to be

cooled all the way down to 300 K prior to being sent to the Selexol unit, the physical absorption process that removes H_2S and CO_2. (63)

The objective of this work is to find a high molecular weight liquid polymeric solvent from the PDMS family of polymers that is capable of absorbing these acid gases at elevated temperatures. The key advantage of this PDMS solvent would be that the exit stream from the WGS reactor would not need to be cooled via heat exchangers and would have less cost to sensible heat loss, meaning energy savings, as well as capital investment savings for equipment associated with the heat exchangers involved in the process. In addition, the H_2O in this fuel stream would not need to be condensed out and because PDMS is hydrophobic the H_2O would then be utilized to produce power downstream in the turbine; according to an in house NETL study this extra mass in the fuel stream could improve the overall plant efficiency by an estimated 1 % - 3 %.

The binary phase behavior diagrams (Px) of various PDMS solvents with CO_2, and binary Px diagrams of PDMS and H_2 at elevated temperatures of 353 K, 373 K, and 393 K have been examined. Our group as well as others have shown PDMS (86) (87) (24) (23) (25) (26) (27) and PDMS modified to incorporate acetate groups in the backbone (28) (29) to be very soluble with CO_2.

4.0 NOVEL OLIGOMERIC SOLVENTS FOR ABSORPTION OF CO_2

4.1 MATERIALS

Poly(propyleneglycol) dimethylether (PPGDME Mn = 230 and 400, average repeat unit of 3.2 and 6.0, RU = 3.2, 6.00, Mn/Mw=1.08) and poly(ethyleneglycol) dimethylether (PEGDME Mn = 250 and 310, RU = 4.6 and 6.0, Mn/Mw=1.12) were purchased from Polymer Source Inc. and used as received. Poly(dimethylsiloxane) (PDMS Mn=237 and 550, RU = 2.0 and 6.24) was purchased from Gelest Inc. and used as received. Perfluoropolyether, PFPE, named Krytox® GPL 100 (Mn = 960, RU = 5.0) was purchased from Miller–Stephenson and used as received. Poly(propyleneglycol) diacetate (PPGDAc, Mn=509, RU = 6.7) and poly(butyleneglycol) diacetate with a linear ($-C_4H_8O-$) monomer unit, also known as poly(tetramethyleneetherglycol) diacetate, (PTMEGDAc Mn=250, RU=3.2) or poly(1-4-butanediol) diacetate, were synthesized by Bayer Material Science using PPG, and PTMEG as the starting materials, and transforming the terminal hydroxyl groups to acetate groups. Poly(butylenegylcol) (PBG) with a branched monomer ($-CH(C_2H_5)CH_2O-$), received from Huntsman International LLC., was transformed into a PBGDAc (Mn=250, RU=3.2) by Bayer Material Science. Glyceryl triacetate (GTA) ≥99.0% was purchased from Fluka and used as received; this compound was considered because it is analogous to a trimer of poly(vinyl acetate), the most CO_2-philic high molecular weight hydrocarbon-based polymer identified to

date. (20) The Selexol™ solvent, which is a mixture of PEGDME oligomers with various repeat units between 3 and 9, produced by Dow and was purchased from Univar, was used as received. The structure of each solvent used is shown in Table 1. Much of the results discussed in this chapter have been published here. (86) (87) CO_2 was purchased from Penn Oxygen and Supply Company with a purity of 99.99% and used without further purification.

4.2 SOLUBILITY OF CO_2 IN OLIGOMERS

4.2.1 Phase behavior apparatus

Phase behavior measurements were carried out at 298 K for all oligomers and hexamers and 313 K for the PEGDME and PPGDME hexamers, PPGDAc, PBGDAc, PTMEGDAc, GTA, PDMS hexamer, and Selexol™. The bubble point loci of all pseudo-binary systems were determined in a windowed, agitated, variable volume view cell (Schlumberger) using standard non-sampling techniques, also known as the synthetic method, also described elsewhere. (32) (41) (86) (88) The schematic of this apparatus is shown in Figure 9 and the variable volume Pyrex tube inside of the cell is shown in Figure 10. The hollow Pyrex tube (1.25 inch ID, 1.75 inch OD) has a maximum capacity of 100 mL, but the sample volume (specified amounts of CO_2 and solvent) of the mixture is lower than this (approximately 30 mL to 90 mL) during a given experiment. An O-ring encircles a floating piston housed inside the tube that separates the cylindrical sample volume above the floating piston from the overburden fluid below the piston. The Pyrex tube is retained within a high pressure stainless steel vessel with 1 ½" thick borosilicate windows on opposing sides. The overburden fluid resides below the floating piston

on the inside of the hollow tube, and also in the gap between the stainless steel cell and the outer surface of the Pyrex tube, thereby eliminating any pressure drop across the wall of the hollow tube. The entire high pressure cell is enclosed in a temperature controlled air bath capable of controlling the temperature between 253 K and 453 K, as measured with a type K thermocouple to an accuracy of ±0.2 K. The thermocouple is used to measure the temperature of the overburden fluid surrounding the sample volume, which was previously determined to be within 0.1 K of the temperature within the sample volume. The cell has an operating pressure of 0.21 MPa to 69 MPa and the pressure in the overburden fluid is measured with a Heise pressure gauge accurate to within ±0.07 MPa.

In a typical experiment, the oligomer sample (about 25g to 70 g) is first loaded by weight from a syringe onto the surface of the floating piston within the Pyrex tube. The Pyrex tube, floating piston and oligomer assembly is then inserted into the high pressure windowed cell and sealed with a cap that houses a magnetic mixer and the port through which gas can enter the sample volume. The piston is then displaced to a position near the top of the cell, thereby minimizing the sample volume and displacing air from the sample volume. The sample volume is then flushed several times with CO_2 (0.1 MPa to 0.5 MPa) in order to assure there is no air present during the experiment. A small amount of high pressure CO_2 then flows into the sample volume from a high pressure positive displacement (PD) pump that contains liquid CO_2 at ambient temperature (~295 K) and a specified pressure (e.g. 10 MPa) and volume (100 cc). The mass of CO_2 that entered the sample volume is determined by calculating the amount of CO_2 that left the PD pump; a NIST correlation is used to determine the CO_2 density at these conditions. (53) Other mixture compositions are attained via the additions of CO_2 to the sample volume. First, the polymer-CO_2 mixture in the sample volume is compressed to the same pressure as the

CO_2 in the PD pump. The valve separating the CO_2 and the sample volume is then opened, and liquid CO_2 is displaced into the sample volume at the exact same volumetric flow rate that the sample volume is expanded. This is achieved by advancing the CO_2 PD pump at the same rate as the overburden fluid PD pump is withdrawn. This results in a well controlled, isothermal and essentially isobaric addition of a specified volume (and thereby mass) of CO_2 into the sample volume. A mixture of known overall concentration is then isolated from the CO_2 source by closing the valve leading to the CO_2 PD pump, and compressing the mixture, via the addition of the overburden fluid and reduction of the sample volume, until a single phase is attained as the mixture is stirred. The mixer is turned off and the system is very slowly depressurized and expanded by withdrawing the overburden fluid from the cell. The bubble point is denoted as the pressure at which a single bubble escapes from the solution and remains in equilibrium above the liquid phase. Bubble points were repeated at least three times; the data were reproducible within the accuracy of the apparatus, ± 0.07 MPa.

Table 1. Structures of CO_2-philic oligomers.

polypropyleneglycol dimethylether (PPGDME)	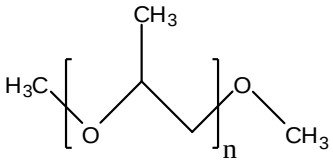
polyethyleneglycol dimethylether (PEGDME)	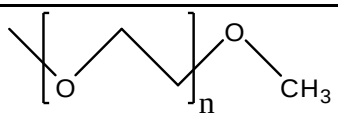
polydimethyl siloxane (PDMS)	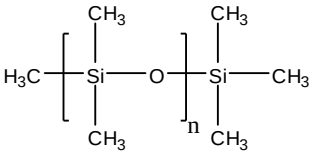
perfluoropolyether (PFPE), or perfluoropropylene glycol	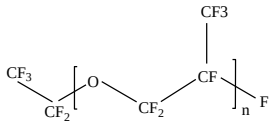
polypropyleneglycol diacetate (PPGDAc)	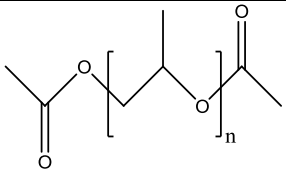
polytetramethyleneether glycol diacetate (PTMEGDAc)	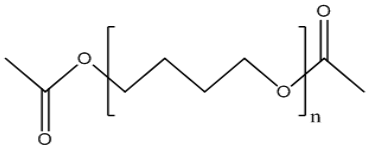
polybutyleneglycol diacetate, branched monomer (PBGDAc)	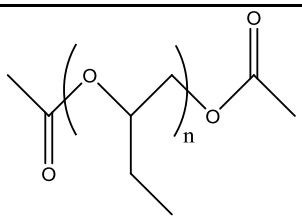
glycerol triacetate (GTA)	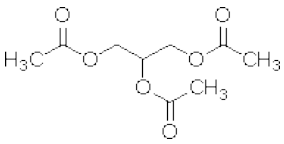

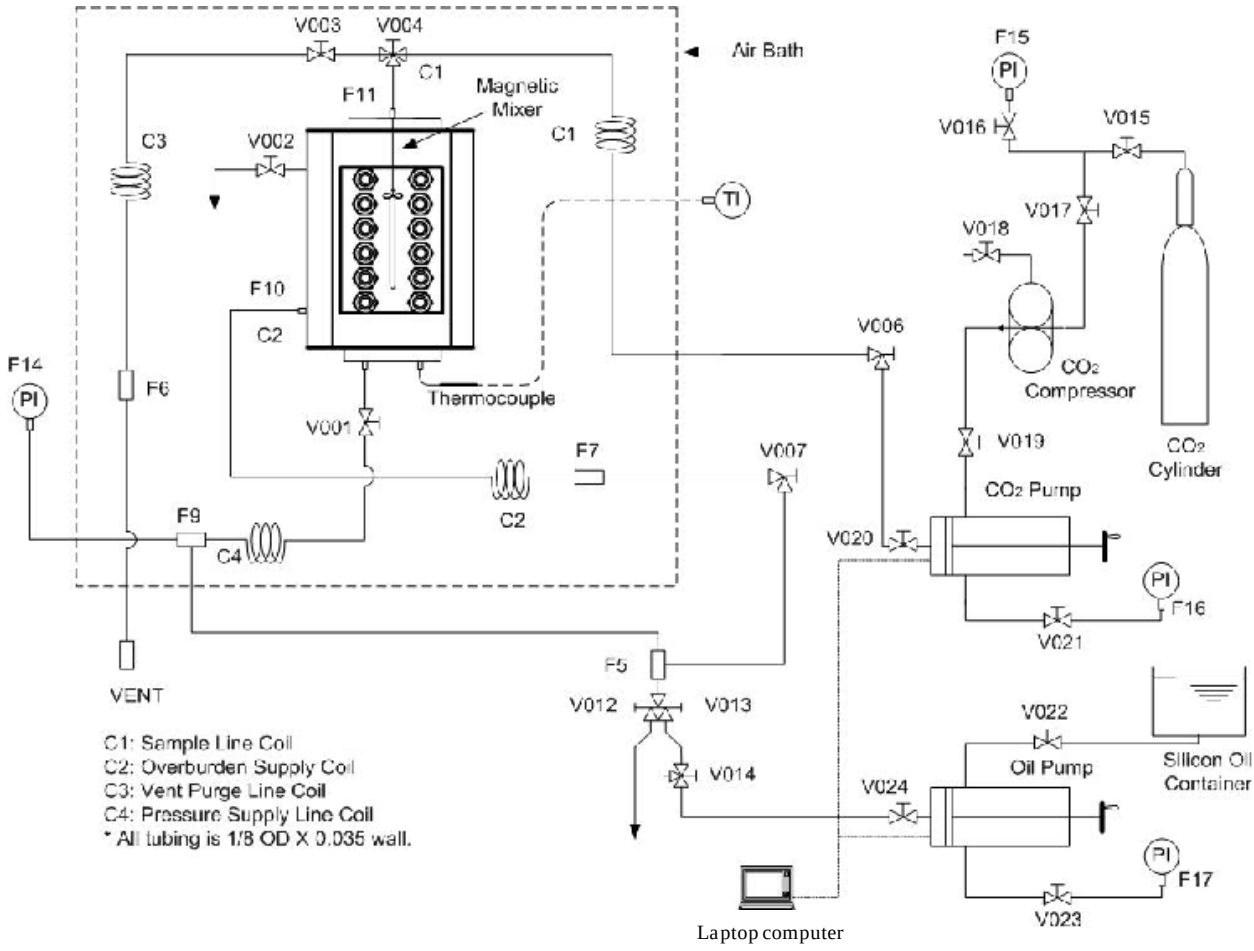

Figure 9. Experimental apparatus used in phase behavior and solubility experiments.

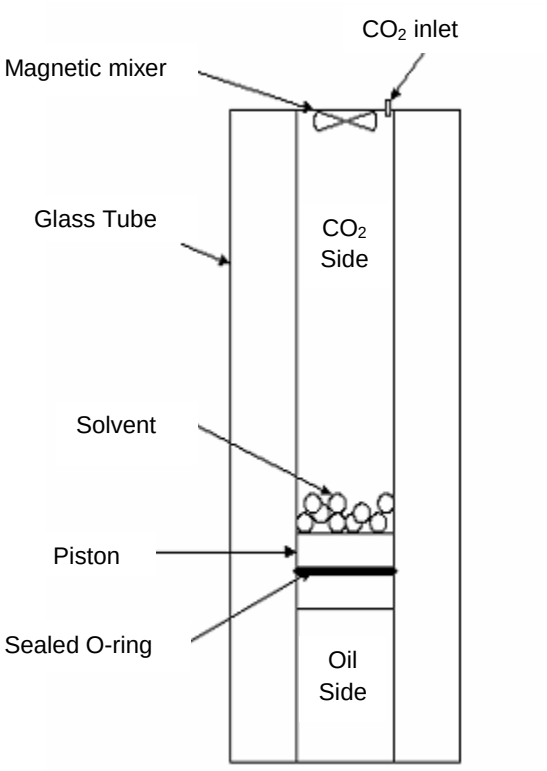

Figure 10. Detailed drawing of the high pressure, variable volume, view cell.

4.2.2 Phase behavior and solubility results

The experimentally measured bubble point loci for the PEGDME250-CO_2, PPGDME230-CO_2, PFPE960-CO_2 and PDMS237-CO_2 pseudo-binary systems can be seen in MPa absolute over the entire range of solvent weight fraction, *w*, in Figure 11 and on the solvent rich end, $w = 0.8 – 1.0$, in Figure 12.

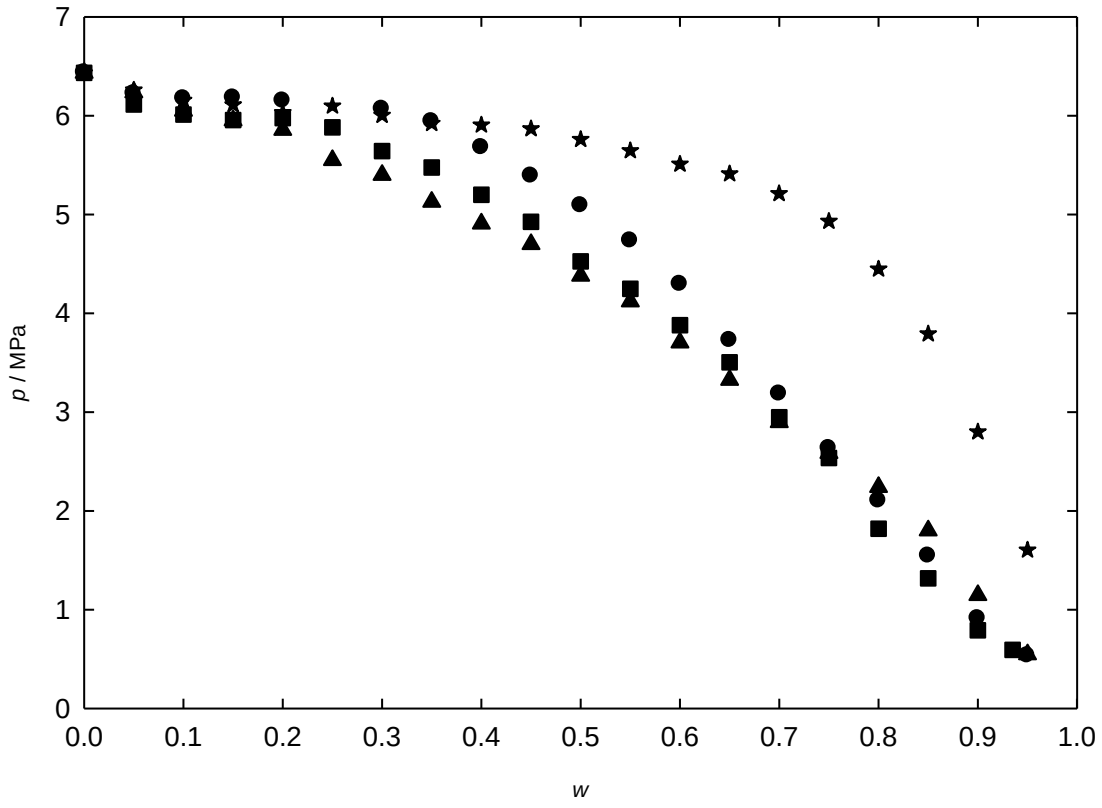

Figure 11. Oligomer-CO_2 bubble point curves of the CO_2-philic solvents at 298.15 K; ● PEGDME 250; ■ PPGDME 230; ★ PFPE 960; ▲ PDMS 237.

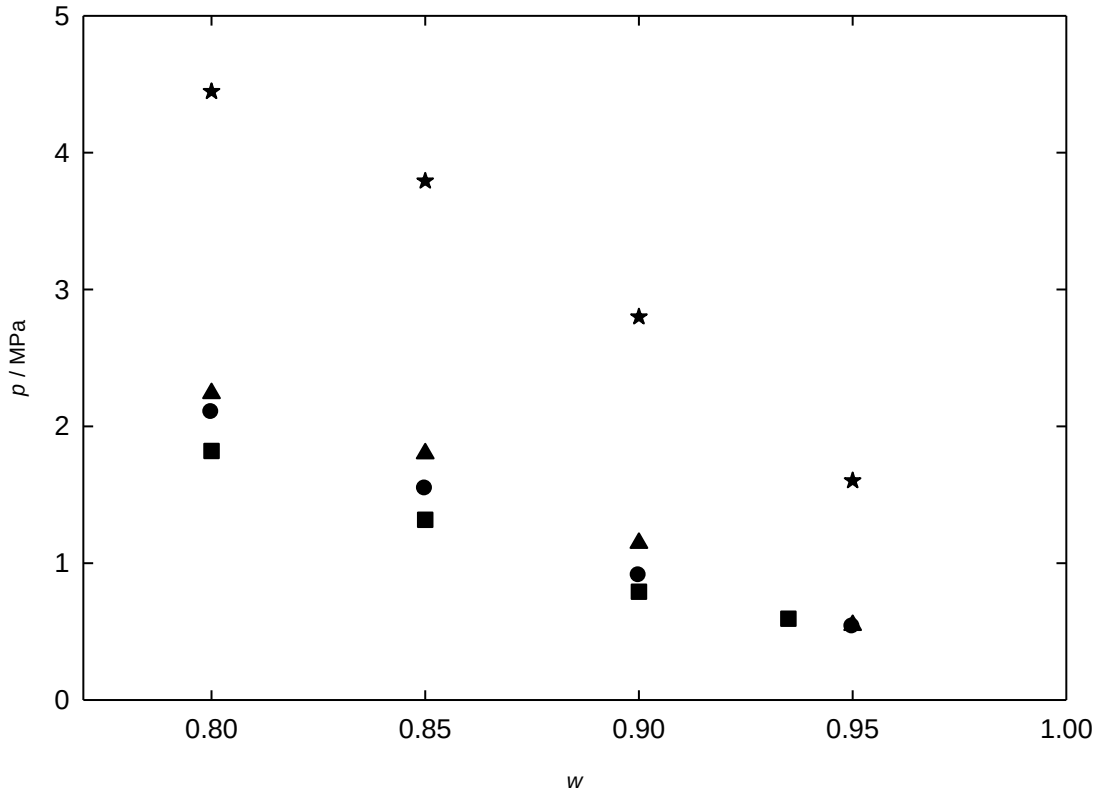

Figure 12. Comparison of the phase behavior of CO_2 in oligomers on the solvent rich side, determined at 298.15 K; ● PEGDME 250; ■ PPGDME 230; ★ PFPE 960; ▲ PDMS 237.

The bubble point curves in Figure 11 are bound by the vapor pressure of CO_2 and by the vapor pressure of the oligomer, which is too low to measure accurately in our experimental apparatus (the apparatus has a lower limit of 0.25 MPa). At pressures above the bubble point loci a single homogeneous liquid phase is reached. Upon depressurization at a given concentration a bubble forms and two phases are present, a less dense CO_2 rich vapor phase and more dense solvent rich liquid phase. The right hand side of the phase behavior diagram shown in Figure 12 (the solvent-rich end) is of particular interest for the CO_2 absorption process. The bubble point pressures for the PPGDME-CO_2, PDMS-CO_2, and PEGDME-CO_2 systems are comparable (within 0.5 MPa) for solvent weight fractions above 0.65. In contrast, much higher pressures (roughly twice that of the other solvents) had to be used in the PFPE-CO_2 system in order to obtain a single homogeneous phase over this same composition range. This result was somewhat unexpected because relatively high molecular weight PFPE oligomers are known to be more CO_2-soluble than PPG carbohydrate oligomers of comparable size.(32)(33)

A closer examination of the composition range of 0.8 – 1.0 solvent weight fraction (0.0 – 0.2 weight fraction of CO_2), PPGDME requires slightly lower pressures to dissolve a specified amount of CO_2 than PEGDME or PDMS. We note that the PPGDME and PEGDME oligomers are terminated with methyl ether groups, rather than hydroxyls, because hydroxyl groups are CO_2-phobic moieties that reduce the solubility of CO_2 in a solvent, while the oxygen of the methyl ether group promotes solubility by providing an additional site for Lewis acid:Lewis base interactions with CO_2.(13)(18)

The ranking of the CO_2-philic nature of these oligomers given above is on a *weight basis*. It is interesting to view the solubility on the basis of the number of moles of repeat units, instead of a weight basis in an effort to eliminate any potential bias caused by comparing solvents on a

weight basis that are different in chain length. This is especially true with the PEG monomer being compared to the PPG monomer where both monomers only differ in a branched methyl group however, the PEG solvent used is on average more than a full repeat unit longer than the PPG oligomer used. The experimental data, as a function of the number of moles of repeat units, are presented in Figure 13. It can be seen that PDMS is clearly the most CO_2-philic solvent on a per repeat units basis, followed by PPGDME, PEGDME, and then PFPE. This means that the repeat unit in PDMS, containing silicon, oxygen and two methyl groups, is the most CO_2-philic monomer of the oligomers tested. Interestingly enough, the poor performance of the PFPE solvent persists. It was far outperformed by the other three solvents when compared on a weight basis and when compared on a molar percent basis the same result precipitates. This is contrary to literature, (88) which found that long chain PFPE polymers outperform hydrocarbon counterparts of similar chain length.

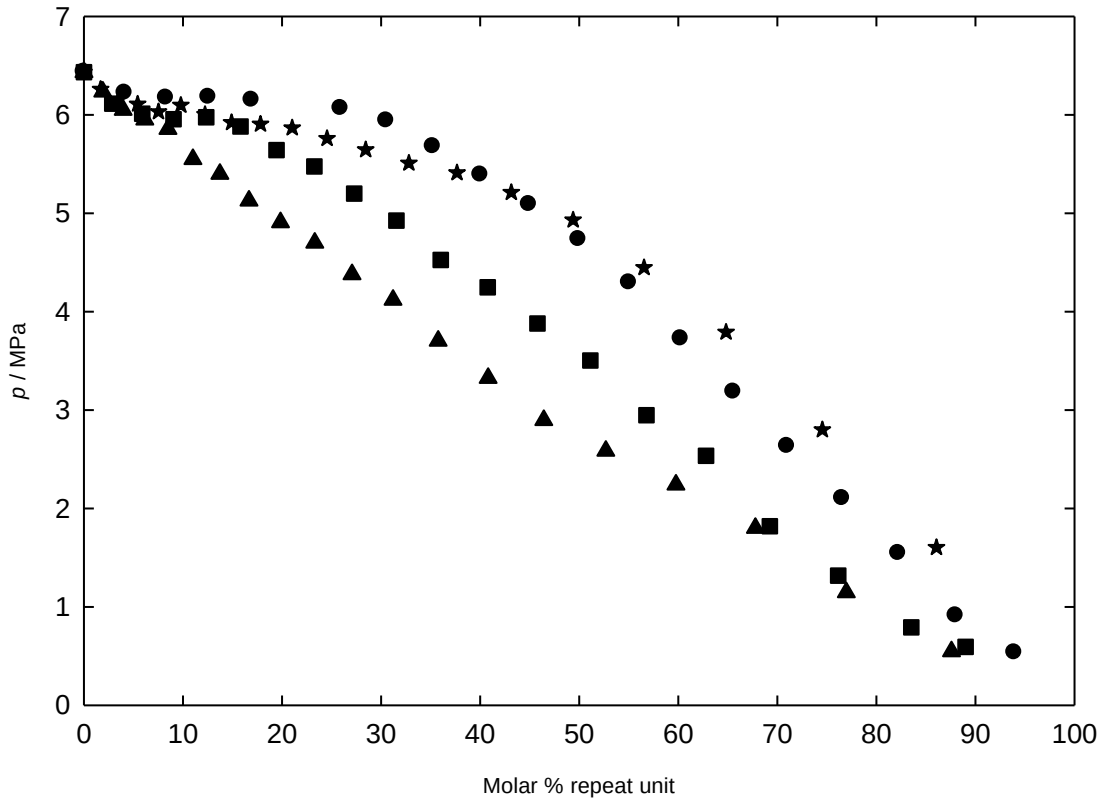

Figure 13. Comparison of the solubility of CO_2 in oligomers with respect to the repeat unit of each oligomer; ● PEGDME 250; ■ PPGDME 230; ★ PFPE 960; ▲ PDMS 237.

The bubble point loci for the pseudo-binary systems of PPGDME400-CO_2, PEGDME310-CO_2, PPGDAc509-CO_2, PTMEGDAc250-CO_2, PBGDAc250-CO_2, Selexol^{TM}-CO_2, PDMS550-CO_2, and the binary system GTA-CO_2 are reported on the solvent-rich end (0.6-1.0 weight fraction of oligomer, *w*) at 298 K (Figure 14) and 313 K (Figure 15). Above the bubble point pressure is a single homogeneous phase while below the bubble point there are two phases present, the less dense vapor phase made up of virtually only CO_2, and the more dense oligomer rich phase still containing dissolved CO_2. Each bubble point was reproduced six times, which resulted in ±0.07 MPa measurement variability. This degree of uncertainty is reflected by the size of the data markers in the figures. Each bubble point locus is bounded at the pure solvent end, *w* = 1.0, of the Px diagram by the vapor pressure of the solvent. These pressures are too low to be measured precisely using our equipment. The perfluoropolyether (PFPE, n = 5.0) results shown in Figure 14 are reproduced from above.

Figure 14 (298 K) illustrates that the solubilities of CO_2 in PEGDME, PPGDME, PDMS, PTMEGDAc, PBGDAc, and GTA are comparable. The greatest difference in the bubble point loci for any of these systems at any composition is only ~ 0.41 MPa for the range of *w* shown. The Selexol^{TM} solvent required similar pressures as compared to these solvents in order to dissolve the same amount of CO_2 on a weight basis. The PPGDAc and PFPE solvents yielded the lowest CO_2 solubility on a weight basis, requiring roughly 0.34 MPa to 0.69 MPa more than the PPGDME, PEGDME, PDMS, PTMEGDAc, PBGDAc and GTA to dissolve the same amount of CO_2. The poor PFPE performance is attributable in part to the results being presented on a weight fraction of interest to engineering design, which favors oligomers with low molecular weight monomers.

The bubble point loci results at 313 K are illustrated in Figure 15. Due to the poor performance at 298 K and great expense of the PFPE solvent, it was not assessed at 313 K. As expected, the increase in temperature decreases the solubility of CO_2 in all the solvents; therefore the bubble point pressures have shifted to higher values for any particular concentration of the solvent. GTA appears to be the best solvent at this temperature, although it must be kept in mind that this is clearly the most volatile of the solvents being considered (normal boiling point 453 K). The oligomeric solvents Selexol^{TM}, PPGDME, PEGDME, PDMS, PBGDAc, and PTMEGDAc give very similar CO_2 solubility results over the composition range. PPGDAc again exhibited the lowest CO_2 solubility as presented.

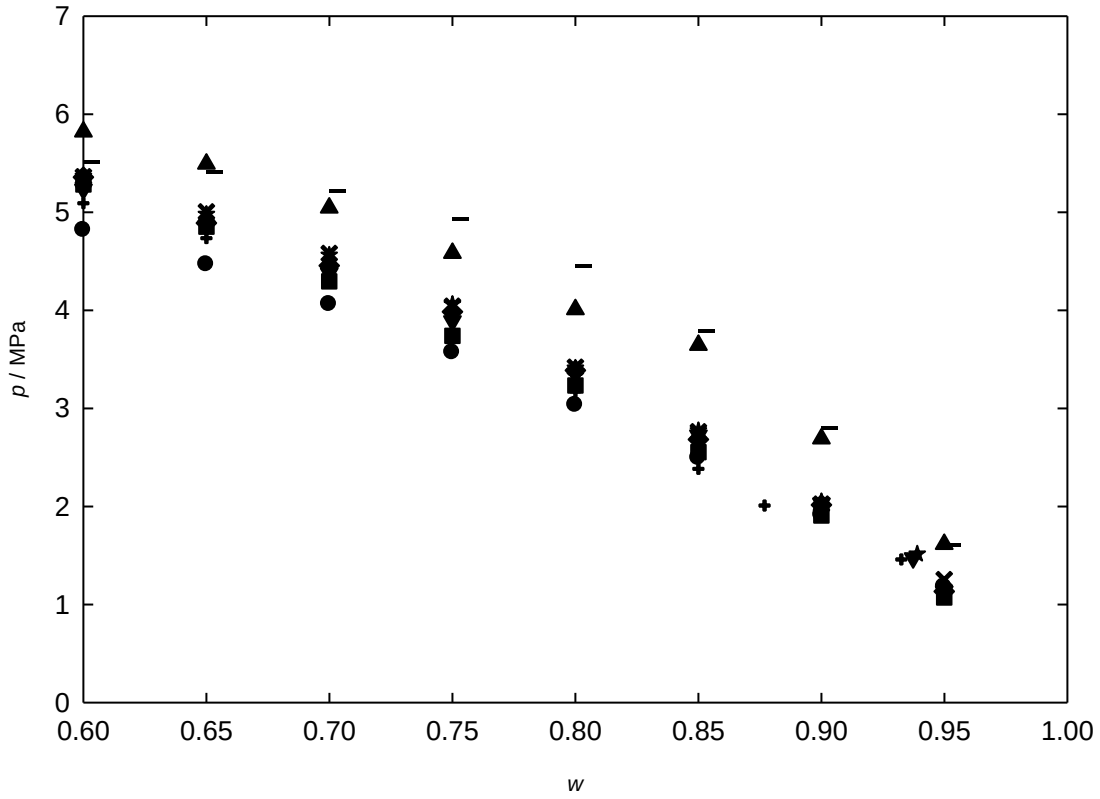

Figure 14. Phase behavior bubble point loci for hexamer solvents tested at 298 K; ◆ PEGDME; ■ PPGDME; ▲ PPGDAc; × PBGDAc; ★ PTMEGDAc; ● GTA; + PDMS; – PFPE; ▼ Selexol.

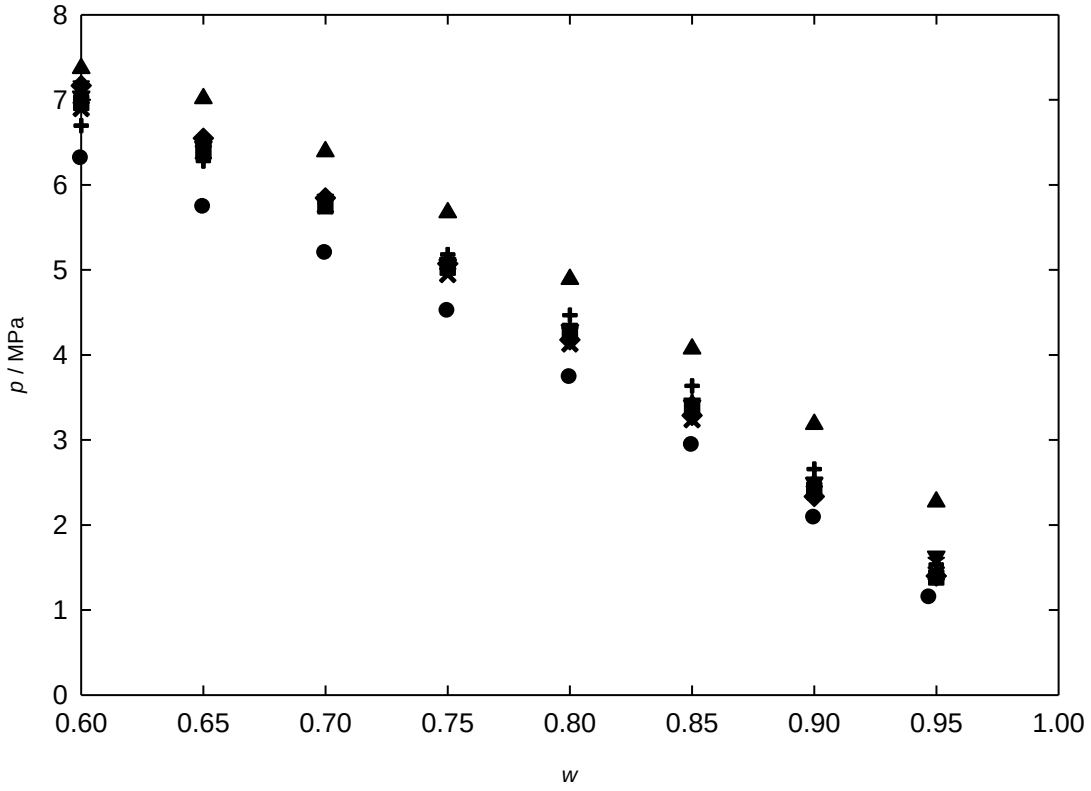

Figure 15. Phase behavior bubble point loci for hexamer solvents tested at 313 K; ◆ PEGDME; ■ PPGDME; ▲ PPGDAc; × PBGDAc; ★ PTMEGDAc; ● GTA; + PDMS; ▼ Selexol.

4.3 VISCOSITY OF OLIGOMERS

4.3.1 Neat solvent viscosity measurements

Neat solvent viscosity measurements were carried out for the higher molecular weight oligomers referred to as hexamers (not PPGDME 230, PEGDME 250 or PDMS 237) using a Brookfield LVDV-II+Pro viscometer with cone spindle CPE-40, capable of measuring viscosities of 0.15 cP to 3,065 cP with a temperature range of 273 K to 473 K and also has temperature ramping capabilities. A Brookfield TC-602 temperature controller with ethylene glycol as the heating/cooling fluid was used in order to maintain the temperature of the sample cup during each experiment.

Each absorbent was tested at three separate shear rates and at two different temperatures; the ambient temperature in the laboratory, 295 K, and 313 K. In each experiment the viscometer was zeroed, and 0.5 mL of the solvent, measured using a Fisherbrand Finnpipette in order to ensure precision and repeatability, was placed in the sample cup. Then the sample cup was attached to the viscometer, and the gap between the cup and spindle was set using the micrometer adjustment ring. Shear rates were then chosen across the viscometer's range in an effort to capture any non-Newtonian behavior. The viscosity of each solvent is an important metric in its potential implementation. In the case of liquid solvents the smaller the viscosity the more mobile the solvent will be from the gas absorber to the flash chambers, via pumping, used for regeneration. In general, the smaller the viscosity of the solvent the better so long as the vapor pressure remains significantly low, as to avoid substantial solvent evaporative losses.

4.3.2 Viscosity comparison of each hexamer and Selexol™

Viscosity is an important property in solvent selection because low viscosity will reduce pumping costs and mass transfer resistances during CO_2 absorption. The viscosity of each solvent was measured at two temperatures, 295 K and 313 K at various shear rates which were determined based on the viscometer's accuracy capability which is a function of the viscosity of each solvent and the shear rate. Lower solvent viscosity leads to an increased range of shear rates, higher viscosity leads to a decreased range of shear rates. The data are illustrated in Figures 16 and 17.

At both temperatures the PDMS has substantially lower viscosity than all other solvents tested with a viscosity of less than 3 cP at both temperatures. The solvents with the next lowest viscosity of approximately 6 cP include PPGDME and Selexol™, and PEGDME that has a viscosity of approximately 8 cP. PBGDAc, GTA, PTMEGDAc, and PPGDAc have higher viscosity values of about 17 cP, 18 cP, 20 cP, and 30 cP, respectively. Upon increasing the temperature to 313 K, the viscosities all decreased as expected, but their ranking was maintained with the exception of the viscosity of GTA decreasing to be slightly less than the viscosity of PBGDAc.

The effect of small amounts of dissolved water on solvent viscosity has been measured for several solvents. For example, 1wt% water was added to Selexol™ and PBGDAc (PDMS is immiscible with water, therefore it was not selected.). The PBGDAc viscosity value decreased from 17 cP to 15 cP, while the change in the Selexol™ viscosity of 6.9 cP was not detectable. Further, upon absorption of CO_2 at elevated pressure, the solvent-CO_2 solution viscosity will diminish, as has been shown in the literature in polymer-CO_2 mixtures. (89) (90) (91) (92) For

example, the viscosity of PDMS saturated with CO_2 at 353 K and 8.69 MPa (8.8 wt% CO_2) was 50% lower than that of neat PDMS at low shear rates. (89)

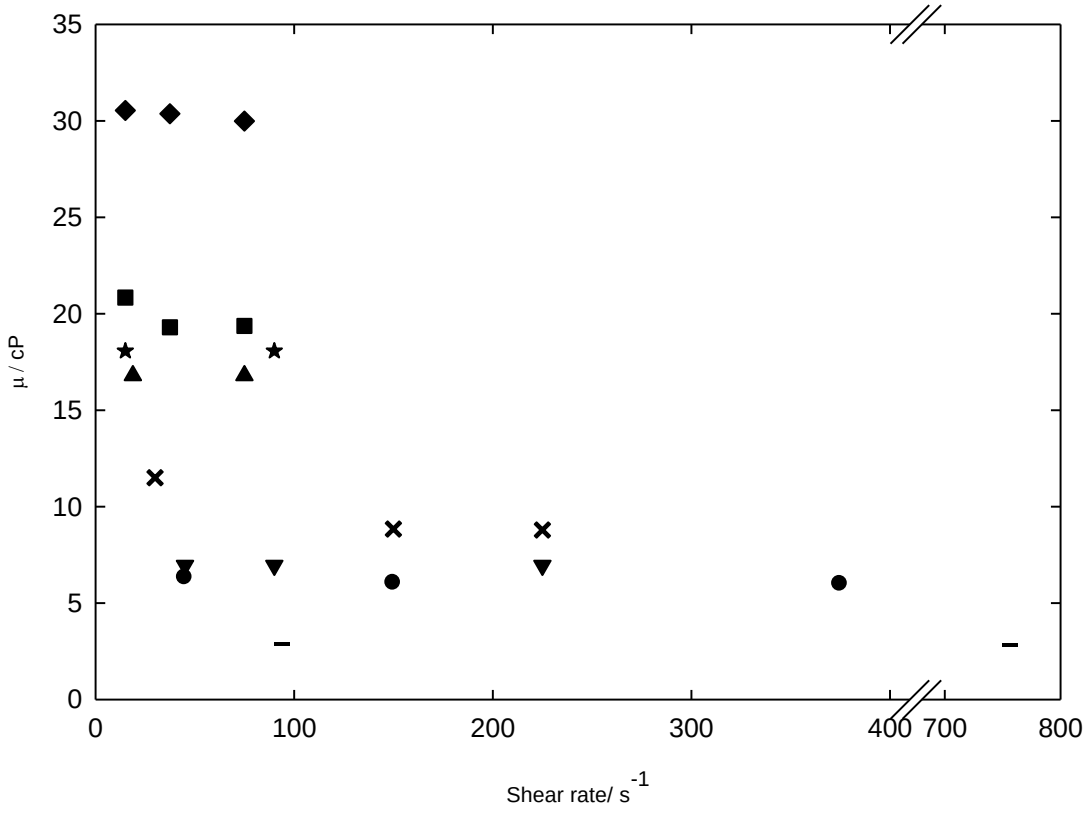

Figure 16. Viscosity of each hexamer at 295 K listed in order of lowest viscosity to highest: ▬ PDMS; ● PPGDME; ▼ Selexol; ✕ PEGDME; ▲ PBGDAc; ★ GTA; ■ PTMEGDAc; ◆ PPGDAc.

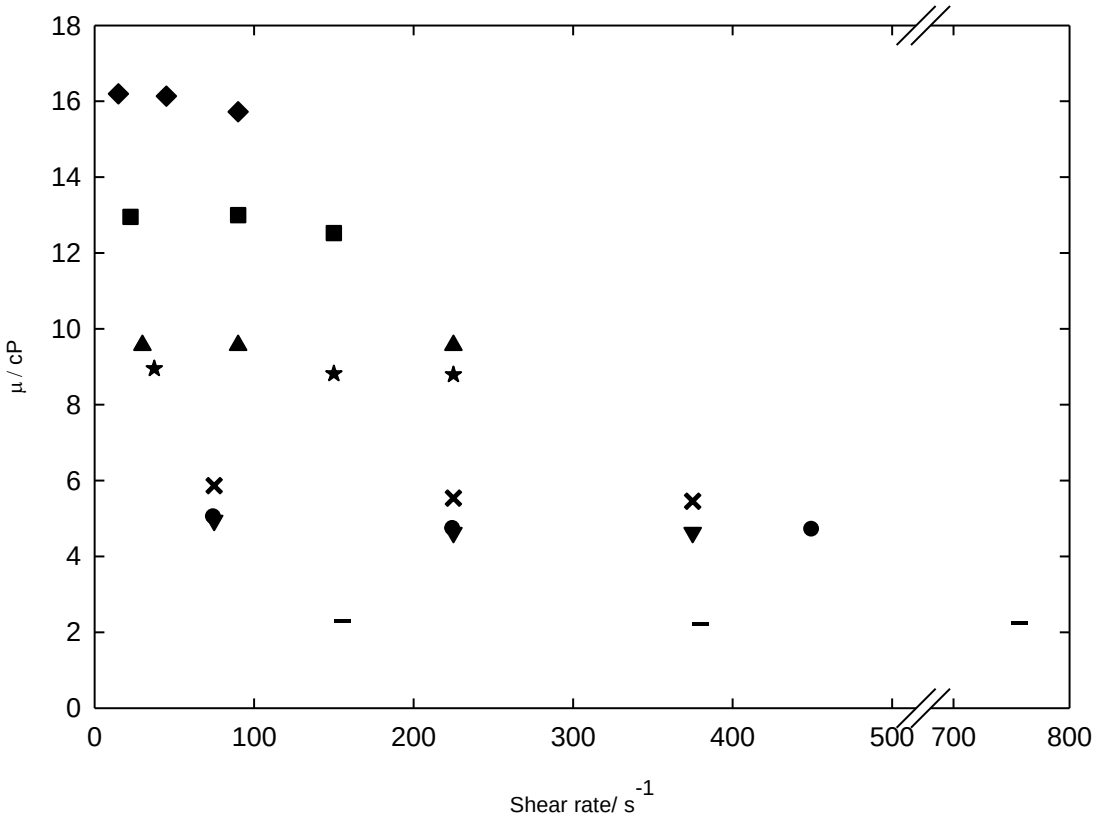

Figure 17. Viscosity of each hexamer at 313 K listed in order of lowest viscosity to highest: : ▬ PDMS; ● PPGDME; ▼ Selexol; ✕ PEGDME; ★ GTA; ▲ PBGDAc; ■ PTMEGDAc; ◆ PPGDAc.

4.4 SOLUBILITY OF WATER IN NEAT SOLVENT

4.4.1 Neat solvent-water cloud point measurement procedure

The solubility of water in each hexamer was also assessed at 295 K and 313 K by slowly adding water to the solvent until a cloud point, indicative of the presence of a small aqueous phase in equilibrium with the solvent, was observed. The hydrophilic nature of each solvent was tested because the mixed gas stream that contains the CO_2 from an IGCC power plant contains various amounts of water and if the water is also absorbed then the TSD step could become very costly due to the specific heat of water. In a typical experiment 10 grams of the solvent was placed in a beaker and distilled water was added to the solvent drop-wise until a cloud point was observed. The temperature of the beaker was controlled with a water bath and heating plate, and mixing was ensured with a magnetic stirbar and stirplate.

4.4.2 Solubility of water in each solvent

The solubility of water in the solvents examined at 295 K and 313 K is shown in Table 2. The PEGDME and Selexol^{TM} are fully miscible with water at all concentrations. This is not ideal because of the presence of water in the mixed gas stream and in order to remove it the solvent would have to go through an energy consuming TSD step in addition to the necessary PSD step. The solubility of water in the other solvents was dramatically lower. PDMS is completely immiscible with water. The solubility of water in PPGDME, PPGDAc, and PTMEGDAc was roughly 2 wt%. The GTA absorbed about 5 wt% water. The ranking of the

oligomers from the greatest to least capability to absorb water is: Selexol^{TM} ~ PEGDME >> GTA > PPGDME ~ PPGdiacetate ~ PBGDAc ~ PTMEGDAc >> PDMS.

Table 2. Bench top water miscibility in solvents, test results at 295 K and 313 K.

Solvent	**Miscibility (g H_2O/g solvent)**	
	295 K	313 K
PDMS	Immiscible	Immiscible
PTMEGDAc	0.017	0.024
PBGDAc	0.018	0.031
PPGDAc	0.022	0.025
PPGDME	0.021	0.028
GTA	0.046	0.062
PEGDME	Fully miscible	Fully miscible
SELEXOL^{TM}	Fully miscible	Fully miscible

4.5 CONCLUSIONS

Oligomeric solvents, including PPGDME, PEGDME, PPGDAc, PTMEGDAc, PBGDAc, PDMS, PFPE, and GTA, have been examined as potential CO_2 absorbents to be implemented in physical absorption processes. With the exception of PEGDME, these solvents have not been previously assessed as CO_2 solvents. In this work, they have been judged based upon three important properties of a physical solvent used for CO_2 capture: solubility of CO_2 in the solvent over a wide range of pressure, solubility of water in the solvent, and neat solvent viscosity.

Phase behavior plots on the solvent-rich end have been constructed illustrating that the Selexol^{TM} solvent's ability to absorb CO_2 is comparable to that of PEGDME, PDMS, PPGDME,

PBGDAc, PTMEGDAc and GTA at 313 K. PPGDAc exhibited much lower solubility than these solvents.

Viscosity testing showed that PDMS and PPGDME have lower viscosities than PEGDME and Selexol^{TM}, which leads to reduced mass transfer resistances and pumping requirements if these solvents are employed. The remaining solvents, PPGDAc, PTMEGDAc, PBGDAc, and GTA, had viscosity values greater than that of Selexol^{TM}.

The ability of the solvents to absorb water differed dramatically at 295 K and 313 K. Selexol^{TM} and PEGDME are fully miscible with water at all proportions, PPGDME, PPGDAc, PBGDAc and PTMEGDAc absorb only 1-3 wt% water, GTA absorbed 4-6 wt% water, and PDMS is completely immiscible with water.

These properties suggest that PDMS and PPGDME may be very viable CO_2 solvents for the IGCC process. Relative to Selexol^{TM} or PEGDME, PDMS exhibited comparable CO_2 absorption, lower viscosity, and complete immiscibility with water. Relative to Selexol^{TM} or PEGDME, PPGDME exhibited comparable CO_2 absorption, comparable viscosity, and dramatically greater hydrophobicity (only 2-3 wt% water dissolves in PPGDME at 295 K to 313 K).

5.0 CO_2 SOLUBILITY IN VOLATILE ORGANIC SOLVENTS

5.1 MATERIALS

The compounds 1,4-dioxane (anhydrous, mass purity of 0.998), 2-(2-butoxyethoxy)ethyl acetate (mass purity of 0.99), 1-nitropropane (mass purity of ≥0.985), 2-nitropropane (mass purity of 0.96), *N*,*N*-dimethylacetamide (mass purity of ≥0.995), acetylacetone (mass purity of ≥0.99), 2-methoxyethyl acetate (mass purity of 0.98), and *N*-*tert*-butylformamide (mass purity of 0.98), were purchased from Sigma Aldrich and used as received. The other compounds, methyl acetate (mass purity of 0.99, and mass purity of water <0.00005), 2-butoxyethyl acetate (mass purity of 0.98), and acetone (mass purity of 0.996), were purchased from Acros Organics through Fisher Scientific and were used as received. The structure, molar mass, and normal boiling point of each solvent discussed, including those examined in this work as well as industrial solvents, are shown in Table 3. CO_2 was purchased from Penn Oxygen and Supply Company with a mass purity of 0.9999 and used without further purification.

5.2 PHASE BEHAVIOR OF CO_2 IN VOLATILE ORGANICS

5.2.1 Experimental apparatus

Phase behavior bubble point loci were generated for these binary mixtures using the same high pressure, variable volume apparatus described for the oligomer-CO_2 pseudo-binary phase behavior construction illustrated in Figures 9 and 10. In a given experiment 25 g to 60 g of solvent is placed in the Pyrex tube and the sample volume is then reduced by pumping in overburden fluid which raises the piston. Then CO_2 is passed through the left over space to vent out all air. After that, known amounts of CO_2 are isothermally and isobarically injected into the sample volume using the dual pump by pumping in CO_2 while simultaneously extracting overburden fluid. Once a desired concentration is reached the sample volume is repeatedly and slowly compressed and then allowed to equilibrate until the single phase solution is attained. The bubble point pressure during compression corresponds to the point at which the last tiny bubble of gas remains in equilibrium with the liquid; further compression will yield a single phase solution. The raw bubble point data corresponds to the pressure of the overburden fluid at this point. All of the raw bubble point data were then corrected by subtracting the small pressure drop required to overcome the frictional resistance of the O-ring around the floating piston as it maintains the seal between the sample volume and the overburden fluid as it slides along the inner surface of the hollow Pyrex tube. Therefore the bubble point pressure data of the overburden fluid obtained during compression corresponds to the sum of the bubble point pressure of the sample and the pressure drop required to displace the piston. This pressure drop was determined to be 0.20 MPa by comparing our experimental bubble point pressures for pure CO_2 with the CO_2 bubble point values listed in the NIST webbook for temperatures between 290

K and 306 K. All experiments were performed at 298.15 K and solvent mass fractions of at least 0.60. The apparatus used has an experimental pressure limitation of 0.2 MPa to 69.0 MPa (accuracy is ±0.07 MPa) and therefore is not used to measure the pure solvent vapor pressures.

5.2.2 Phase behavior results

The phase behavior at 298.15 K for the binary systems of CO_2 and all 15 solvents shown in Table 3 has been presented in the form of bubble point measurements at the solvent-rich end of the phase behavior diagram on a weight basis in Figure 18. Much of the results discussed in this chapter have been published here. (93) At pressures above the bubble point pressure a single homogenous liquid phase exists. Upon reaching the bubble point two phases become present, one less dense CO_2 rich vapor phase and a more dense solvent rich liquid phase. Also illustrated in Figure 18 are the bubble point loci of acetone and 1,4-dioxane generated in this work compared to literature data which shows good agreement falling within the experimental error. All bubble point measurements represent the average of six individual measurements with an uncertainty of ±0.07 MPa, as reflected by the size of the data markers in each Px diagram. Table 3 presents the relative rank of the ability to absorb CO_2 on a mass and molar basis according to experimentally determined phase behavior.

Table 3. Solvent structures, molar mass, and normal boiling point as given by the supplier, and relative CO_2 solubility rankings on a weight and molar basis according to experimental results and COSMOtherm predictions.

Solvent * This work # Literature reference	Structure	*Mw* (g/mol)	*T*(P=101.325 kPa, K)	Solvent strength on weight basis (exp)	(calc)	Solvent strength on molar basis (exp)	(calc)
acetone*	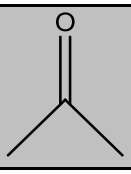	58.08	329	1	1	5	7
methyl acetate*	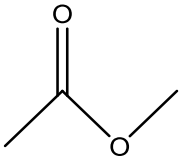	74.08	330	2	3	2	9
1,4-dioxane*	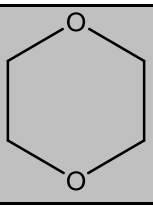	88.11	373	3	4	4	6
methanol	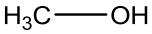	32.04	338	4	8	15	15
2-methoxy ethyl acetate*	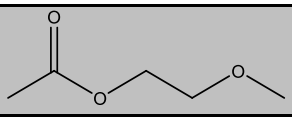	118.13	418	5	6	3	5
2-nitro propane*	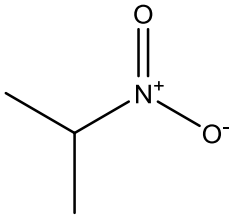	89.09	393	6	10	7	12
N,*N*-dimethyl acetamide*	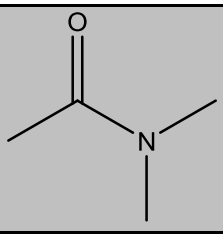	87.12	439	7	2	8	2
acetyl acetone*	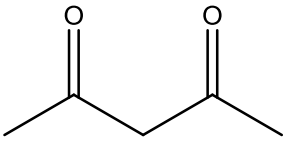	100.12	414	8	7	6	8
1-nitro propane*	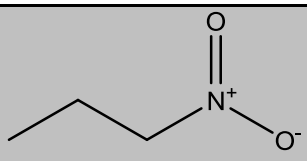	89.09	404	9	9	10	11

Table 3. (continued)

isooctane	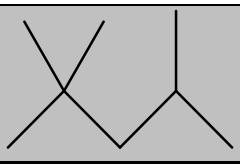	114.23	371	10	15	9	13
2-(2-butoxy ethoxy) ethyl acetate*	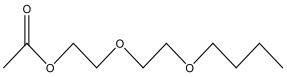	204.26	518	11	12	1	1
N-formyl morpholine	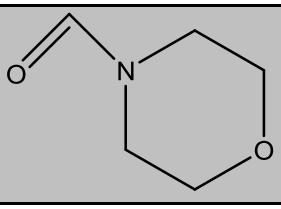	115.13	509	12	5	12	4
propylene carbonate	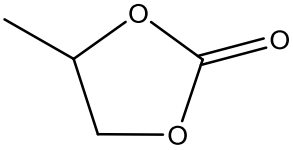	102.09	513	13	13	13	14
2-butoxyethyl acetate*	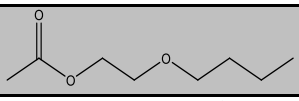	160.21	465	14	14	11	3
N-tert-butyl formamide*	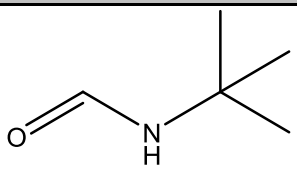	101.15	475	15	11	14	10

On a weight basis, as shown in Figure 18, acetone exhibits the greatest ability to absorb CO_2 due to its low molar mass (58.08 g/mol) and inclusion of a CO_2-philic carbonyl group. The volatility of acetone (bp 329.15 K), which could result in significant evaporative losses and flammability concerns, is the likely reason that acetone has not been used as a commercial CO_2 solvent. Methyl acetate (bp 330 K) requires only slightly higher pressures than acetone to dissolve a specified amount of CO_2. Although its molar mass (74.08 g/mol) is greater than that of acetone, methyl acetate contains two CO_2-philic oxygen atoms in the ether and carbonyl functionalities that enhance its solvent strength. The next best solvent, 1-4,dioxane (bp 373 K) has a slightly greater molar mass (88.11 g/mol) and also contains two CO_2-philic ether oxygen atoms in its six-member ring structure. The bubble point data for methanol (bp 337.85 K) and 1,4-dioxane are comparable. Although the hydroxyl group is a CO_2-phobic moiety, methanol's very low molar mass (32.04 g/mol) favors high solubility values on a weight basis. The next best solvent, 2-methoxyethyl acetate (118 g/mol, bp 418 K), has a significantly higher molar mass and is substantially less volatile than acetone, methyl acetate, 1,4-dixoane, and methanol. The presence of two ether oxygens and a carbonyl oxygen in 2-methoxyethyl acetate accounts for its ability to be a relatively good solvent.

The remaining solvents, in order of descending solvent strength on a mass basis, are 2-nitropropane, *N*,*N*-dimethylacetamide, acetylacetone, 1-nitropropane, isooctane, 2-(2-butoxyethoxy)ethyl acetate, *N*-formylmorpholine, propylene carbonate, 2-butoxyethyl acetate, and *N*-*tert*-butylformamide. The nitro, secondary amine and tertiary amine groups associated with the nitrogen atoms in 2-nitropropane, *N*,*N*-dimethylacetamide, 1-nitropropane, *N*-formylmorpholine, and *N*-*tert*-butylformamide apparently are not as CO_2-philic as the ether and carbonyl oxygen atoms associated with the best solvents. Although isooctane has comparable

molar mass (114.23 g/mol) and boiling point (371 K to 372 K) to 1,4-dioxane, it does not contain any CO_2-philic oxygen atoms and is therefore a poorer solvent. Propylene carbonate is a low molar mass solvent that contains three oxygen atoms, however the carbonate functionality has been previously shown to be less CO_2-philic than oxygens found in ether, carbonyl and acetate groups and that trend continues in this work. (29) (93) Finally, the terminal butyl group of 2-(2-butoxyethoxy)ethyl acetate and 2-butoxyethyl acetate diminish the solvent strength of these compounds relative to their methyl-terminated lower molar mass analog, 2-methoxyethyl acetate.

Bubble point loci shown in Figure 19 depict the CO_2 solubility data on a molar basis, and the relative rank of each compound's solvent strength on a molar basis is presented in Table 3. When compared on a molar basis, the six best solvents, in descending order of solvent strength, are 2-(2-butoxyethoxy)ethyl acetate, methyl acetate, 2-methoxyethyl acetate, 1,4-dioxane, acetone and acetylacetone. Five of these six possess multiple ether and/or carbonyl oxygen atoms, with the only exception being acetone, which has only one carbonyl group. The worst solvent when measured on a molar basis is methanol, a very low molar mass solvent (which favors its ranking on a mass basis) which possesses a CO_2-phobic hydroxyl group.

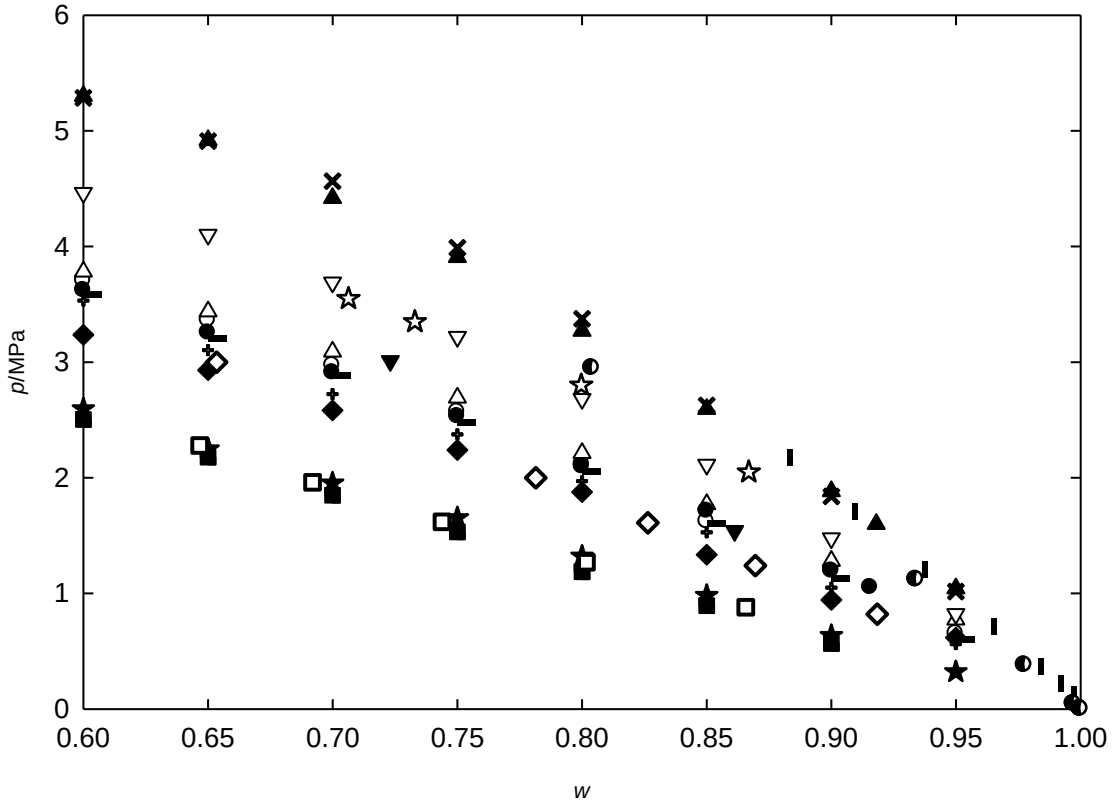

Figure 18. . Solubility of CO_2 in all volatile solvents presented in mass fraction of solvents, w, listed in order of solvent strength from best to worst: ■ acetone (this work); □ acetone (95); ★ methyl acetate; ◆ 1,4-dioxane (this work); ◇ 1,4-dioxane (75); ▼ methanol (62); ✤ 2-methoxyethyl acetate; ━ 2-nitropropane; ○ *N*,*N*-dimethylacetamide; ● acetylacetone; △ 1-nitropropane; ☆ isooctane (61); ▽ 2-(2-butoxyethoxy)ethyl acetate; ◐ *N*-formylmorpholine (96); ❙ propylene carbonate (60); ▲ 2-butoxyethyl acetate; ✕ *N*-*tert*-butylformamide.

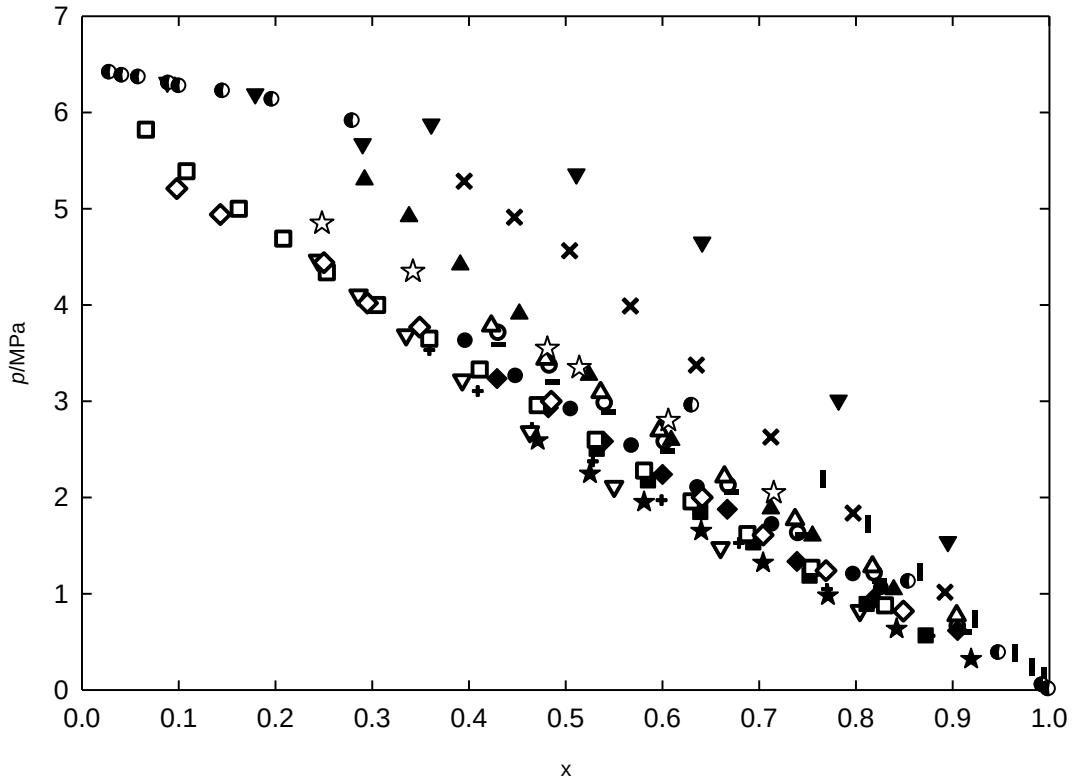

Figure 19. Phase behavior of volatile solvents on a molar basis listed in order of solvent strength from best to worst: ▽ 2-(2-butoxyethoxy)ethyl acetate; ★ methyl acetate; ✚ 2-methoxyethyl acetate; ◆ 1,4-dioxane (this work); ◇ 1,4-dioxane (75); ■ acetone (this work); □ acetone (95); ● acetylacetone; ▬ 2-nitropropane; ○ *N*,*N*-dimethylacetamide; ☆ isooctane (61); △ 1-nitropropane; ▲ 2-butoxeythyl acetate; ◑ *N*-formylmorpholine (96); ❙ propylene carbonate (60); ✖ *N*-*tert*-butylformamide; ▼ methanol (62).

5.2.3 A priori calculation of phase behavior via COSMOtherm

A vital part of this work was conducted in conjunction with Dr. De-Li Chen using the Conductor-like Screening Model for Real Solvents (COSMO-RS), referred to as COSMOtherm, and developed by Klamt et al. (96) (97) COSMOtherm is based on unimolecular quantum chemical calculations of individual species and is widely used to predict thermodynamic properties of fluids. (98) (99) (100) In this work it is used to predict the solubility of CO_2 in these various volatile solvents through the construction of binary phase behavior diagrams. COSMOtherm was chosen because it is capable of qualitatively, and to some degree, quantitatively capturing intermolecular interactions such as hydrogen bonding and Lewis acid:base interactions. This has been shown by Freire et al. (101) (102) where COSMOtherm was used to predict liquid-liquid equilibria of mixtures of water and various ionic liquids and alcohols and various ionic liquids. Ouni et al. used COSMOtherm to predict the vapor-liquid equilibria for 2-methylpropane with various short chain alcohols. (103) Finally, Schroder et al. were able to predict the aqueous solubilities of solid carboxylic acids with COSMOtherm. (104) In this study COSMOtherm was used as a screening tool in order to determine whether or not some volatile organics could be used as CO_2-philic solvents and whether or not they should be examined experimentally. The calculated bubble point data of the 15 solvents that were chosen will be compared with experimental results in an attempt to determine if COSMOtherm can be used to qualitatively rank the solvent strength of small, volatile, organic solvents.

5.2.4 Computational methods for COSMOtherm

The standard procedure for COSMO-RS calculations consists of two steps. Quantum chemical calculations are performed in the first step for all molecules in the system. The density function theory (DFT) based functional, B88-PW86,(106)(107) together with a triple zeta valence polarized basis set (TZVP)(108) and the RI approximation(109) is used throughout this study. The continuum solvation model COSMO is used in these calculations in order to simulate a virtual conductor environment for the molecules. During the quantum chemical self-consistency algorithm the solute molecule is converged to its energetically optimal state in a conductor with respect to electron density and geometry. The output of these calculations is the so-called σ-profile, or polarization charge density.(110)(111) All DFT/COSMO-RS calculations were performed using the quantum chemical program TURBOMOLE.(112)

In the second step of COSMO-RS calculations the σ-profiles are used to quantify the interaction energy of pair-wise interacting surface segments with regards to the most important molecular interaction modes such as electrostatics and hydrogen bonding. All COSMO-RS calculations were implemented with the COSMOtherm program,(113) which offers an efficient implementation of the COSMO-RS method. The BP_TZVP_C21_0107 parameterization(113) was adopted in this work. The CO_2 vapor pressure value of 6.43 MPa(114) at 298.15 K was used as the only experimental input parameter in the COSMOtherm calculations. The model was not adjusted in any manner to fit the bubble point results for the binary mixtures.

5.2.5 Assessment of calculated phase behavior

The bubble point curves have been computed by COSMOtherm for all compounds listed in Table 3 at 298.15 K. The computed data were used to determine the relative rank of each solvent near a solvent mass fraction of 0.80. Table 3 presents the relative rank of each solvent on a weight and molar basis based on the bubble point loci generated by COSMOtherm predictions. A numerical analysis of the predicted bubble point loci was performed by calculating the average absolute deviation (AAD) and average absolute percent deviation (AAPD) and can be seen in Table 4.

A comparison of the COSMOtherm ranking of the solvent strength to the ranking based on experimental results, seen in Table 3, indicates that COSMOtherm is not able to correctly rank all the solvents. If the focus is shifted solely to oxygenated hydrocarbons with oxygen atoms in CO_2-philic functionalities (e.g. carbonyl, acetate, ether, carbonate), however, COSMOtherm performs very well, correctly predicting the order of solvent strength as acetone, methyl acetate, 1,4-dioxane, 2-methoxyethyl acetate, acetylacetone, 2-(2-butoxyethoxy)ethyl acetate, propylene carbonate, and 2-butoxyethyl acetate. The only oxygenated hydrocarbon whose relative solvent strength was incorrect was methanol, which contains a CO_2-phobic hydroxyl group. Figure 20 gives comparison on a weight basis of each of the oxygenated hydrocarbons bubble point loci determined experimentally and predicted by COSMOtherm. Overall, COSMOtherm under predicts the bubble point pressures, or alternatively, it over predicts the CO_2 solubility in each solvent, but is still able to accurately predict the relative solvent strength.

Quantitatively, COSMOtherm suffers from drawbacks. Firstly, the solubilities of CO_2 in each solvent compared to one another are incorrect thus making the overall ranking of solvents

incorrect both on a weight and molar basis. Presented in Table 4 are the average absolute deviation (AAD) and average absolute percent deviation (AAPD) calculated via equations 1 and 2, respectively:

$$AAD = \frac{1}{N}\sum_{i=1}^{N}\left|P_i^{exp} - P_i^{calc}\right| \quad (1)$$

$$AAPD = \frac{1}{N}\sum_{i=1}^{N}\frac{\left|P_i^{exp} - P_i^{calc}\right|}{P_i^{exp}} \times 100\% \quad (2)$$

where P_i^{exp} and P_i^{calc} are the pressures at a given concentration determined experimentally or calculated, respectively, and N is the number of data points. The results of the AAD and AAPD calculation for each solvent, over the composition ranges shown in Figures 18-19, indicates the most accurately predicted solvent is methyl acetate with an AAD of 0.13 MPa and an AAPD of 12.48 %. Other solvents that were reasonably well predicted include methanol, isooctane, 1,4-dioxane, acetone, 2-methoxyethyl acetate and 2-nitropropane, all having AADs around 0.49 MPa and AAPDs ranging from 10.73 % to 27.89 %. Overall the better predicted solvents are those that have smaller molecular weights and are made up of only C, H, and O. The solvents that were in poorest agreement with calculations were 2-butoxyethyl acetate, n-tert-butylformamide, and n,n-dimethylacetamide with AAD values of 1.38 MPa, 1.56 MPa, and 1.24 MPa, respectively and AAPD values of 40.39 %, 45.53 %, and 54.02 %, respectively. The poorest predictions involved the larger compounds that also had N or N^+ as a part of the compound's makeup. This lack of accuracy is also reflected in the relative ranking for the compounds that contain nitrogen groups such as nitro, amide, and secondary or tertiary amines as they were unsuccessfully predicted with the COSMO-RS approach. This was seen especially in predictions for *N*,*N*-dimethylacetamide and *N*-formylmorpholine with each of these solvents containing a tertiary amine. Shown in Figure 21 is a comparison on a weight basis of the remaining solvents

whose relative solvent strength was not accurately predicted by COSMOtherm compared to the experimental results.

It is important to note that Kholod et al. (115) predicted the water solubility for nitrogen containing compounds using the COSMO-RS approach and found significant disagreement between calculated and experimental values. Accordingly, Kholod made an ad-hoc modification to the COSMO-RS approach in order to improve the agreement between predicted and experimental solubility values. It appears that properties of molecules with nitrogen-containing groups are not always accurately modeled within the COSMOtherm formalism and that the error can be ascribed to problems with the COSMO-RS part of the calculation. It is clear that COSMOtherm would need to be optimized or tailored in some way in order to achieve good agreement with all experimental data, however, this alteration would take away from any potential predictability it might have. At present we have no adequate explanation for this. The failure to predict the correct ordering for the methanol/CO_2 system may be due to specific hydrogen bonding interactions not adequately described in COSMOtherm, although previous studies have been able to accurately predict properties of systems containing hydrogen bonding liquid mixtures. (102) (103)

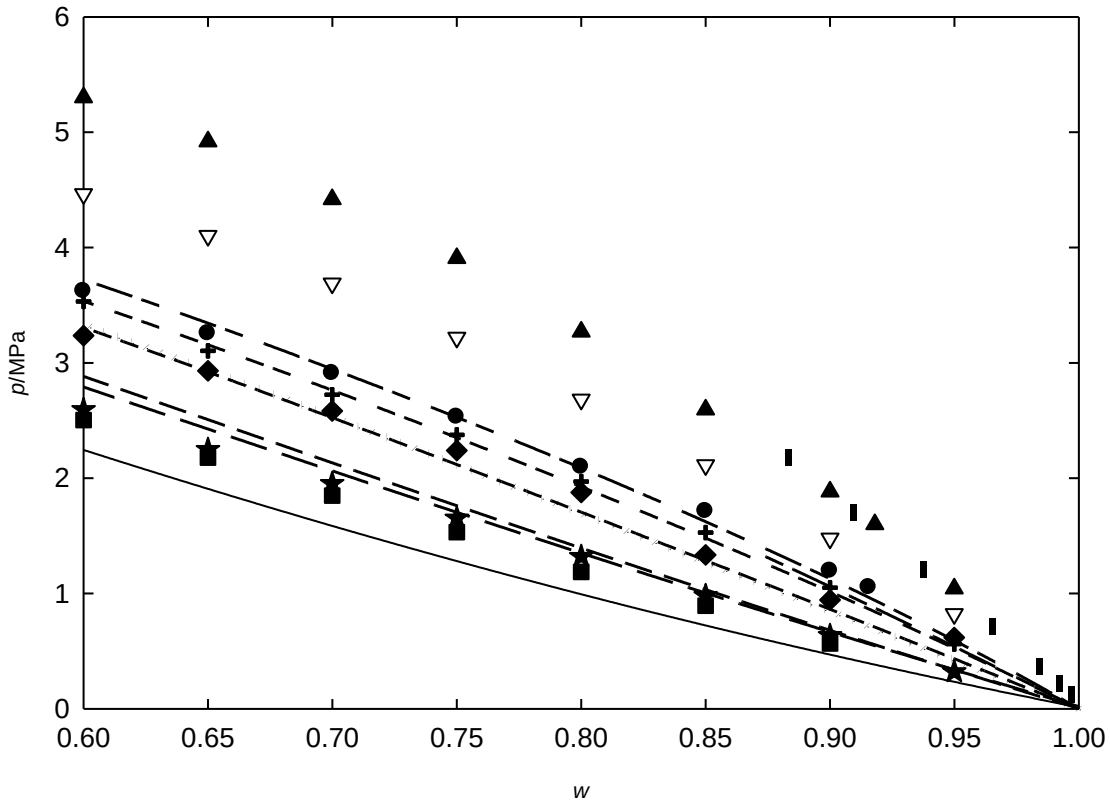

Figure 20. Comparison of solubility of CO_2 in the eight oxygenated hydrocarbons, presented in mass fraction of solvents, w, COSMOtherm (lines) and experimental (symbols) listed in descending solvent strength order according to experimental results: ■, ———— acetone; ★, — — — methyl acetate; ◆, — — — — 1,4-dioxane; ✚, – – – – – – 2-methoxyethyl acetate; ●, ▪▪▪▪▪▪▪▪▪▪▪▪ acetylacetone; ▽, – – – – 2-(2-butoxyethoxy)ethyl acetate; ▮, — – — – propylene carbonate[55]; ▲, – — – — 2-butoxyethyl acetate.

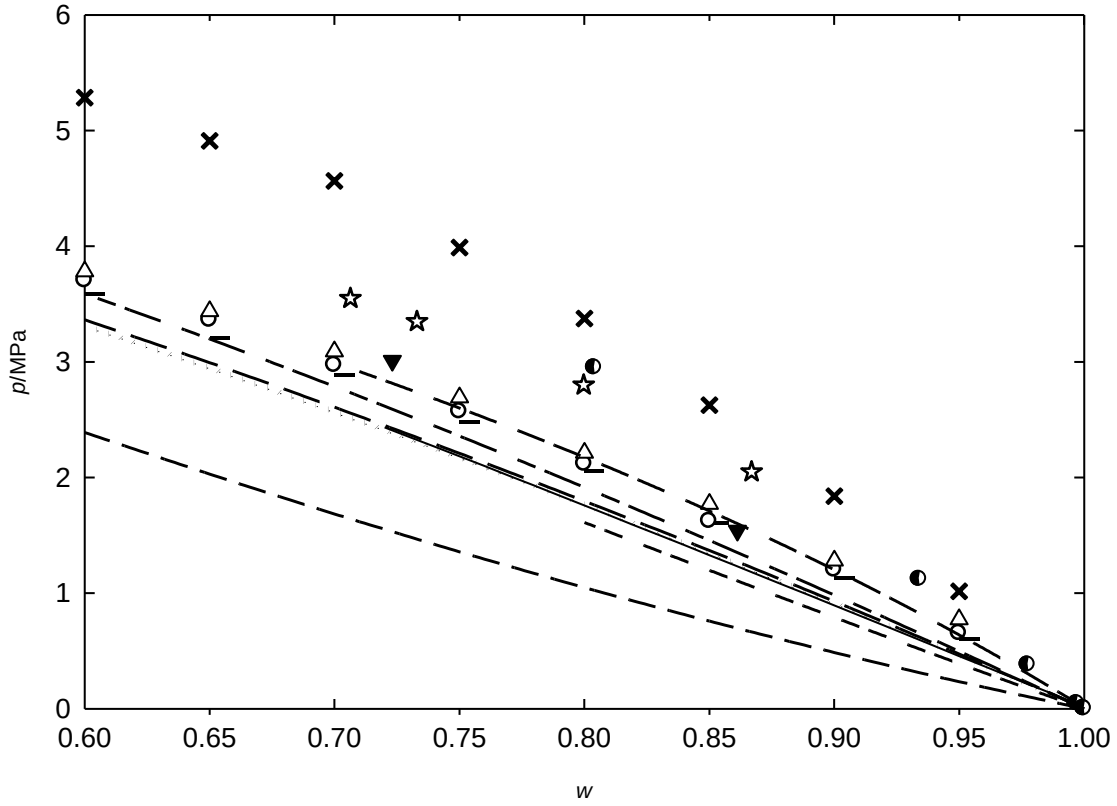

Figure 21. Solubility of CO_2 in the seven remaining solvents, presented in mass fraction of solvents, w, COSMOtherm (lines) and experimental (symbols) listed in descending solvent strength order according to experimental results: ▼, _____ methanol[62]**;** – , — — — 2-nitropropane; ○ , — — — — *N*,*N*-dimethylacetamide; △, ····· 1-nitropropane; ☆, — — — — — — isooctane[53]; ◑, – – – – – – *N*-formylmorpholine[54]**;** ×, — – — – — – *N*-*tert* -butylformamide.

Table 4. The average absolute deviation and average absolute percent deviation of the solubility pressures computed from COSMOtherm relative to the experimental data and presented in order of solvent strength on a weight basis according to COSMOtherm.

Compound	Average Absolute Deviation (AAD), MPa	Average Absolute Percent Deviation (AAPD)
acetone	0.42	27.10
propylene carbonate	0.39	35.07
n,n-dimethylacetamide	1.24	54.02
isooctane	0.53	16.83
methyl acetate	0.13	12.48
1,4-dioxane	0.46	27.89
n-formylmorpholine	0.75	24.35
acetylacetone	0.58	24.26
2-methoxyethyl acetate	0.42	22.32
1-nitropropane	0.66	29.32
2-nitropropane	0.44	21.87
n-tert-butylformamide	1.56	45.53
2-(2-butoxyethoxy)ethyl acetate	0.94	33.80
2-butoxyethyl acetate	1.38	40.39
methanol	0.42	10.73

5.3 CONCLUSIONS

The solubility of CO_2 in various "small molecule" solvents has been determined at 298.15 K. To the best of our knowledge, these results have not been previously reported for 2-butoxyethyl acetate, 2-(2-butoxyethoxy)ethyl acetate, 1-nitropropane, 2-nitropropane, *N*,*N*-dimethylacetamide, 2-methoxyethyl acetate, and *N*-*tert*-butylformamide.

When compared on a weight basis, acetone exhibits the greatest capacity for the absorption of CO_2 solubility. Three of the next four best solvents, methyl acetate, 1,4-dioxane and 2-methoxyethyl acetate, are rich in carbonyl and/or ether groups that favor Lewis acid : Lewis base interactions with CO_2, and the solvent strength decreases with increasing molar mass and increasing boiling point. Although methanol possesses a CO_2-phobic hydroxyl group, the very low molar mass of this alcohol enables it to exhibit a solvent strength comparable to that of 1,4-dioxane when measured on a weight basis.

When the solvents were compared on a molar basis, the six best solvents, 2-(2-butoxyethoxy)ethyl acetate, methyl acetate, 2-methoxyethyl acetate, 1,4-dioxane, acetone, and acetylacetone, were rich in highly CO_2-philic carbonyl and/or ether oxygen atoms. The poorest solvent on a molar basis was methanol. In general, when compared on either basis, solvents containing butyl, t-butyl, nitro, and secondary or tertiary amines exhibited poorer solvent strength than the carbonyl and ether-rich solvents.

Despite its ability to accurately predict carbon dioxide gas solubility in oligomeric solvents,(86) and ionic liquid membranes,(116) the COSMOtherm formalism did not accurately predict the relative solubility of CO_2 in all the volatile, small molecule solvents. However, a closer evaluation of the data revealed that COSMOtherm was able to correctly predict the relative solvent strengths of those compounds containing only C, H, and O, except for methanol.

It appears that COSMOtherm is not able to correctly account for the interactions in the systems with nitrogen-containing molecules and for methanol. Similar problems have been noted previously,(115) with the failure linked to the COSMO-RS part of the formalism. A modification of COSMO-RS is apparently needed to correctly account for nitrogen-containing systems.

6.0 NOVEL PHASE CHANGE SOLVENTS FOR CO_2 ABSORPTION

Solid CO_2-philes that can melt in the presence of high pressure CO_2 at pressures commensurate with the IGCC process, form low viscosity liquids that would reduce mass transfer resistance in an adsorption column, selectively absorb significant amounts of CO_2, and (most significantly) be regenerated in a separate vessel by reducing the pressure to a value just below that required for the CO_2-phile to solidify and release the captured CO_2. This would allow for the development of a novel absorption solvent that could be regenerated at a pressure much higher than that associated with conventional liquid solvents. This, in turn, would greatly reduce the power required to compress the released CO_2 to a liquid or supercritical state suitable for transportation to a sequestration site (e.g. ~15 MPa). The power consumption required to perform this compression ranges approximately between 40 % - 50 % of the total power consumed by the carbon capture process based on CO_2 removal goals, and overall plant design. (63) (117) (118) (119) Equation 3 is used to determine the power by an isothermal compressor derived from the Bernoulli equation comparable to those used in carbon capture processes and are defined by

$$P_B = \frac{1.97 T_a q_0}{\eta} \ln \frac{p_b}{p_a} \quad (3)$$

where P_B is the power supplied to the pump (kW), p is the pressure at point a or b, q_0 is the volume of gas compressed (std m^3/s evaluated at 273.15 K and 101.325 kPa), T_a is the inlet temperature (K), and η is the mechanical efficiency of the pump. Important assumptions include

the mechanical, kinetic and potential energies do not appreciably change, the velocity and static head terms can be dropped the compressor is frictionless, and the ideal gas law is assumed valid. (120) This equation is dependent upon the natural logarithm of the compression ratio. In the case of physical solvents CO_2 is released at approximately 0.1 MPa (1 atm) and then compressed to 15 MPa. The ln of this compression ratio is close to 5. CO_2 released from a phase change solvent would be in the vapor phase at ~5 MPa, and need to be compressed up to 15 MPa. The ln (15/5) is roughly unity, therefore, the compression of CO_2 released during the regeneration process conducted at 5 MPa would require ~20 % of the work associated with the compression of CO_2 released during the regeneration of conventional liquid solvents at ~0.1 MPa. Aspen simulations completed using an isentropic compressor and the Peng-Robinson equation of state reveal that the compression of CO_2 through the vapor phase, from 2 MPa up to 7.3 MPa, starting at 303 K, requires 20 % of the energy to compress CO_2 at the same conditions and starting at 0.1 MPa. The impacts of these potential economic and energetic savings are the major motivation behind this work.

Three of these CO_2-philic solids, tri-*tert*-butylbenzene (TTBB), maltose octaacetate (MOA), and tri-*tert*-butylphenol (TTBP), have been previously discovered by our group and others in the past; the binary phase behavior for TTBB, MOA, and TTBP is presented in Figures 22 – 24, respectively. In order for these compounds to be effective solvents for the capture of CO_2 from a mixed gas stream, the solubility of H_2 in the CO_2-rich molten solid needs to be very low. Binary experiments conducted by our group with the solid and pure H_2 demonstrate that these compounds do not experience a similar melting point depression with H_2 present; these compounds are not H_2-philic. Also, in order for there not to be excessive "evaporative" losses of the molten solvent, its solubility in the high pressure CO_2/H_2 mixture should be low.

Although each of the binary mixtures illustrated in Figures 22 – 24 present different phase behavior than the other, they share some common attributes that may be taken advantage of for CO_2 capture. It can be seen Figure 22 that in the presence of CO_2 at 298 K and a pressure of about 4 MPa, the TTBB melts and a liquid phase containing as much as 90 wt% TTBB forms. This liquid phase can be slightly depressurized back below 4 MPa in order to reproduce a solid TTBB powder that releases all CO_2 just absorbed to yield a high pressure CO_2 phase that contains no TTBB. This same melting point depression is seen in Figures 23 and 24 where MOA is able to form a liquid at ~5 MPa and as much as 50 % MOA, and TTBP will melt and dissolve into CO_2 above 6.7 MPa and up to 8 % TTBP. (It should be noted that this small pressure change is accompanied by a large density change as the CO_2 transforms from a liquid-like density to a high-pressure gas-like density). Upon compression each of the solids are able to form a single, clear, homogeneous liquid phase. These three solids helped in the judicious selection of all the solids tested in this work. Each of these three solids will be tested in the tertiary phase behavior, explained in greater detail below, due to their success in experiencing a melting point depression in the binary mixture with CO_2. The complex phase behaviors seen by these three solids and formed by each of the solids examined in this work are also discussed in greater detail below, in an effort to find a solid CO_2-phile capable of becoming a physical absorbent for a CO_2 capture process.

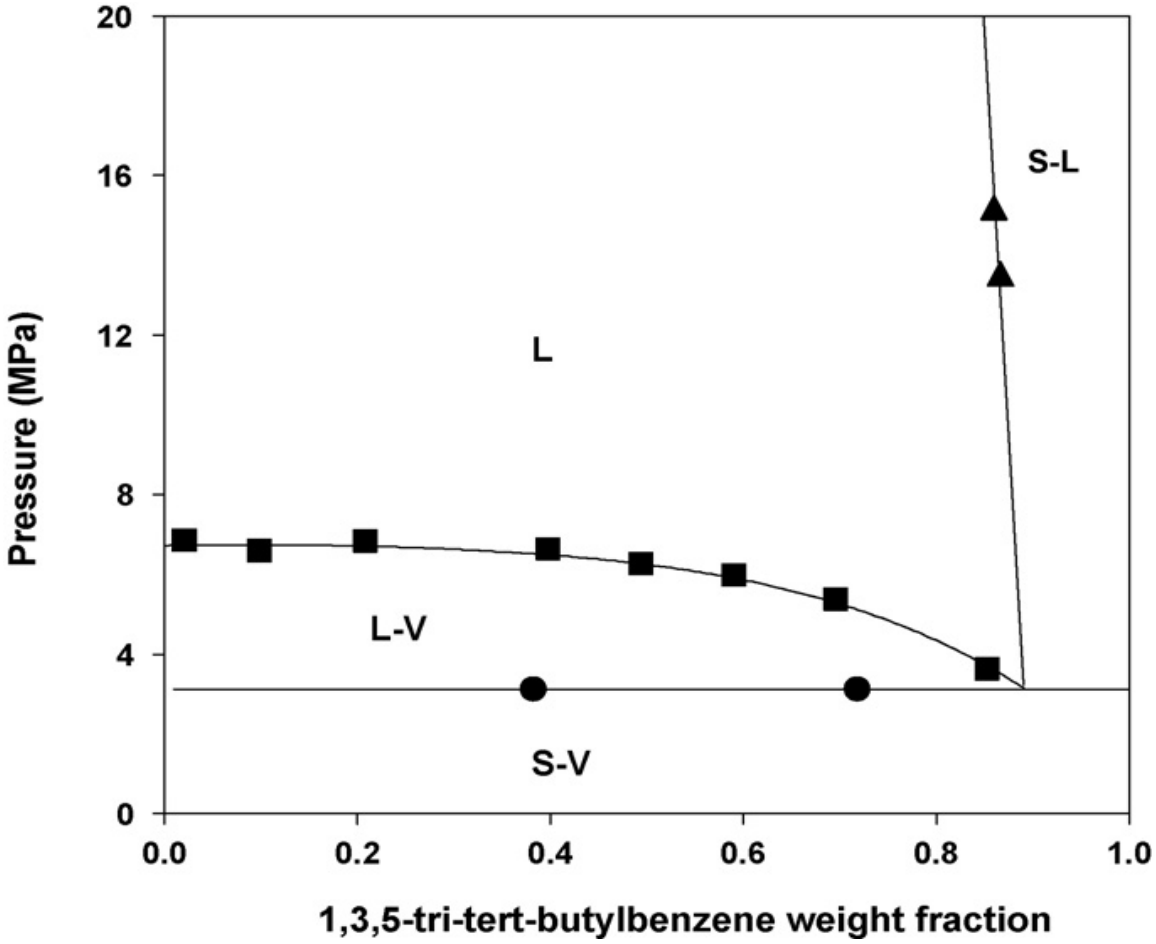

Figure 22. Binary phase behavior of 1,3,5-tri-tert-butylbenzene, T=298K. By absorbing CO_2 the melting point of TTBB can be lowered by approx. 50K (50).

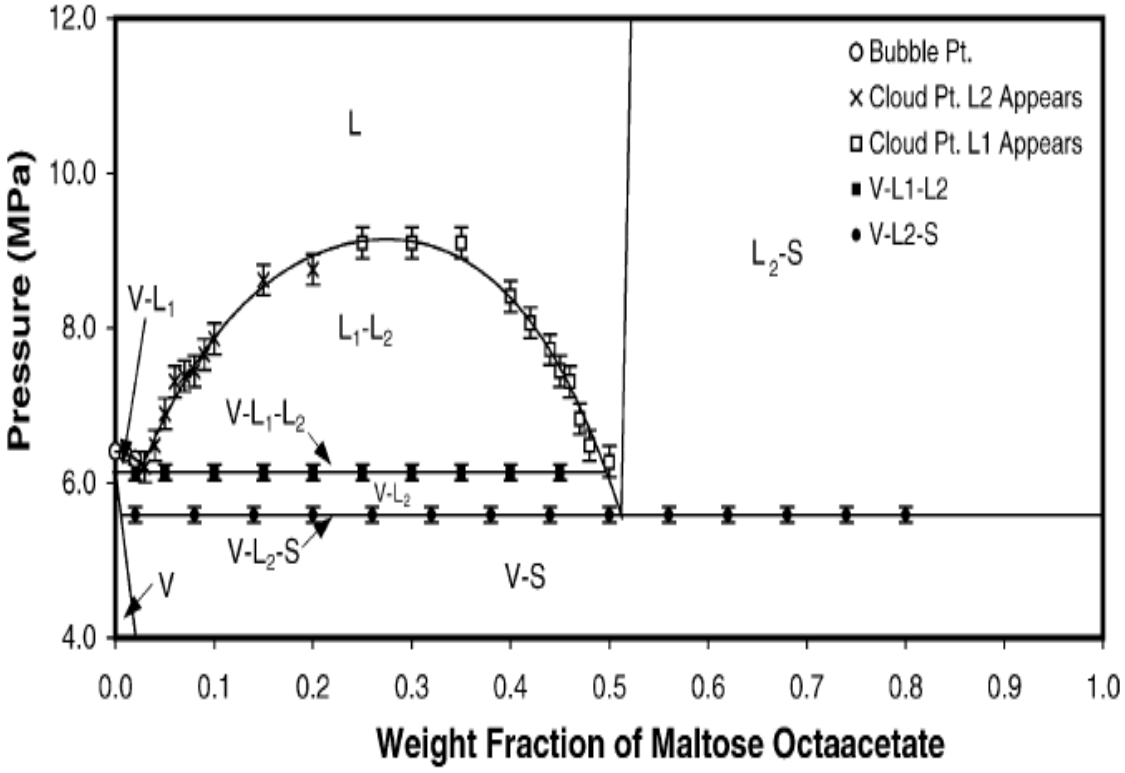

Figure 23. Phase behavior of the binary system of maltose octaacetate and CO_2, T=298K (37).

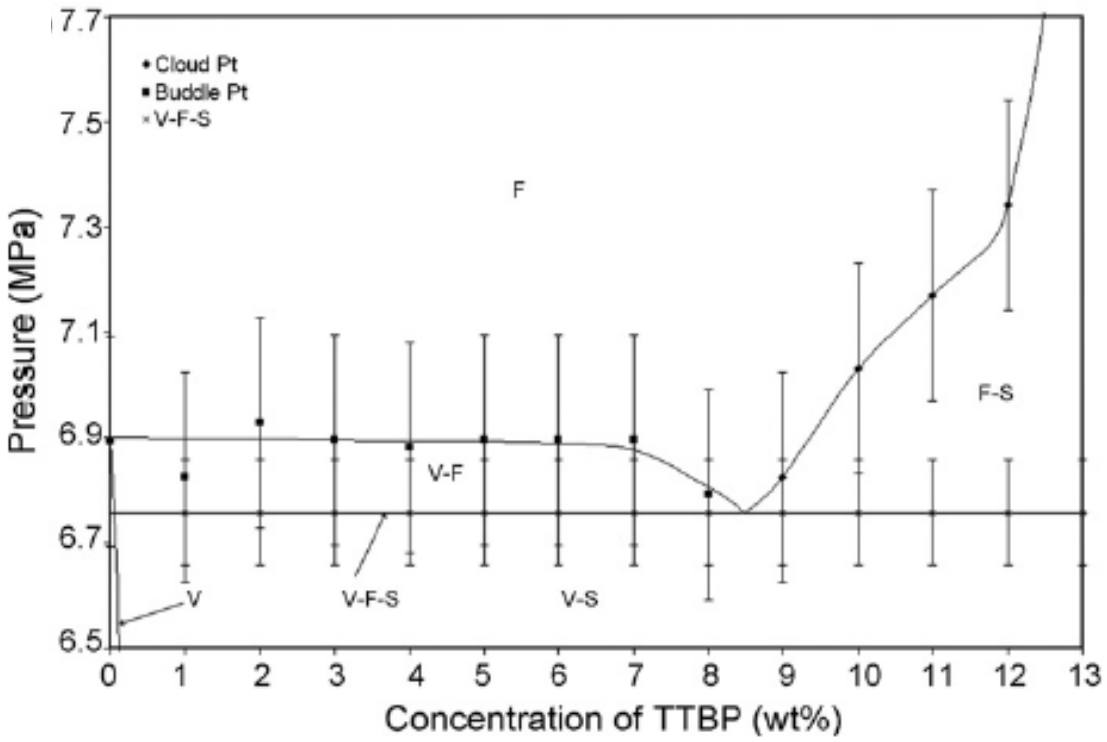

Figure 24. Phase behavior for the binary system of TTBP and CO_2 at 301 K. (51)

6.1 MATERIALS

All 12 solid CO_2-philes were purchased from Sigma Aldrich including, β-D-ribofuranose tetraacetate (mass purity of 0.98), D-(+)-sucrose octaacetate (mass purity of 0.98), β-D-maltose octaacetate, α-D(+)-glucose pentaacetate (mass purity of 0.99), β-D-galactose pentaacetate (mass purity of 0.98), 2,6-di-*tert*-butyl-4-methylphenol (mass purity of ≥0.99), 1,2,4-triacetoxybenzene (mass purity of 0.97), 2,4-di-*tert*-butylphenol (mass purity of 0.99), 1,3,5-trioxane (mass purity of ≥0.99), 2,4,6-tri-*tert*-butylphenol (mass purity of 0.98), 1,3,5-tri-*tert*-butylbenzene (mass purity of 0.97), 3,5-di-*tert*-butylphenol (mass purity of 0.99). Listed in Table 5 are the structures of all solids examined in this work as well as their melting points (mp) at ambient pressure as given by the supplier. CO_2 was purchased from Penn Oxygen and Supply Company with a purity of 0.9999 and used without further purification. The CO_2/H_2 mixed gas was purchased from Matheson Tri-Gas and has a certified molar composition of 0.4993 CO_2 and 0.5007 H_2 measured with an accuracy of ±0.02.

Table 5. Structures and normal melting points of all solid CO_2-philes examined in this study.

Solid CO_2-phile	Structure	Melting point / K
β-D-ribofuranose 1,2,3,5-tetraacetate	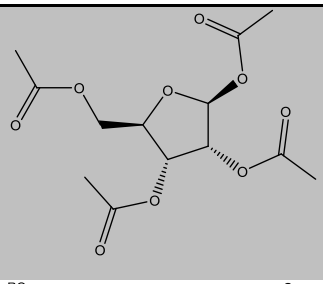	354 - 356
D-(+)-sucrose octaacetate	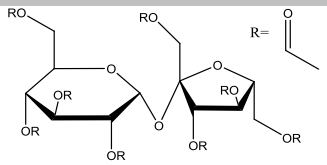	355 - 358
β-D-maltose octaacetate	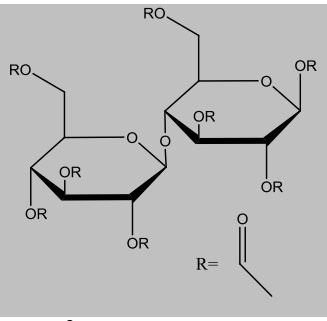	433 - 434
α-D(+)-glucose pentaacetate	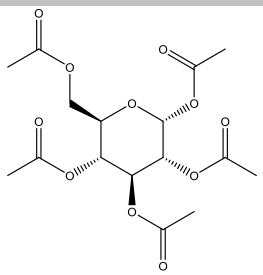	382 - 384
β-D-galactose pentaacetate	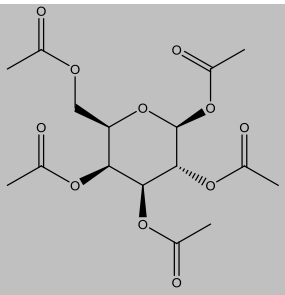	416 - 417

Table 5. (continued)

2,6-di-*tert*-butyl-4-methylphenol	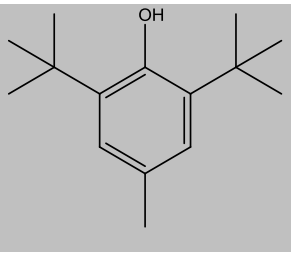	342 - 346
1,2,4-triacetoxybenzene	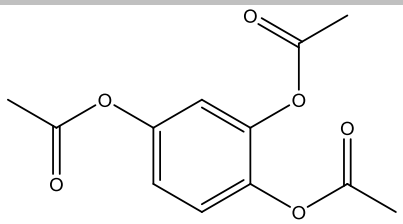	371 - 373
2,4-di-*tert*-butylphenol	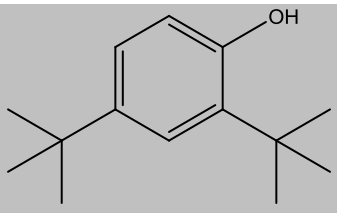	326 - 329
1,3,5-trioxane	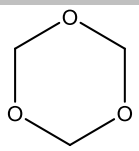	332 - 335
2,4,6-tri-*tert*-butylphenol	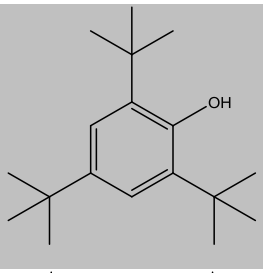	398 - 403
1,3,5-tri-*tert*-butylbenzene	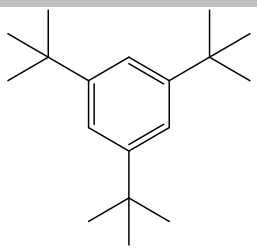	340 – 345

Table 5. (continued)

3,5-di-*tert*-butylphenol	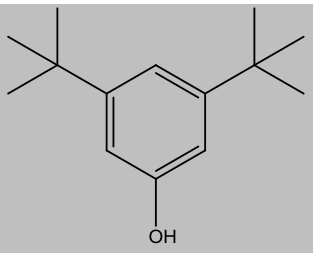	360 - 362

6.2 PHASE BEHAVIOR OF SOLID CO_2-PHILES IN CO_2

6.2.1 Experimental apparatus

The phase behavior of each binary system was generated using the same high pressure, windowed, agitated, variable volume view cell (Schlumberger Ltd.) as illustrated in Figures 9 and 10. In a given experiment between 0.25 g to 10 g of the solid is placed in the Pyrex tube and the tube is then sealed in the cell and the sample volume is reduced by pumping in the overburden fluid. The remaining air present in the tube is then vented out with the CO_2 or CO_2/H_2 mixed gas, depending on the experiment. After that known amounts of gas are isobarically and isothermally pumped into the sample volume while simultaneously withdrawing the overburden oil via a dual positive displacement pump. This enables the sample volume to be expanded at the same volumetric rate as the gas mixture is being introduced. Once the desired mass fractions are achieved the sample volume is compressed up to 68.95 MPa, when using pure liquid CO_2, or 34.5 MPa, when using the CO_2/H_2 mixed gas. At the elevated pressures either a single, clear, homogeneous, fluid phase, fluid-liquid equilibrium (FLE), or fluid-solid equilibrium (FSE) would result. (The term "liquid" or "solid" in the FLE and FSE designations refer to CO_2-philic compound's state, while the term "fluid" refers to the CO_2-rich vapor phase or the (CO_2/H_2)-rich mixed gas phase.) The sample volume was then slowly expanded and phase behavior transitions were observed. Bubble points are defined as the equilibrium coexistence of a liquid phase and a minute amount of a vapor or fluid phase. The liquid-liquid cloud points correspond to the pressure at which the mixture within the sample volume starts separating into two liquid phases, most commonly occurring in the form of a cloud point at which point it is no longer possible to see through the sample volume due to the appearance of droplets of a second

phase, and can be seen in Figure 24. To confirm that the two-phase conditions were attained, the cell is then left in a quiescent state at the cloud point pressure until the fluid phase is clear and a very small liquid phase is observed wetting the bottom of the sample volume. Three phase equilibrium is characterized by vapor-liquid-liquid equilibrium (VLLE), vapor-liquid-solid equilibrium (VLSE), and fluid-liquid-solid equilibrium (FLSE).

6.2.2 Solid CO_2-philes and CO_2, binary mixtures

Phase behavior results, in the form of pressure vs. weight fraction of the solid (w), for the binary systems of β-D-galactose pentaacetate (BGAL-Ac), β-D-ribofuranose tetraacetate (BRF-Ac), α-D(+)-glucose pentaacetate (AGLU-Ac), trioxane, D-(+)-sucrose octaacetate (SOA), 2,4-di-*tert*-butylphenol, and 2,6-di-*tert*-butyl-4-methylphenol with CO_2 have been examined. All of these solids were capable of experiencing melting point depressions and were successful in forming a single homogeneous liquid phase at elevated pressures with CO_2. Two of the solids, 3,5-di-*tert*-butylphenol and 1,2,4-tri-acetoxybenzene, however, were not able to mix with CO_2 in any proportions up to the pressure limit of our apparatus (68.95 MPa). Due to this shortcoming, they were not examined with the equimolar CO_2/H_2 mixed gas. To the best of our knowledge, phase behavior for β-D-ribofuranose tetraacetate, 2,4-di-*tert*-butylphenol, 2,6-di-*tert*-butyl-4-methylphenol and trioxane with CO_2 have not been previously reported.

The CO_2-(CO_2-philic compound) pressure-composition diagrams observed during this study fall into two categories, as shown in Figures 25 and 26. In the first, illustrated in Figure 25, a single VLS three-phase pressure line bounds three two-phase regions, the vapor-liquid (VL) and liquid-solid (LS) regions above the VLS pressure, and the vapor-solid (VS) region below the VLS pressure. This behavior is exhibited by binary mixtures of CO_2 with either

BGAL-Ac, BRF-Ac, or AGLU-Ac in Figures 27 – 29, respectively. The second type of phase behavior, illustrated in Figure 26, is characterized by two three-phase pressures, VL_1L_2 and VL_2S, where L_1 and L_2 correspond to CO_2-rich and CO_2-philic compound-rich liquids, respectively. The VL_1L_2 line bounds the VL_1, L_1L_2, and VL_2 regions, while the VL_2S line bounds the VL_2, L_2S and VS regions. This behavior is exhibited by binary mixtures of CO_2 with either 1,3,5-trioxane, SOA, 2,4-di-*tert*-butylphenol, or 2,6-di-*tert*-butyl-4-methylphenol in Figures 30 – 33, respectively. In Figures 27 – 33 solid curves have been drawn through data points corresponding to these phase behavior transitions. In each diagram, the dashed curves are qualitative extrapolations included solely to assist the reader in understanding how the experimental data correspond to the generalized Px diagrams shown in Figures 25 and 26, and are not representative of actual measured data points.

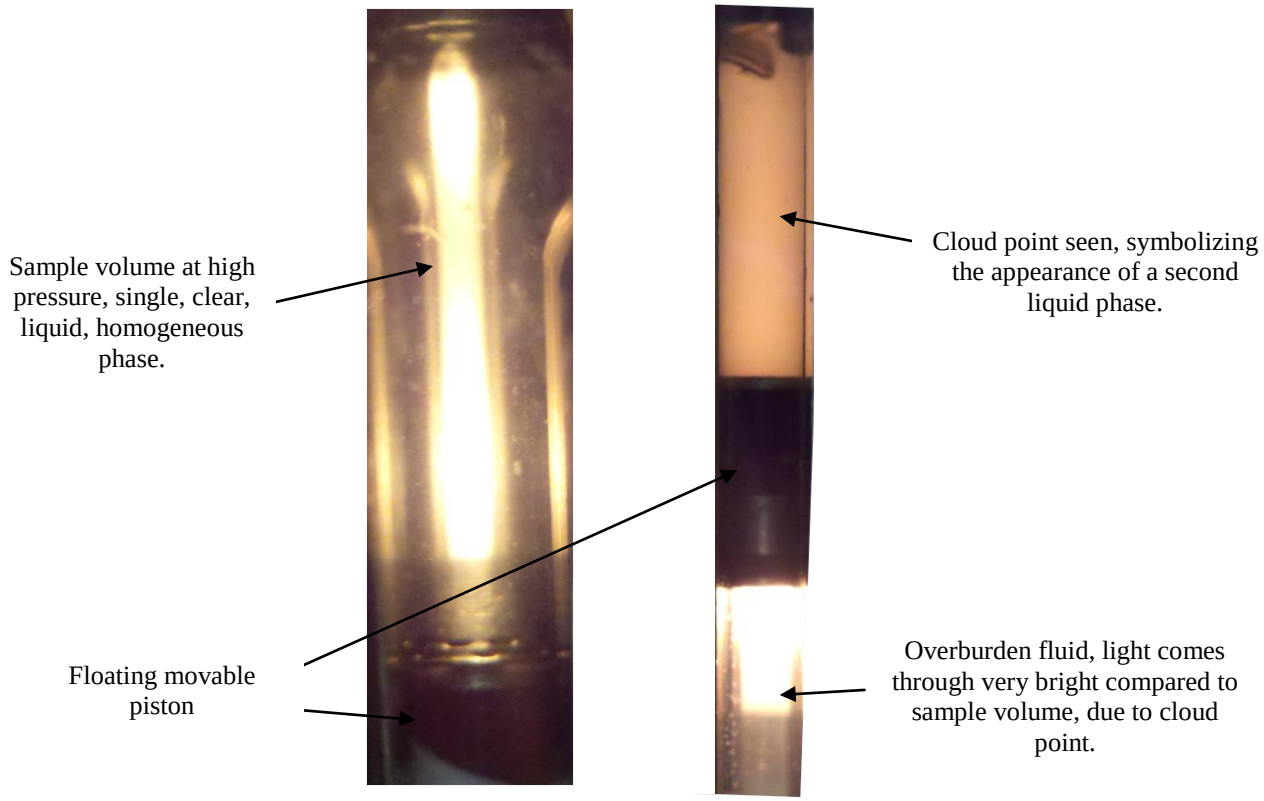

Figure 25. Images of cloud point transitions for high pressure phase behavior.

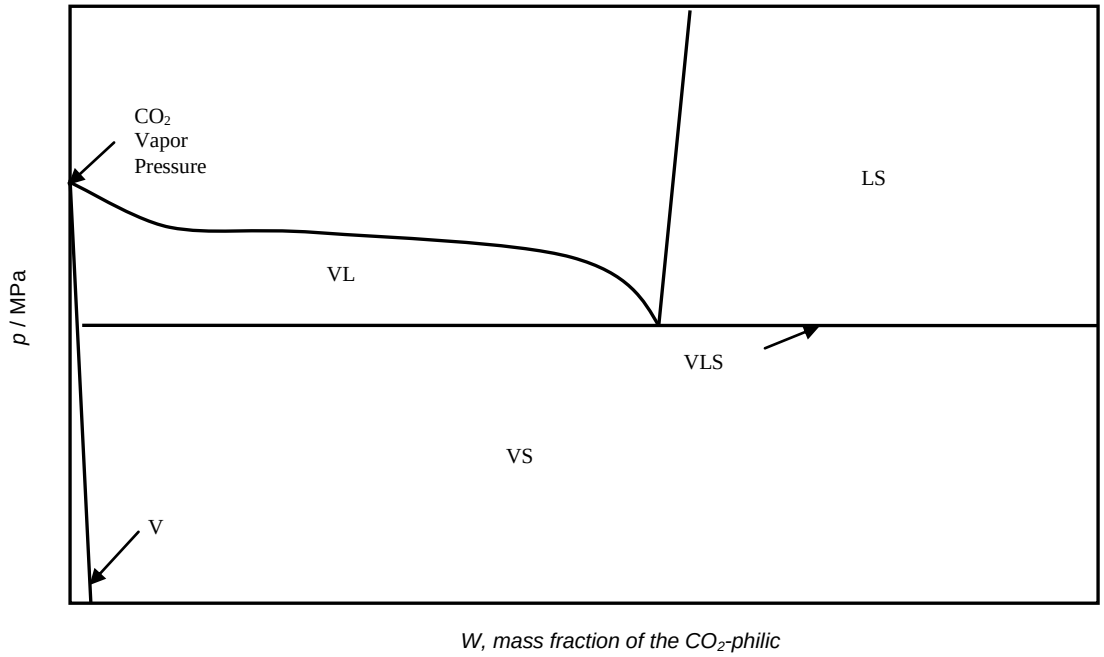

Figure 26. General Px diagram, type one; Mixtures of CO_2 and a CO_2-philic solid that exhibit a single three-phase equilibrium line.

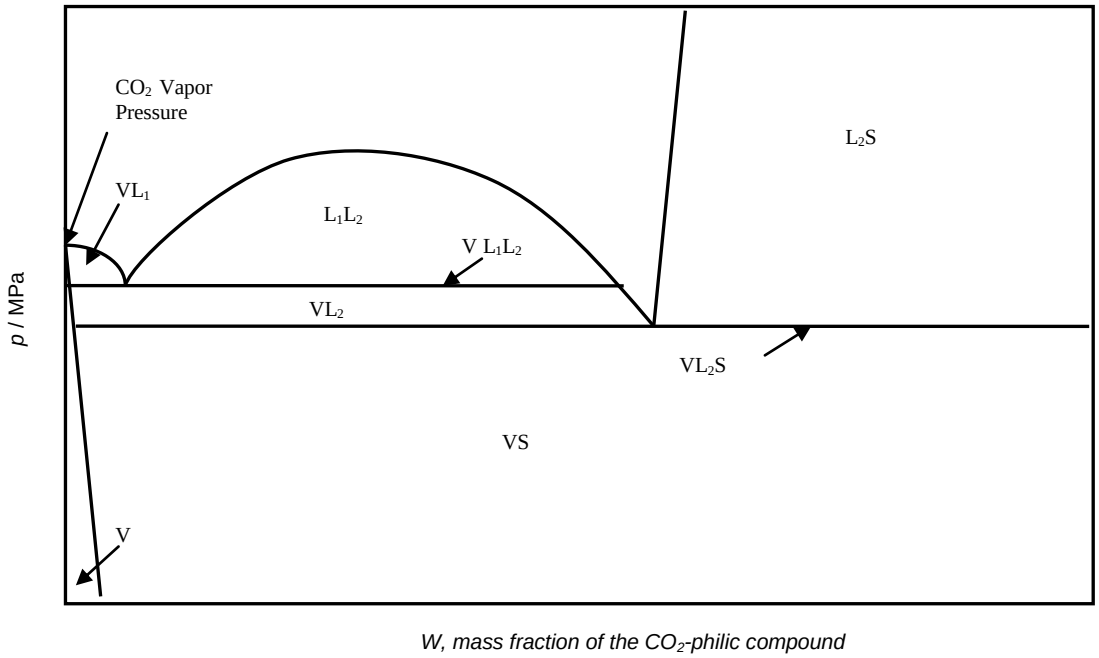

Figure 27. General Px diagram, type two; Mixtures of sub-critical CO_2 and a CO_2-philic solid that exhibits two three-phase equilibrium lines. (37)

6.2.2.1 CO_2 - β-D-galactose pentaacetate, BGAL-Ac

As illustrated in Figure 27 a clear single homogeneous liquid (L) is realized at elevated pressures and BGAL-Ac weight fractions of 0.35 and less. At BGAL-Ac weight fractions greater than 0.35 the system is immiscible up to the pressure limits of the apparatus (68.95 MPa) resulting in two phases, the solid BGAL-Ac and the other being comprised of liquid CO_2. The boundaries of this SL region are illustrated by the SL phase boundary line and the extrapolated VLS three phase pressure line, which meet the LV bubble point locus.

At lower concentrations of the BGAL-Ac ($w < 0.4$), expansion of the L phase results in the appearance of CO_2 rich vapor bubbles. These data terminate at the CO_2 vapor pressure at 298 K, and define the VL bubble point curve; the two-phase boundary of the VL region.

Upon further expansion of the VL phase the VLS three-phase pressure is reached. At this point the system goes through an isobaric expansion where all CO_2 still in the liquid phase evaporates as the BGAL-Ac in the liquid phase freezes.

Below the three-phase boundary is the VS phase which is comprised of CO_2 rich vapor with practically no BGAL-Ac and a BGAL-Ac – rich solid. The system could not be expanded enough to obtain visual observations of VS phase behavior.

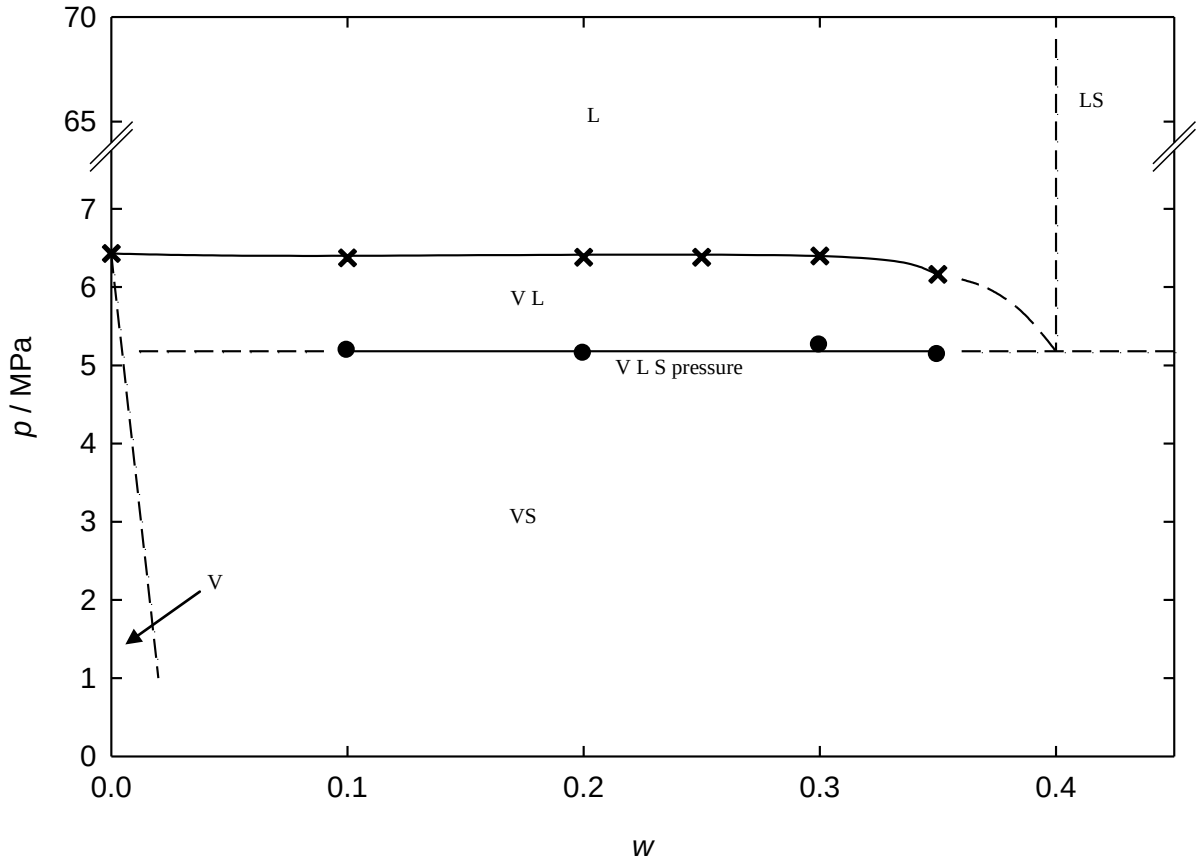

Figure 28. Phase behavior of CO_2 and β-D-galactose pentaacetate at 298 K; × VL; ● VLS. At VLS conditions, the L phase contains roughly 60wt% CO_2. VLS pressure variability = ±0.3 MPa.

6.2.2.2 CO_2 – ribofuranose tetraacetate, BRF-Ac and CO_2 – α-D-glucose pentaacetate, AGLU-Ac

Mixtures of CO_2 with either BRF-Ac or AGLU-Ac, Figures 28 and 29, exhibit similar behavior as the CO_2 – BGAL-Ac mixture shown in Figure 27. In both cases, it was not possible to charge the vessel with high enough proportions of the CO_2-philic compound to observe SL phase equilibrium. The boundaries of this SL region are qualitatively illustrated by the vertical dashed SL phase boundary and the extrapolated SLV three phase pressure line, which meet the LV extrapolated line.

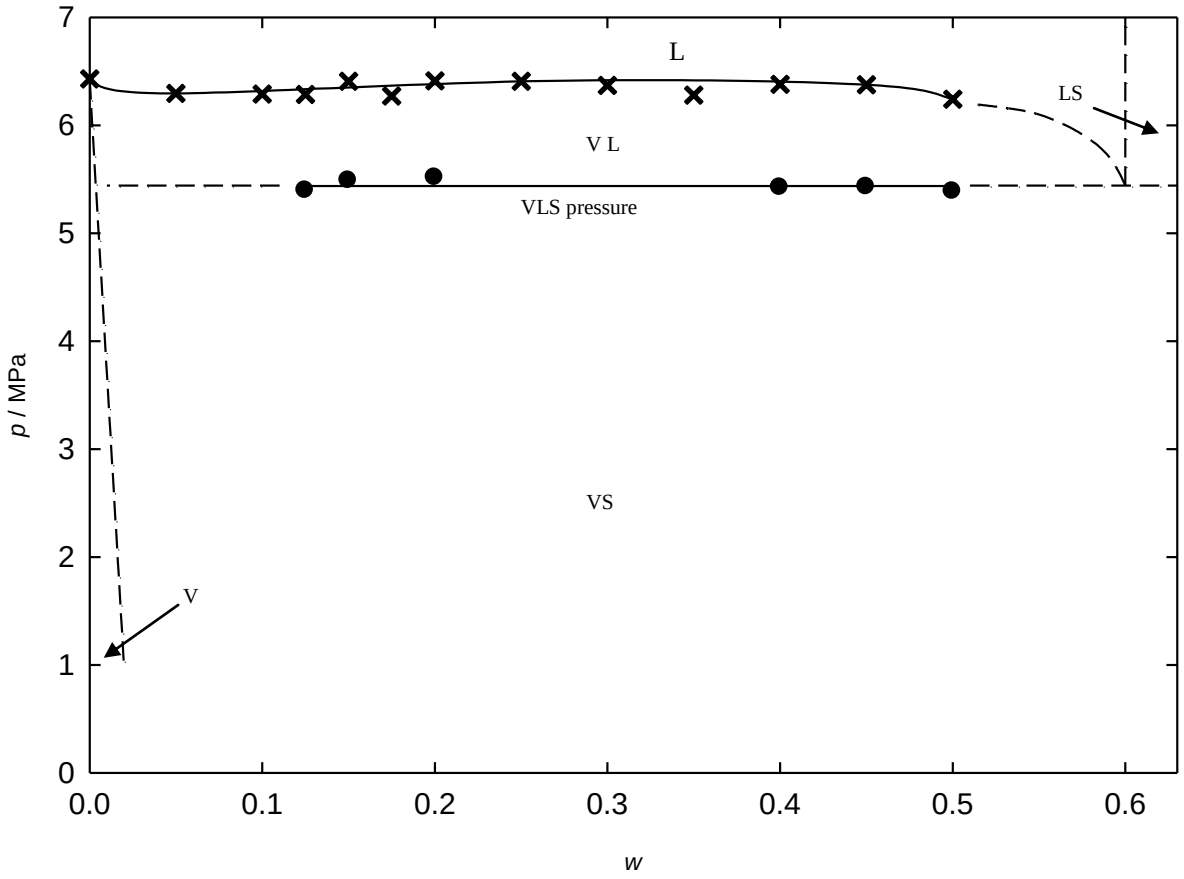

Figure 29. Phase behavior of CO_2 and β-D-ribofuranose 1,2,3,5-tetraacetate at 298 K; ✕ VL; ● VLS. At VLS conditions, the L phase contains roughly 40wt% CO_2. VLS pressure variability = ±0.61 MPa.

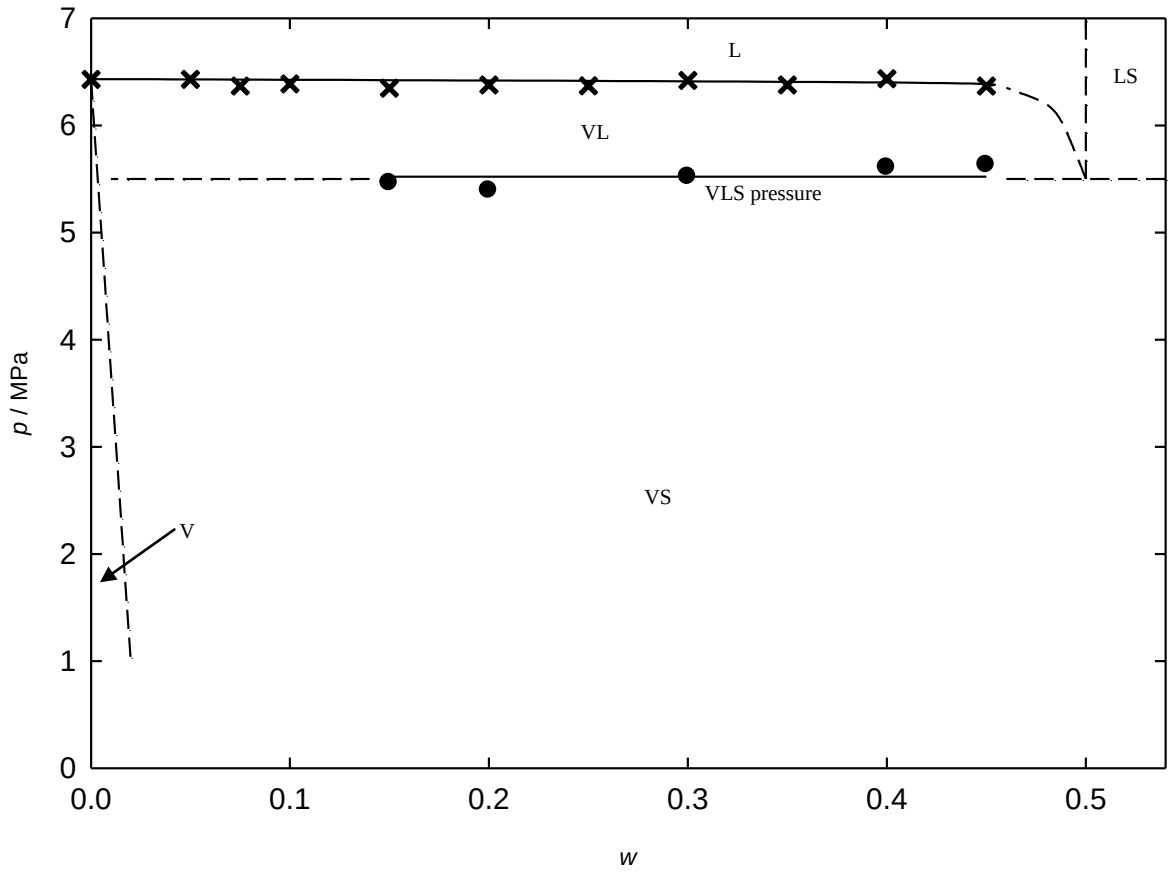

Figure 30. Phase behavior of CO_2 and α-D(+)-glucose pentaacetate at 298 K; ✕ VL; ● VLS. At VLS conditions, the L phase contains roughly 50wt% CO_2. VLS pressure variability = ±0.31 MPa.

6.2.2.3 CO_2 -1,3,5-trioxane

The second type of phase behavior, qualitatively illustrated in Figure 26, was exhibited by several binary systems, such as the CO_2 and trioxane binary shown in Figure 30. An immiscible liquid-solid region is realized at trioxane weight fractions greater than 0.6 and pressures above the three phase VL_2S line. This L_2S phase is comprised of solid trioxane, S, and a trioxane-rich liquid phase L_2. This region is bounded by the vertical L_2S line, which occurs at trioxane weight fractions greater than 0.60 but less than 0.65 (LS behavior was observed at w = 0.65), the VL_2S line, and the neat trioxane boundary.

The expansion of the single homogeneous liquid (L), at trioxane weight fractions less than 0.10, results in liquid-liquid cloud points. This region that contains these two liquid phases is labeled L_1L_2. At weight fractions between 0.05 and 0.10, droplets of the more dense L_2 phase appeared. The L_1L_2 region is bounded by the VL_1L_2 three phase boundary line, the L_1L_2 binodal curve, and the small (un-detected) VL_1 region illustrated by the dashed line.

The expansion of the single homogeneous liquid (L) at trioxane weight fractions ranging from greater than 0.10 and less than 0.65 resulted in CO_2 rich vapor bubbles being formed on the VL_2 bubble point boundary of the VL_2 region. The VL_2 region is also observed upon further expansion from the L_1L_2 region across the VL_1L_2 three-phase pressure line and the VL_2 phase region results.

Further expansion of the VL_2 phase region results in the formation of solid trioxane at the VL_2S three phase pressure. Isobaric expansion through this boundary causes all liquid trioxane to freeze into solid leaving the two phase system made up of CO_2 rich vapor with practically no trioxane and a trioxane rich solid with practically no CO_2.

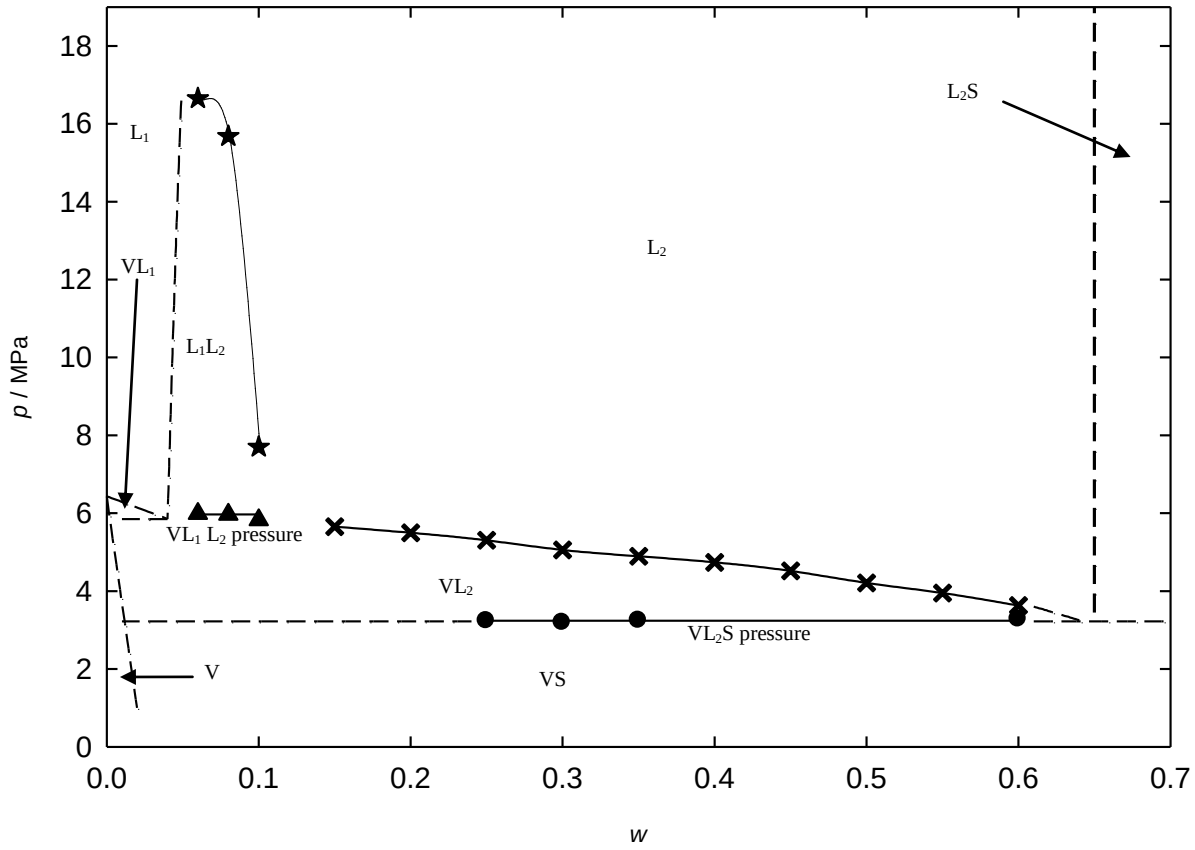

Figure 31. Phase behavior of CO_2 (1) and 1,3,5-trioxane (2) at 298 K; ● V L_2S; ★ L_1 L_2; ▲ V L_1 L_2; × V L_2. At VL_2S conditions, the L_2 phase contains roughly 35wt% CO_2. VL_2S pressure variability = ±0.22 MPa.

6.2.2.4 CO_2 and D-(+)-sucrose octaacetate, SOA

The binary mixture of CO_2 and SOA, illustrated in Figure 31, exhibit a more typical depiction of phase behavior illustrated in Figure 26. At SOA weight fractions less than 0.05 the expansion of the single homogenous L phase results in the VL_1 two phase region being observed, represented qualitatively by dashed lines in Figure 31. The VL_1 binodal boundary begins at the pure vapor pressure of CO_2 at 298 K and terminates at the VL_1L_2 three phase boundary line.

At SOA weight fractions greater than 0.05 and less than 0.5, expansion of the L phase results in the L_1L_2 binodal line and region. At weight fractions of 0.25 and above, liquid droplets of the less dense CO_2-rich liquid L_1 formed and upon quiescence settle to the top of the sample volume. This signifies that the SOA rich liquid, L_2, is the continuous phase at these conditions and the points on the L_1L_2 binodal line at weight fractions from 0.25 to 0.50 are known as "bubble" points. At SOA weight fractions less than 0.20, down to 0.05, liquid droplets of the more dense L_2 droplets formed and sank to the bottom of the sample volume upon quiescence. This results in L_1 being the continuous phase at these conditions and the points on the L_1L_2 binodal line at weight fractions 0.05 to 0.20 are known as "dew" points. The L_1L_2 region is bounded by the VL_1L_2 three phase boundary line, the L_1L_2 binodal curve, and the small (un-detected) VL_1 region illustrated by the dashed line.

Further expansion of the L_1L_2 region at all weight fractions tested results in the VL_1L_2 three phase boundary being reached. This three phase line is bound by three two phase regions, the VL_1 region, the L_1L_2 region, and the VL_2 region. An isobaric expansion across the VL_1L_2 line results in the two phase VL_2 region.

Upon expansion of the two phase VL_2 region solid SOA becomes visible at the VL_2S three phase pressure line. This three phase line is bounded by the VL_2S region, the VS region

and the L_2S region. Upon isobaric expansion of the three phase line, all CO_2 becomes vapor, containing virtually no SOA, and all SOA becomes a solid, containing virtually no CO_2.

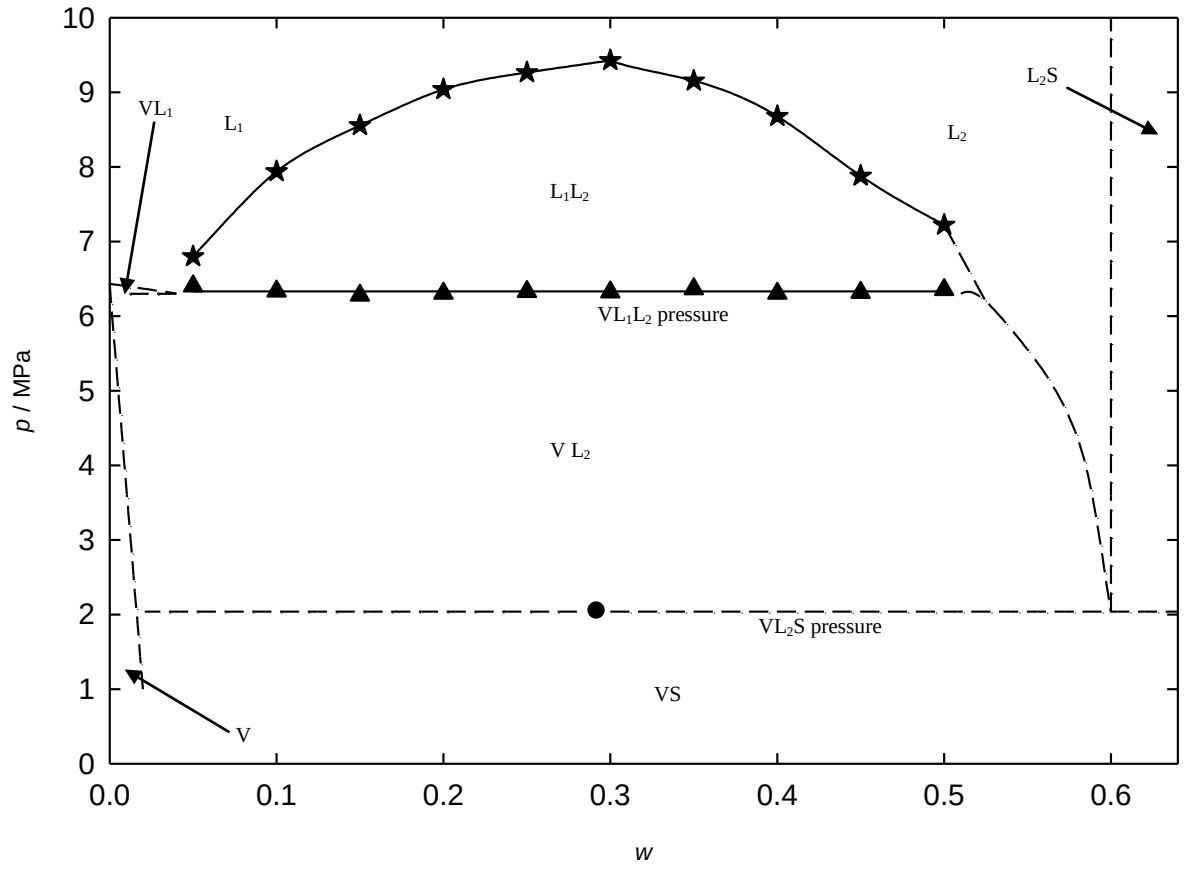

Figure 32. Phase behavior of CO_2 (1) and D-(+)-sucrose octaacetate (2) at 298 K; ● VL_2 S; ★ L_1L_2; ▲ V L_1 L_2. The L_1L_2 critical point composition is in the w = 0.20 – 0.25 range. At VL_2S conditions, the L_2 phase contains roughly 40wt% CO_2. VL_2S pressure variability = ±0.72 MPa.

6.2.2.5 CO_2 – 2,4-di-*tert*-butylphenol and CO_2 – 2,6-di-*tert*-butyl-4-methylphenol

Mixtures of CO_2 with either 2,4-di-*tert*-butylphenol or 2,6-di-*tert*-butyl-4-methylphenol, Figures 32 and 33, respectively, exhibit similar behavior as the CO_2 - SOA mixture shown in Figure 31. In both cases, the binodal VL_1 line was seen and measured. The VL_1L_2 line was not found below a weight fraction of 0.12 and 0.2 however, and is illustrated by dashed lines in both figures. In Figure 33 the pressure difference between the L_1L_2 binodal line and the VS region is only 1 MPa, so isothermal expansions must be conducted slowly and carefully in order to be able to view and record all boundary lines and phase regions observed.

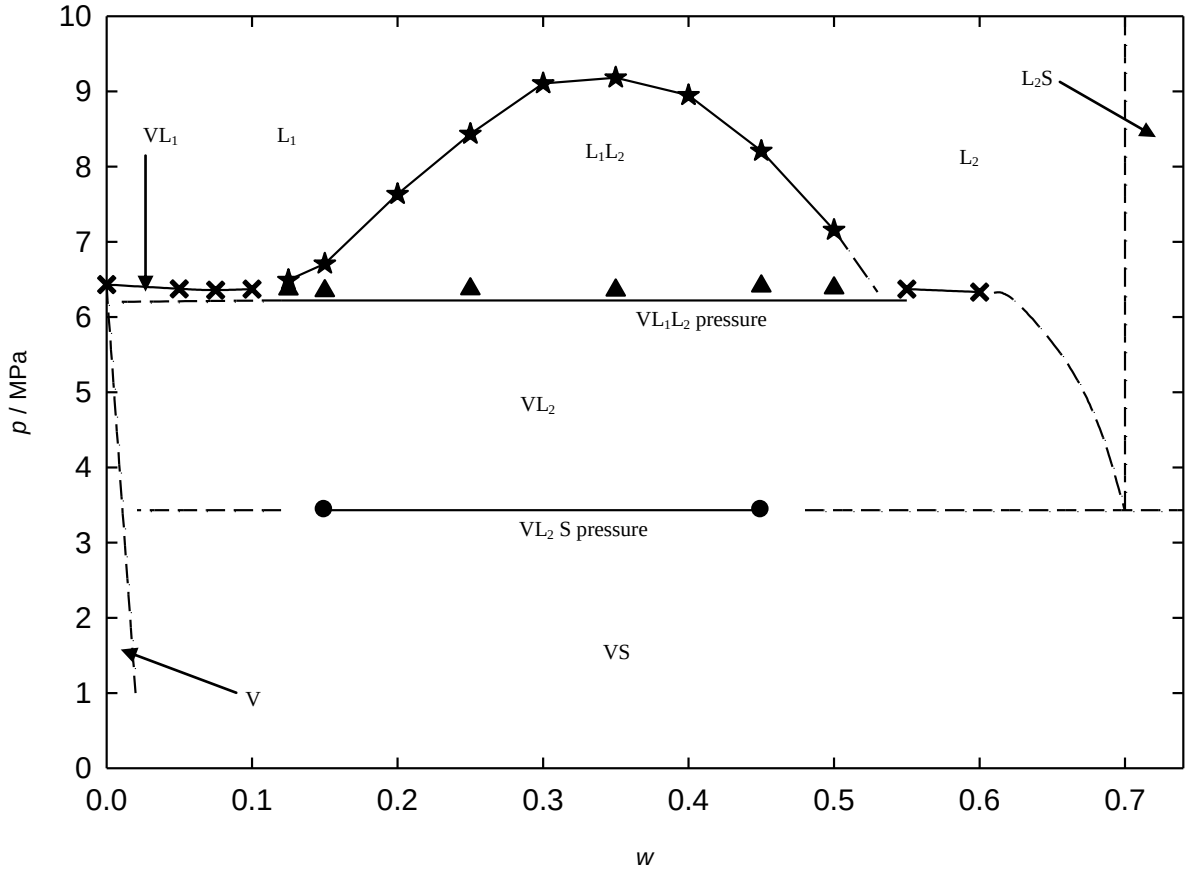

Figure 33. Phase behavior of CO_2 (1) and 2,4-di-*tert*-butylphenol (2) at 298 K; ● V L_2S; ★ L_1 L_2; ▲ VL_1L_2; ✖ V L_2. At VL_2S conditions, the L_2 phase contains roughly 30wt% CO_2. VL_2S pressure variability = ±0.56 MPa.

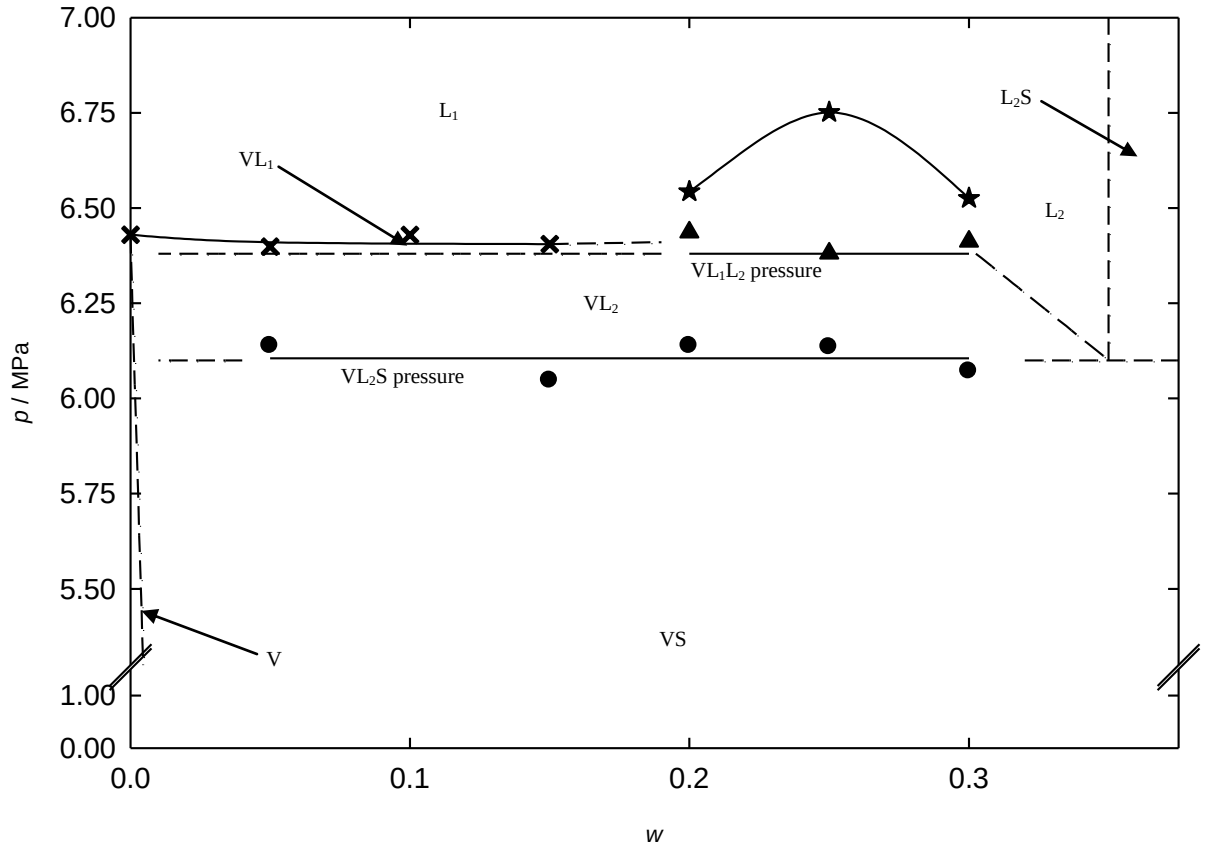

Figure 34. Phase behavior of CO_2 (1) and 2,6-di-*tert*-butyl-4-methylphenol (2) at 298 K; ● V L_2 S; ★ L_1 L_2; ▲ VL_1 L_2; ✖ V L_1. At VL_2S conditions, the L_2 phase contains roughly 65wt% CO_2. VL_2S pressure variability = ±0.33 MPa.

6.2.2.6 The three phase pressure lines

It is worth noting that the three different three phase lines, the VLS line in Figure 25 and the VL_1L_2 and VL_2S lines in Figure 26, must all be straight horizontal lines and are illustrated as such. This is due to Gibb's phase rule. In these binary systems there are two components in the system and 3 phases which results in one degree of freedom. In our apparatus the temperature is set at 298 K thus resulting in zero degrees of freedom, making the three phase pressure of these three different boundaries independent of composition and thus a constant pressure value with a slope of zero.

6.2.3 Solid CO_2-philes and CO_2/H_2, tertiary mixtures

All seven solid CO_2-philes that were able to mix with CO_2 and experienced melting point depressions, as seen in Figures 27 – 33, were tested with the equimolar CO_2/H_2 mixed gas. In addition to these seven CO_2-philes, MOA, TTBP, and TTBB were also tested with the mixed gas. Each of these three solids were examined in the past by our group or others and showed phase behavior similar to that seen with the solids examined in this work. To our knowledge the tertiary phase behavior involving these 10 solids has never been studied before.

Of the 10 solid CO_2-philes examined with the mixed gas 1,3,5-trioxane, TTBB, 2,4-di-*tert*-butylphenol and SOA experienced a melting point depression. They were tested at various weight fractions of each solid and the results are illustrated as a pseudo-binary phase behavior diagram in Figure 34 and the complete list of solids tested is in Table 6. The other six solids tested at various solid weight fractions, down to 0.01, with the mixed gas did not experience any melting while being examined and were immiscible up to 34.5 MPa.

The data in Figure 34, and pressures listed in Table 6, are the pressures at which each ternary system exhibited a three phase boundary labeled the fluid-liquid-solid (FLS) boundary with an average variability of ± 1.5 MPa. At pressures above this three phase boundary resides a two phase region consisting of a supercritical fluid made up of the CO_2/H_2 mixed gas and a liquid phase comprised mostly of the solid in question and small amounts of dissolved CO_2 and/or H_2. This result is encouraging because it means the solids are capable of forming a liquid that could be used to selectively absorb CO_2 from a supercritical mixed stream. Also the solids did not completely mix with the fluid, meaning that it is not fully miscible with the fluid, likely due to the presence of H_2. Upon expansion across the FLS line, the two phase region comprised of solid and fluid is recovered. Unfortunately the experimental apparatus used is incapable of sampling any of the phases present in the cell as it is a closed system.

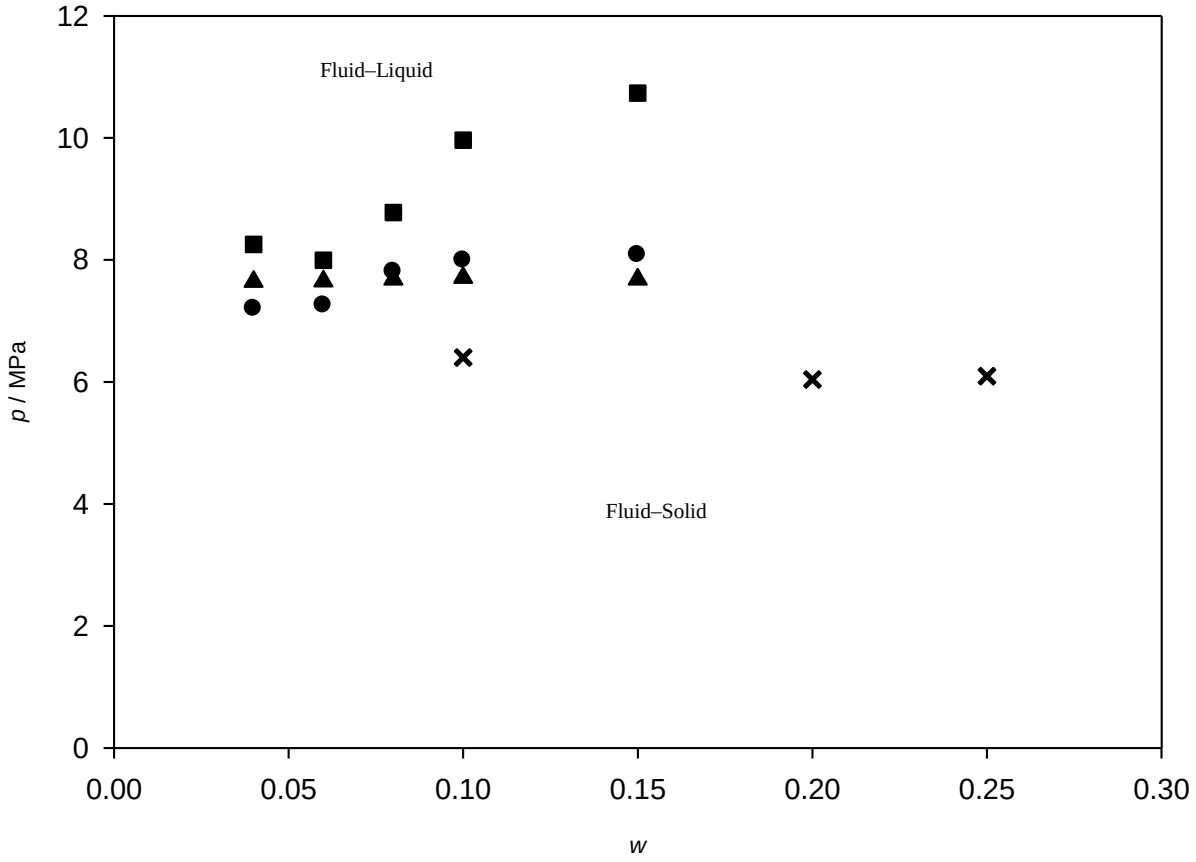

Figure 35. Phase behavior of tertiary systems made up of 50:50 mol CO_2:H_2 and solid CO_2-philes at 298 K: ● 1,3,5-trioxane; ▲ 1,3,5-tri-*tert*-butylbenzene; ■ 2,4-di-*tert*-butylphenol; ✕ D-(+)-sucrose octaacetate.

Table 6. Results of the ternary systems comprised of each solid CO_2-phile and an equimolar CO_2/H_2 mixed gas.

Solid CO_2-phile	Melted in CO_2/H_2?	Average fluid-liquid-solid pressure (MPa)	Solid weight fraction tested
α-D-glucose pentaacetate	No	-	-
β -D-ribofuranose tetraacetate	No	-	-
2,6-di-*tert*-butyl-4-methylphenol	No	-	-
2,4,6-tri-*tert*-butylphenol	No	-	-
β -D-maltose octaacetate	No	-	-
β–D-galactose pentaacetate	No	-	-
1,3,5-trioxane	Yes	7.66	0.04 – 0.15
1,3,5-tri-*tert*-butylbenzene	Yes	7.67	0.04 – 0.15
2,4-di-*tert*-butylphenol	Yes	9.14	0.04 – 0.15
sucrose octaacetate	Yes	6.18	0.10 – 0.25

6.3 CONCLUSIONS

The binary phase behavior of mixtures of CO_2 and each of the following compounds has been determined at 298 K: β-D-galactose pentaacetate, β-D-ribofuranose tetraacetate, α-D(+)-glucose pentaacetate, 1,3,5-trioxane, D-(+)-sucrose octaacetate, 2,4-di-*tert*-butylphenol, 2,6-di-*tert*-butyl-4-methylphenol, 1,2,4-tri-acetoxybenzene and 3,5-di-*tert*-butylphenol. 3,5-di-*tert*-butylphenol and 1,2,4-triacetoxybenzene were essentially insoluble in CO_2. Only 3,5-di-*tert*-butylphenol and 1,2,4-tri-acetoxybenzene did not melt in the presence of dense CO_2. The remaining solids were quite soluble in CO_2, as evidenced by Px diagrams that exhibited either one or two three-phase equilibrium lines. Further, the CO_2-philic compound liquid phase contained 30 – 65wt% CO_2 at three phase equilibrium conditions.

The ternary phase behavior for mixtures of each promising CO_2-philic solid identified in this study or prior investigations (β-D-galactose pentaacetate, β-D-ribofuranose tetraacetate, α-D(+)-glucose pentaacetate, trioxane, D-(+)-sucrose octaacetate, 2,4-di-*tert*-butylphenol, 2,6-di-*tert*-butyl-4-methylphenol, 2,4,6-tri-*tert*-butylphenol, 1,3,5-tri-*tert*-butylbenzene, and β-D-maltose octaacetate) with an equimolar CO_2/H_2 gas blend has also been determined. Only four of the solids, 1,3,5-trioxane, 2,4-di-*tert*-butylbenzene, 1,3,5-tri-*tert*-butylbenzene, and sucrose octaacetate, melted in the presence of this gas mixture at pressures comparable to those occurring in IGCC plants. These four compounds are viable candidates for pre-combustion, phase-changing, CO_2-selective sorbents.

7.0 SOLUBILITY OF CO_2 AND H_2 IN PDMS AND PEGDME AT HIGH TEMPERATURES

7.1 MATERIALS

All three different molecular weights of PDMS used in this study were purchased from Gelest Inc. listed here including properties given by the supplier, PDMS10 (viscosity, μ, equals 10 cSt at 298.15 K, and average molar mass, $\overline{MW}$ equals 1,250 g/mol), PDMS 20 (μ = 20 cSt at 298.15 K and $\overline{MW}$ = 2,000 g/mol), and PDMS50 (μ = 50 cSt at 298.15 K and $\overline{MW}$ = 3,780 g/mol). PEGDME (repeat unit, n, equals 6, $\overline{MW}$ = 310) was purchased from Polymer Source Inc and used as received. CO_2 was purchased from Penn Oxygen and Supply Company with a purity of 0.9999 and used without further purification. H_2 was purchased from Matheson Gas Products with a purity of 0.9999 and used without further purification.

7.2 SOLUBILITY OF CO_2 AND H_2 IN PDMS AND PEGDME

7.2.1 Experimental apparatus

The phase behavior cell used for this work is the same as described and illustrated in Figures 9 and 10. In a given experiment between 40 g and 60 g of PDMS or PEGDME are loaded into the Pyrex tube which is then loaded into the view cell and sealed. The floating piston

is then pushed up to decrease the volume of the air in the tube. CO_2 or H_2, depending on the experiment, is then vented in the tube and back out again in order to remove any excess air still remaining in the tube. Next, CO_2 or H_2 is pumped into the sample volume to the desired weight fraction while simultaneously removing the overburden fluid, assuring an isobaric and isothermal addition. After the first weight fraction is loaded, the environmental chamber is closed and heated to the desired temperature, either 353 K, 373 K, or 393 K. When the experimental temperature is reached the sample volume is compressed, up to 68.95 MPa for CO_2 or 34.50 MPa for H_2. At elevated temperatures either a single, clear, homogeneous liquid phase (L), a two phase vapor-liquid phase (VL), or a two phase fluid-liquid phase (FL) is achieved depending on pressure. The term "fluid" or "vapor" both refer to the less dense of the two phases inside the sample volume that is made up of either a supercritical fluid phase or a vapor phase of CO_2 or H_2. The sample volume is then expanded in order to witness phase behavior transitions and phenomena. Bubble points are defined as the equilibrium coexistence of a liquid phase and a minute amount of a vapor or fluid phase. During operation at high temperatures the isobaric addition of gases was carried out by accounting for density changes in the gases, upon increasing from room temperature to operational temperature, using density values taken from the NIST webbook for pure CO_2 and pure H_2. The pumps were then run simultaneously while taking into account the change in density by operating the overburden fluid pump faster than the gas pump and extracting a correspondingly larger amount of volume of overburden fluid from the view cell.

7.2.2 Solubility results of CO_2 in PDMS and PEGDME

Phase behavior results, in the form of pressure vs. weight fraction of PDMS (w) and PEGDME (w), for the binary systems of PDMS10 at 353 K, PDMS20 at 373 K, PDMS50 at 393 K, PEGDME at 353 K, 373 K, and 393 K with CO_2 are illustrated in Figure 35. All bubble point measurements represent the average of at least four individual measurements with an uncertainty of ± 0.07 MPa as reflected by the size of the data points. To our knowledge phase behavior for PDMS10, PDMS20, PDMS50, and PEGDME at these temperatures with CO_2 has not been previously reported.

As shown in Figure 35 at elevated pressure each binary mixture is capable of forming a single, clear, homogeneous L phase with the CO_2 over the range of weight fractions illustrated, $0.60 \leq w \leq 0.95$. Upon expansion of the L phase, bubble points are recorded upon realization of minute amounts of CO_2 bubbles evolving out of the L phase forming the binodal fluid-liquid (FL) line. Further expansion results in the two phase, fluid-liquid (FL) region consisting of supercritical CO_2 (or vapor CO_2 depending upon the pressure) with virtually no PDMS or PEGDME in the fluid phase and liquid PDMS or PEGDME with varying amounts of CO_2 still dissolved in the liquid phase.

The PDMS10 and PEGDME at 353 K exhibit the greatest ability to absorb CO_2. This is because of two correlations that complement each other at these conditions. The first is that PDMS10 has the lowest molar mass of the three PDMS solvents (1,250 g/mol) and hence the shortest chain length. Shorter chain lengths lead to increased entropy of mixing, thus more favorable mixing conditions according to Flory and Huggins.(121) Our group has illustrated that chain length directly correlates with CO_2 miscibility in the past by comparing various chain lengths of PEGDME, poly(propylene glycol) di-methyl ether, and PDMS and the ability of the smaller solvents to exhibit higher miscibility with CO_2.(86)(87) The second correlation, that is

also in favor of PDMS10 having the highest capacity of CO_2, is that as temperature increases the solubility of CO_2 in these solvents, and almost all solvents, decreases. Thus, the smallest solvent, PDMS10, at the lowest temperature, 353 K, has the greatest ability to mix with CO_2 out of the three solvents studied and the three temperatures chosen. Both of these correlations are also illustrated as PDMS20 at 373 K has a greater affinity for CO_2 than PDMS50 at 393 K.

The PEGDME used throughout these experiments is the same, so while there are no advantages in size or chain length, the mixture at the lowest temperature will have the highest capacity for CO_2. When PEGDME and PDMS are compared against each other at each temperature, the solubility results are comparable, as seen in Figure 35. This has also been shown at 298 K and 313 K above; however, in that case the size of the PDMS and PEGDME were comparable. Here the PDMS is substantially larger in molar mass and chain length, indicating that the temperature dependence of the solubility of CO_2 in solvents plays a larger role when determining CO_2-philicity than the size of the solvents being compared. The ability of the PDMS to absorb a comparable amount of CO_2 gives it a major commercial advantage in that it is capable of operating at these higher temperatures with negligible evaporative losses due to its larger size and hence lower vapor pressure at these elevated temperatures.

7.2.3 Solubility results of H_2 in PDMS

Illustrated in Figure 36 are the results for H_2 miscibility with each of the various PDMS solvents. All bubble point measurements represent the average of at least four individual measurements with a variability of ± 3.25 MPa. The pump that controls the loading of the sample gas into the Pyrex tube measures the change in volume upon addition of the gas. The NIST webbook is then later used to determine weight fractions; because H_2 is a much more

compressible fluid than CO_2 and due to small, but not negligible, leaking at high pressure, the variability of H_2 experiments is substantially larger than with CO_2. Similar to the CO_2-PDMS pseudo-binary results, each PDMS solvent and H_2 were capable of forming a single, clear, homogeneous L phase, although at much higher pressures and also a much less expansive range of weight fractions, $0.995 \leq w \leq 0.999$. It is unable to determine which solvent is more miscible with H_2 as reported. This result is not entirely unexpected however. When H_2 and each of the PDMS solvents at each temperature mix together there are two competing effects. The first is the entropy of mixing of the PDMS solvent and the H_2 which favors shorter chain, smaller polymers regardless of the solute that is trying to be dissolved. As illustrated in Figure 35, where CO_2 is dissolved in PDMS, the entropy of mixing, coupled with temperature change can result in a difference in bubble point pressures at a given weight fraction can be as much 6 MPa. The second, and competing factor, is that H_2 solubility in solvents increases with increasing temperature, opposite that of CO_2's relationship with temperature. As the temperature increases the density of the solvent decreases providing more space or pockets for the small diatomic H_2 to fill. There are very few interactions occurring between the H_2 and the PDMS solvent other than typical van der Waals forces that allows the H_2 to fill vacancies provided by the rise in temperature.

7.3 WATER MISCIBILITY IN PDMS AND PEGDME

7.3.1 Experimental procedures

Bench top experiments were carried out to test water miscibility in PEGDME at one atmosphere and up to 373 K. PEGDME and distilled water were combined in a vial and placed in an oil bath to control temperature throughout the experiment. The temperature was slowly increased while observing any phase transitions. In a typical experiment approximately 5 g each of water and PEGDME were placed in the vial.

Each of the three PDMS solvents was combined with water in the phase behavior cell at their respective temperatures. Once in the Pyrex tube the piston was raised to remove all gas present in the sample volume. Once the gas was vented the temperature of the apparatus was raised to the corresponding temperature, either 353 K, 373 K, or 393 K. At the desired temperature, the PDMS and H_2O liquid mixture is compressed up to 69 MPa and mixed for approximately 25 minutes. After mixing, the mixer is turned off and the sample volume is expanded back down to one atmosphere while observing any phase transitions. Typically 25 g of the PDMS is loaded into the Pyrex tube with approximately 10 g of H_2O.

7.3.2 Water miscibility results

As illustrated at 298 K and 313 K in Table 2 and continuing up to 373 K, the water and PEGDME are fully miscible, at which point the water begins boiling out of solution. This characteristic of PEGDME is what causes the need for the fuel gas stream from the gasifier to be

cooled down to 313 K. Much of the water has to be condensed out in order to avoid having to remove it from the rich solvent via costly heating.

The PDMS on the other hand is completely immiscible up to 69 MPa. Although the weight fraction of PDMS and water loaded into the cell was not expected to form a single clear liquid phase, this experiment still illustrates immiscibility. If any of the water would have mixed in the PDMS (or if any of the PDMS would have mixed with the water) then upon expansion a phase transition in the form of a cloud point would have been visible in the PDMS phase. Instead, upon expansion both phases, for all three PDMS solvents at their respective temperatures, stayed perfectly clear and the interface quiescent throughout the expansion. This feature is important as it would allow the PDMS solvents to selectively absorb only CO_2 from the mixed gas fuel stream. In addition the heat exchangers and condensing step associated with the removal of water could be avoided and the mass associated with the water in the fuel stream can be expanded downstream to produce more power.

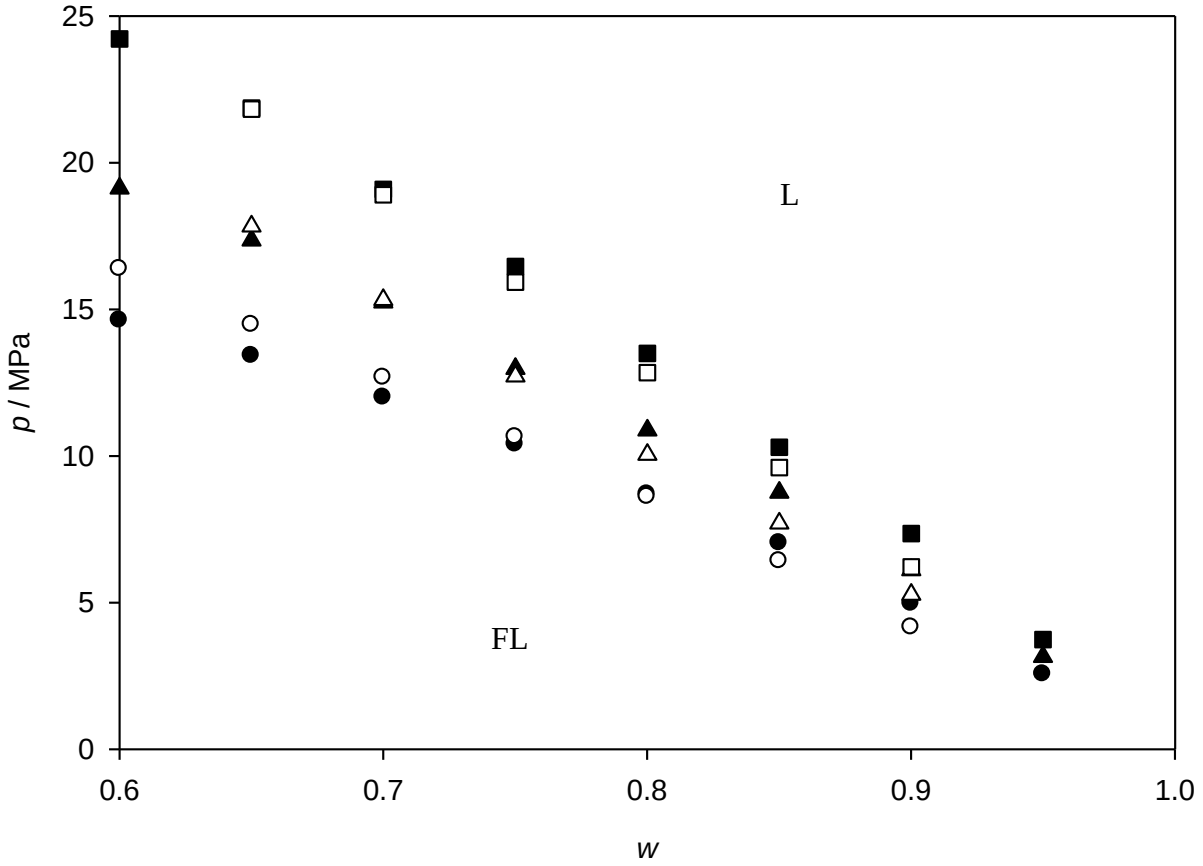

Figure 36. Phase behavior diagram of CO_2 with each PDMS solvent and PEGDME: ● PDMS10 at 353 K; ▲ PDMS20 at 373 K; ■ PDMS50 at 393 K; ○ PEGDME at 353 K; △ PEGDME at 373 K; □ PEGDME at 393 K.

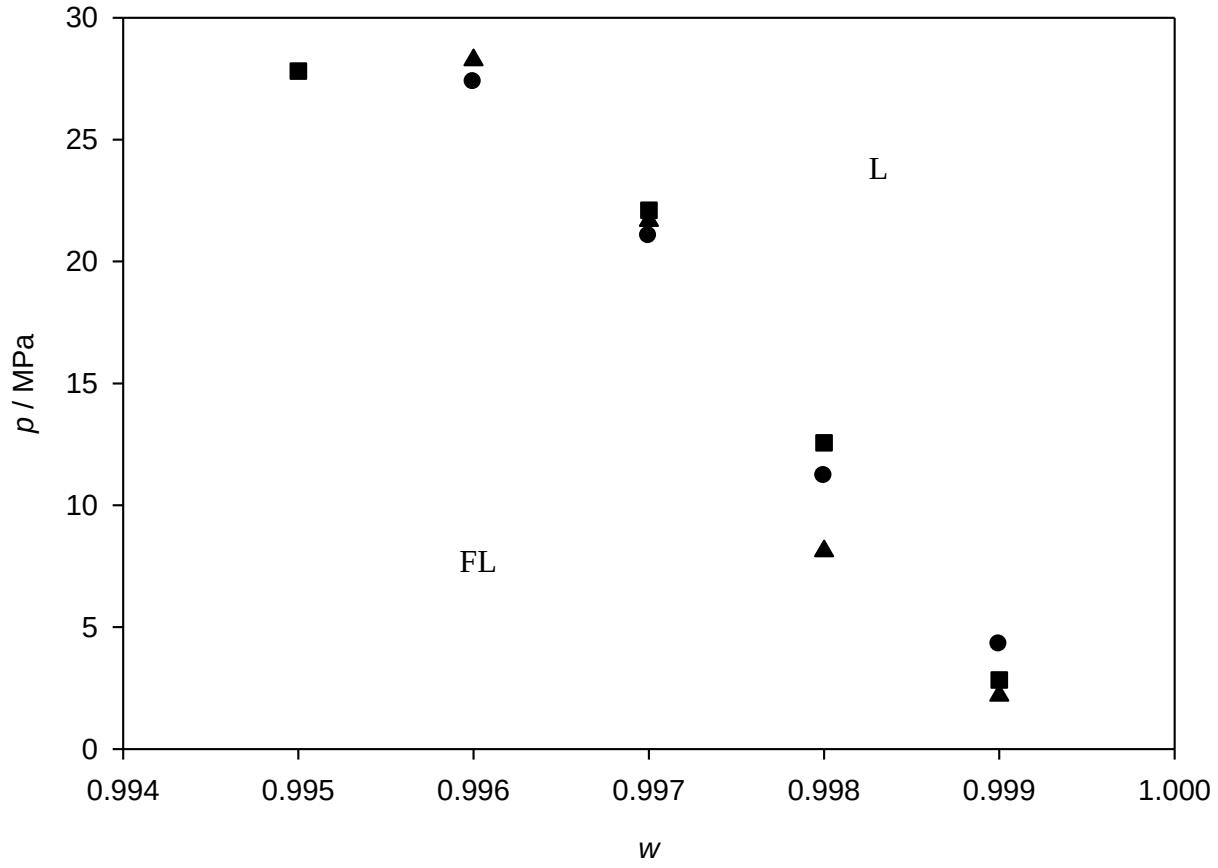

Figure 37. Phase behavior diagram of H_2 with each PDMS solvent: ● PDMS10 at 353 K; ▲ PDMS20 at 373 K; ■ PDMS50 at 393 K. Variability of measurements = ±3.25 MPa, error bars have been left out to for ease of reading.

7.4 CONCLUSIONS

The binary phase behavior of PDMS10 at 353 K, PDMS20 at 373 K, PDMS50 at 393 K, and PEGDME at 353 K, 373 K, and 393 K with CO_2 have been determined. The binary phase behavior of PDMS10 at 353 K, PDMS20 at 373 K, and PDMS50 at 393 K with H_2 has been determined. To the best of our knowledge all binary phase behavior studied in this work have never been presented before.

All three PDMS solvents as well as PEGDME were capable of mixing and forming a single homogenous L phase at weight fractions between 0.60 and 0.95 at modest pressures ranging from 2.5 MPa to 25 MPa. PDMS10 and PEGDME at 353 K were the most soluble with CO_2 as they were capable of mixing at the lowest pressures out of the four solvents studied. They are the most miscible due to complimenting factors based on the entropy of mixing and also because it is at the most favorable mixing temperature, the lowest, 353 K. Further, all three PDMS solvents showed comparable CO_2 solubility with the PEGDME at each temperature.

All PDMS solvents were able to mix and form a single homogeneous L phase with H_2 at slightly higher pressures than CO_2, 2.5 MPa to 30 MPa, but only at much higher weight fractions of PDMS, 0.996 to 0.999. It is unclear which solvent is most miscible with H_2 due to competing factors involved with the miscibility of H_2. The entropy of mixing favors the smallest, short chain PDMS solvent, PDMS10 at 353 K, to be the most miscible. At the same time, H_2 miscibility has a direct correlation to increasing temperature, favoring PDMS50 at 393 K to be the most miscible. In order to determine which solvent is most miscible with H_2 a more systematic approach would need to be carried out. Phase behavior experiments with H_2 in this study are meant as an illustration to compare the selectivity of CO_2 to the selectivity of H_2 in these solvents.

Lastly, PEGDME is fully miscible with water at all concentrations up to 373 K at atmospheric pressure. Conversely all three PDMS solvents are completely immiscible with water up to 68.95 MPa at each respective temperature.

8.0 FUTURE WORK

All solvents examined in this work including low volatility, oligomeric CO_2-philes, organic, volatile solvents, and solid CO_2-philes that melt in the presence of CO_2 and H_2 must be examined in a high pressure cell with sampling capabilities. In a set up such as this ideally the composition of the less dense phase could be examined at will as well as the gas absorbed in the solvent phase, presumably after withdrawing a small amount of the dense liquid phase at high pressure. After this, the solvents capable of selectively absorbing CO_2 can be chosen for testing at the Wilsonville Power Systems Development Facility in order to be examined at pilot scale.

After solubilities and relative selectivities for various gases (CO_2, H_2S, H_2O) in the most promising oligomeric solvents have been determined the physical absorption process can be modeled via Aspen Plus® simulation program. Although Aspen Plus does not have any of the liquid oligomeric solvents within its library of compounds, it is still capable of performing its function once parameters based on solubility and the physical properties of each solvent are defined with the help of the perturbed-chain statistical associating fluid theory, PC-SAFT, an advanced equation of state capable of performing calculations on mixtures of gases and solvents including polymers.(122)(123)(124) With Aspen it is possible to model specific unit operations within the carbon capture system, the entire carbon capture system, or the entire power plant including the carbon capture system. Developing Aspen simulations is necessary for economic analysis as well as optimization of each process in order to determine the most likely

commercially viable CO_2 capture solvent and/or process. In addition a priori calculations and predictions of solvent-CO_2 phase behavior and solubility could be made and is advantageous because of the time and money saved compared to testing all binary systems.

All solid CO_2-philes in this work were tested only at 298 K. Examining these same solvents at temperatures above their melting point would be of interest. Typically the carbon capture process in an IGCC plant occurs at or around 313 K which requires a cooling stage that cools the fuel gas stream to 313 K from approximately 400 K and condenses out much of the water present in the fuel stream. The loss of this water vapor reduces the mass of the fuel stream and the mass flow through the turbine resulting in a decrease of power production. This loss in power production is estimated to decrease overall plant efficiency by 1 – 3 %. The solid CO_2-philes would already be liquid at this un-cooled temperature and if they were capable of absorbing CO_2 at this temperature then this cooling stage would not be required, similarly to the high molar mass PDMS previously discussed. Therefore cost of energy and initial capital cost would decrease due to the removal of the cooling stage and there would be no decrease in the plant's overall efficiency. Two things of note are that the solvent would need to have low vapor pressure at these conditions, as it is now a liquid, and it would have to be hydrophobic because now there would be substantially more water vapor present compared to the fuel gas stream at 313 K.

BIBLIOGRAPHY

1. International Energy Agency, Key World Energy Statistics. Paris, France, 2010.

2. U.S. Geological Survey, Mineral commodity summaries, Washington, DC, U.S. Geological Survey, 2010.

3. SRI Consulting, [Online] SRI Consulting, January 2010. [Cited: January 14, 2011.] http://www.sriconsulting.com/WP/Public/Reports/eo/.

4. Richards, M., Shenoy, A., Schultz, K., Brown, L., Harvego, E., McKellar, M., Coupey, J-P, Moshin Reza, S.M., Okamoto, F., Handa, N., Int. J. Nuclear Hydrogen Production and Applications, (2006) **1**, 36-50.

5. U.S. Energy Information Administration, International Energy Outlook 2010, Washington DC, U.S, Department of Energy, 2010.

6. U.S. Environmental Protection Agency, Inventory of U.S. Greenhouse Gas Emissions and Sinks: 1990-2008, Washington, DC, U.S. Environmental Protection Agency, 2010.

7. International Energy Agency (IEA) Greenhouse Gas R&D Programme, Opportunities for early application of CO_2 sequestration technologies, Cheltenham, International Energy Agency, 2002.

8. Descamps, C., Bouallou, C., Kanniche, M., Energy, (2008) **33**, 874-881.

9. CCSReg Project Engineering and Public Policy Department, College of Engineering, Carnegie Mellon University, [Online] 2008 [Cited: June 17, 2011.] http://www.ccsreg.org/technologies.html.

10. Reynolds, L., Gardecki, A. J., Frankland, S., Horng, L. M., Maroncelli, M., J. Physical Chemistry , (1996) **100**, 10337-10354.

11. Kauffman, F. J., J. Physical Chemistry A, (2001) **105**, 3433-3442.

12. Raveendran, P., Wallen, S. L., J. American Chemical Society, (2002) **124**, 12590-12599.

13. Beckman, E. J., Chemical Communications, (2004) **17**, 1885.

14. Fulton, J. L., Yee, G., Smith, R. D., J. American Chemical Society, (1991) **113**, 8327-8334.

15. Pearson, R. G., J. American Chemical Society, (1963) **85**, 3533-3539.

16. Pearson, R. G., J. Chemical Education, (1968) **45**, 581-587.

17. Nelson, M. R., Borkman, R. F., J. Physical Chemistry A, (1998) **102**, 7860-7863.

18. Kazarian, S. G.. Vincent, M. F.. Bright, F. V.. Liotta, C. L.. Eckert, C. A., J. American Chemical Society, (1996) **118**, 1729.

19. Rindfleisch, F, DiNoia, T. P., McHugh, M. A., J. Physical Chemistry, (1996) **100**, 15581-15587.

20. Wang, Y., Hong, L., Tapriyal, D., Kim, I. C., Paik, I-H., Crosthwaite, J. M., Hamilton, A. D., Thies, M. C., Beckman E.J., Enick R.M., Johnson, J. K., J. Physical Chemistry B, (2009) **113**, 14971-14980.

21. Palamara, J. E., Davis, P. K., Suriyapraphadilok, U., Danner, R. P., Duda, J. L., Kitzhoffer, R. J., Zielinski, J. M., Industrial Engineering Chemistry Research, (2003) **42**, 1557-1562.

22. Sato, Y., Takikawa, T., Takishima, S., Masuoka, H., J. Supercritical Fluids, (2001) **19**, 187-198.

23. Hoefling, T. A., Newman, D. A., Enick, R. M., Beckman, E. J., J. Supercritical Fluids, (1993) **6**, 165-171.

24. Ganapathy, H. S., Hwang, H. S., Jeong, Y. T., Lee, W-K., Lim, K. T., European Polymer Journal, (2007) **43**, 119-126.

25. Wang, R., Cheung, H.M., J. Applied Polymer Science, (2004) **93**, 545-549.

26. Wang, W., Griffiths, R. M. T., Naylor, A., Giles, M. R., Irving, D. J., Howdle, S. M., Polymer, (2002), **43**, 6653-6659.

27. Yates, M. Z., Li, G., Shim, J. J., Maniar, S., Johnston, K. P., Lim, K. T., Webber, S., Macromolecules, (1999) **32**, 1018-1026.

28. Fink, R., Hancu, D., Valentine, R., Beckman, E. J., J. Phys. Chem. B, (1999) **103**, 6441-6444.

29. Kilic, S., Michalik, S., Wang, Y., Johnson, J. K., Enick, R. M., Beckman, E. J., J. Industrial & Engineering Chemistry Research, (2003) **42**, 6415-6424.

30. O'Neill, M. L., Cao, Q., Fang, M., Johnston, K. P., Industrial Engineering Chemistry Research, (1998) **37**, 3067.

31. Drohmann, C., Beckman, E. J., J. Supercritical Fluids, (2002) **22**, 103-110.

32. Shen, Z., McHugh, M. A., Xu, J., Belardi, J., Kilic, S., Mesiano, A., Bane, S., Karnikas, C., Beckman, E. J., Enick, R. M., Polymer, (2003) **44**, 1491-1498.

33. Desimone, J. M., Guan, Z., Elsbernd, C. S., Science, (1992) **257**, 945.

34. Laintz, K. E., Wai, C. M., Yonker, C. R., Smith, R. D. J., J. Supercritical Fluids, (1991) **4**, 194-198.

35. Raveendran, P., Wallen, S. L., J. Physical Chemistry B, (2003) **107**, 1473-1477.

36. Johnston, K. P., Harrison, K. L., Clarke, M. J., Howdle, S. M., Heitz, M. P., Bright, F. V., Carlier, C., Randolph, T. W., Science, (1996) **271**, 624-626.

37. Hong, L., Thies, M. C., Enick, R. M., J. Supercritical Fluids, (2005) **34,** 11.

38. Raveendran, P., Wallen, S. L., J. American Chemical Society, (2002) **124**, 7274-7275.

39. Ma, S.-L., Wu, Y.-T., Hurrey, M. L., Wallen, S. L., Grant, C. S., J. Physical Chemistry B, (2010) **114**, 3809-3817.

40. Haines, A. H., Steytler, D. C., Rivett, C., J. Supercritical Fluids, (2008) **44**, 21-24.

41. Potluri, V. K., Xu, J., Enick, R. M., Beckman, E. J., Hamilton, A. D., Organic Letters, (2002) **4**, 2333-2335.

42. Dilek, C., Manke, C. W., Gulari, E., Fluid Phase Equilibria, (2006) **239**, 172-177.

43. Serhatkulu, G. K., Dilek, C., Gulari, E., J. Supercritical Fluids, (2006) **39**, 264-270.

44. Kim, J., Novick, B. J., DeSimone, J. M., Carbonell, R. G., Langmuir, (2006) **22,** 642-657.

45. Kim, J., Carbonell, R. G., Langmuir, (2006) **22**, 2117-2129.

46. Potluri, V. K., Hamilton, A. D., Karanikas, C. F., Bane, S. E., Xu, J., Beckman, E. J., Enick, R. M., Fluid Phase Equilibria, (2003) **211**, 211-217.

47. Filardo, G., DiBlasi, M., Galia, A., Ponchel, A., Bricout, H., Sayede, A. D., Monflier, E., J. Supercritical Fluids, (2006) **36**, 173-181.

48. Eastoe, J., Dupont, A., Steytler, D. C., Thorpe, M., Gurgel, A., Heenan, R. K., J. Colloid and Interface Science, (2003) **258**, 367-373.

49. Eastoe, J., Paul, A., Nave, S., Steytler, D. C., Robinson, B. H., Rumsey, E., Thorpe, M., Heenan, R. K., J. American Chemical Society, (2001) **123,** 988-989.

50. Dilek, C., Manke, C. W., Gulari, E., J. Supercritical Fluids, (2008) **43**, 421.

51. Hong, L., Fidler, E., Enick, R. M., Marentis, R., J. Supercrit. Fluids, (2008) **44,** 1-7.

52. Bamberger, A., Schmelzer, J., Walther, D., Maurer, G., Fluid Phase Equilibria, (1994) **97**, 167-189.

53. Isaacs, E., Otto, F. D., Mather, A. E., J. Chemical Engineering Data, (1980) **25,** 118-120.

54. Diguillo, R. M., Lee, R. J., Schaeffer, S. T., Brasher, L. L., Teja, A. S., J. Chemical Engineering Data, (1992) **37**, 239.

55. Shen, K., Li, M., J. Chemical Engineering Data, (1992) **37**, 96.

56. Chakravarty, T., Phukan, U. K., Weiland, R. H., Chemical Engineering Progress, (1985) **April** 32.

57. Diao, Y., Zheng, X., He, B., Chen, C., Xu, X., Energy Conversion and Management, (2004) **45**, 2283.

58. Pereira, F. E., Keskes, E., Adjiman, C. S., Galindo, A., Jackson, G., Philadelphia, PA, Presentation at AIChE annual meeting, November, 2008.

59. Uhde, Morphysorb Uhde's physical solvent for acid gas removal informational page, Uhde, http://www.uhde.eu/cgi-bin/byteserver.pl/pdf/broschueren/Oil_Gas_Refinery/Morphysorb.pdf

60. Murrieta-Guevara, F., Romero-Martinez, A., Trejo, A., Fluid Phase Equilibria, (1988) **44**, 105.

61. Mutelet, F., Vitu, S., Privat, R., Jaubert, J., Fluid Phase Equilibria, (2005) **238**, 157-168.

62. Reighard, T. S., Lee, S. T., Olesik, S. V., Fluid Phase Equilibria, (1996) **123**, 215.

63. National Energy Technology Laboratory, Cost and Performance Baseline for Fossil Energy Plants Volume 1: Bituminous Coal and Natural Gas to Electricity, DOE/NETL, 2010.

64. Kohl, A., Nielson, R., Gas Purification 5th Edition. Houston, Gulf Professional Publishing, 1997.

65. Energy Information Administration, Official Energy Statistics from the U.S. Government. [Online] www.eia.doe.gov.

66. Aiken, R., Ditzel, K.H., Morra, F., Wilson, D.S., Coal-Based Integrated Gasification Combined Cycle (IGCC): Market Penetration Recommendations and Strategies, study for the Deparment of Energy's National Energy Technology Laboratory, September 2004, ES-1.

67. McKetta, J.J., Encyclopedia of chemical processing and design, New York, M. Dekkar, 1976.

68. Net Resources International, [Online] 2011. [Cited: June 17, 2011.] http://www.power-technology.com/projects/isab/isab1.html.

69. AG, Lurgi Oil-Gas-Chemical GmbH and Linde, Hydrocarbon Process, Gas Processes Handbook, 1996, 134.

70. Kohl, A. L., Buckingham, P. A., Petroleum Refiner., (1960) **39**, 193.

71. Bucklin, R. W., Schendel, R. L., Acid and Sour Gas Treating Processes, Houston, Gulf Publishing Co., 1985.

72. Hochgesand, G., Industrial Engineering Chemistry, (1970) **62**, 37.

73. Hossain, M.M., deLasa, H.I., Chemical Engineering Science, (2008), **63**, 4433-4451.

74. Kassim, D. M., Zainel, H. A., Al-asaf, S. A., Talib, E. K., Fluid Phase Equilibria, (1988) **41**, 287-294.

75. Kordikowski, A., Schenk, A. P., Van Nielen, R. M., Peters, C. J., J. Supercritical Fliuds, (1995) **8,** 205-216.

76. Chester, T. L., Haynes, B. S., J. Supercritical Fluids, (1997) **11**, 15-20.

77. Reaves, J. T., Griffith, A. T., Roberts, C. B., J. Chemical Engineering Data, (1998) **43**, 683-686.

78. Day, C.-Y., Chang C.J., Chen C.-Y., J. Chemical Engineering Data, (1996) **41**, 839-843.

79. Day, C-Y., Chang C.J., Chen, C-Y., J. Chemical Engineering Data, (1999) **44**, 365-372.

80. Chang, C. J., Chiu, K.-L., Day, C.-Y., J. Supercritical Fluids, (1998) **12,** 223-237.

81. Adrian, T., Maurer, G., J. Chemical Engineering Data, (1997), **42**, 668-672.

82. Byun, H.-S., Choi, M.-Y., Lim, J.-S., J. Supercritical Fluids, (2006) **37**, 323-332.

83. Leites, I. L., Separation and Purification Technology, (1997) **12**, 201-213.

84. Schwinghammer, S., Siebenhofer, M., Marr, R., J. Supercritical Fluids, (2006) **38**, 1-6.

85. Ashraf-Khorassani, M., Combs, M. T., Taylor, L. T., Talanta, (1997) **44**, 755-763.

86. Miller, M. B., Chen, D., Xie, H., Luebke, D. R., Johnson, J. K., Enick, R. M., Fluid Phase Equilibria, (2009) **287,** 26-32.

87. Miller, M. B., Luebke, D. R., Enick, R. M., Energy and Fuels, (2010) **24,** 6214-6219.

88. Enick, R. M, Beckman, E.J., Yazdi, A., Krukonis, V., Schonemann, H., Howell, J, J. Supercritical Fluids, (1998) **13**, 121.

89. Gerhardt, L. J., Manke, C. W., Gulari, E., J. Polymer Science Part B-Polymer Physics, (1997), **35**, 523-534.

90. Flichy, N. M. B., Lawrence, C. J., Kazarian, S. G., Industrial Engineering Chemistry Research, (2003) **42**, 6310-6319.

91. Royer, J. R., Gay, Y. J., Adam, M., DeSimone, J. M., Khan, S. A., Polymer, (2002) **43**, 2375-2383.

92. Dimitrov, K., Lubomir, B., Tufeu, R., Macromolecular Chemistry Physics, (1999) **200**, 1626-1629.

93. Heller, J. P., Dandge, D. K., Card, R. J., Donaruma, L. G., Society Petroleum Engineering J., (1985) **25**, 679.

94. Chang, C. J., Day, C-Y., Ko, C-M., Chiu, K-L, Fluid Phase Equilibria, (1997) **131**, 243-258.

95. Jou, F. Y., Deshmukh, R. D., Otto, F. D., Mather, A. E., J. Chemical Society, Faraday Trans. 1, (1989) **85**, 2675-2682.

96. Klamt, A., J. Physical Chemistry, (1995) **99,** 2224.

97. Klamt, A., Schuurmann, G., J. Chemical Society Perkin Trans. 2, (1993) 799.

98. Constantinescu, D., Klamt, A., Geana, D., Fluid Phase Equilibria, (2005) **231,** 231.

99. Klamt, A., Eckert, F., Fluid Phase Equilibria, (2000) **172**, 43-72.

100. Lee, M. T., Lin, S. T., Fluid Phase Equilibria, (2007) **254**, 28-34.

101. Freire, M. G., Ventura, S.P.M., Santos, L.M.N.B.F., Marrucho, I.M., Coutinho, J.A.P., Fluid Phase Equilibria, (2008) **268**, 74-84.

102. Freire, M.G., Santos, L.M.N.B.F., Marrucho, I.M., Coutinho, J.A.P., Fluid Phase Equilibria, (2007) **255**, 167-178.

103. Ouni, T., Zaytseva, A., Uusi-Hyyny, P., Pokki, J-P., Aittamaa, J., Fluid Phase Equilibria, (2005) **232**, 90-99.

104. Schroder, B., Santos, L.M.N.B.F., Marrucho, I.M., Coutinho, J.A.P., Fluid Phase Equilibria, (2010) **289**, 140-147.

105. Perdew, J. P., Physical Review B, (1986) **33,** 8822.

106. Becke, A. D., Physical Review A, (1988) **38**, 3098.

107. Schafer, A., Huber, C., Ahlrichs, R., J. Chemical Physics, (1994) **100**, 5829.

108. Ahlrichs, R., Bar, M., Haser, M., Horn, H., Kolmel, C., Chemical Physics Letters, (1989) **162,** 165.

109. Eckert, F., Klamt, A., AIChE J., (2002) **48**, 369.

110. Klamt, A. COSMO-RS from quantum chemistry to fluid phase thermodynamics and drug design, Elsevier, 2005.

111. Eichkorn, K., Treutler, O., Ohm, H., Haser, M., Ahlrichs, R., Chemical Physics Letters, (1995) **240**, 283.

112. Eckert, F., Klamt, A., COSMOtherm Users Manual: Version C2.1 Release 01.07, COSMOlogic, Leverkusen, Germany, GmbH & Co.KG, 2004.

113. Roland, S., Wolfgang, W, J. Physical Chemical Reference Data, (1996) **25**, 1509.

114. Kholod, Y.A., Muratov, E.N., Gorb, L.G., Hill, F.C., Artemenko, A.G., Kuz'min, V.E., Qasim, M., Leszczynski, J. Environmental Science Technology, (2009) **43**, 9208-9215.

115. Shimoyama, Y., Akira, I., Fluid Phase Equilibria, (2010) **297**, 178-182.

116. Rao, A. B., Rubin, E. S., Environmental Science Technology, (2002) **36** 4467-4475.

117. Ordorica-Garcia, G., Douglas, P., Croiset, E., Zheng, L, Energy Conversion and Management, (2006) **47**, 2250-2259.

118. The Cost of CCS...Setting Criteria, Guidelines to Provide Defendable and Realistic Estimates for Decisionmakers, Rubin, E, Pittsburgh, PA, Carbon Capture and Sequestration meeting, 2011.

119. McCabe, W. L., Smith, J. C., Harriott, P., Unit Operations of Chemical Engineering 6th Edition, Boston, Burr Ridge, IL, Dubuque, IA, Madison, WI, New York, San Francisco, St. Louis, McGraw-Hill, 2001.

120. Flory, P. J., Principles of Polymer Chemistry, Ithaca, NY, Cornell University Press, 1953.

121. Gross, J, Sadowski, G., Industrial and Engineering Chemical Research, (2001) **40,** 1244-1260.

122. Gross, J., Sadowski, G., Industrial and Engineering Chemical Research, (2002) **41**, 1084-4093.

123. Gross, J., Sadowski, G., Industrial and Engineering Chemical Research, (2002) **41**, 5510-5515.